INFORMATION TO USERS

This manuscript has been reproduced from the microfilm master. UMI films the text directly from the original or copy submitted. Thus, some thesis and dissertation copies are in typewriter face, while others may be from any type of computer printer.

The quality of this reproduction is dependent upon the quality of the copy submitted. Broken or indistinct print, colored or poor quality illustrations and photographs, print bleedthrough, substandard margins, and improper alignment can adversely affect reproduction.

In the unlikely event that the author did not send UMI a complete manuscript and there are missing pages, these will be noted. Also, if unauthorized copyright material had to be removed, a note will indicate the deletion.

Oversize materials (e.g., maps, drawings, charts) are reproduced by sectioning the original, beginning at the upper left-hand corner and continuing from left to right in equal sections with small overlaps.

Photographs included in the original manuscript have been reproduced xerographically in this copy. Higher quality 6" x 9" black and white photographic prints are available for any photographs or illustrations appearing in this copy for an additional charge. Contact UMI directly to order.

ProQuest Information and Learning
300 North Zeeb Road, Ann Arbor, MI 48106-1346 USA
800-521-0600

EFFECT OF SURFACTANT TRANSPORT ON THE MOBILITY OF BUBBLES IN LIQUIDS

AN EXPERIMENTAL AND COMPUTATIONAL STUDY

by

RAVICHANDRA PALAPARTHI

A Dissertation submitted to the Graduate Faculty in Engineering in partial fulfillment of the requirements for the degree of Doctor of Philosophy, The City University of New York

2001

UMI Number: 3008859

UMI Microform 3008859

Bell & Howell Information and Learning Company
300 North Zeeb Road
P.O. Box 1346
Ann Arbor, MI 48106-1346

This manuscript has been read and accepted for the Graduate Faculty in Engineering in satisfaction of the dissertation requirements for the degree of Doctor of Philosophy.

3/02/01 — Charles Maldarelli

Date — Charles Maldarelli

Chair of Examining Committee

March 2, 2001 — Mumtaz K. Kassir

Date — Mumtaz K. Kassir

Executive Officer

Morton Denn

Alexander Couzis

David Rumschitzki

Andreas Acrivos

Supervisory Committee

THE CITY UNIVERSITY OF NEW YORK

Abstract

EFFECT OF SURFACTANT TRANSPORT ON THE MOBILITY OF BUBBLES IN LIQUIDS AN EXPERIMENTAL AND COMPUTATIONAL STUDY

by

Ravichandra Palaparthi

Advisor: Professor Charles Maldarelli

When a bubble rises in an infinite liquid containing trace amount of surfactant, the surfactant adsorbs on to the front end of the bubble and is swept by surface convection to the trailing end. As the surface concentration of surfactant at the trailing pole is greater than the concentration at the leading pole, the leading pole is of higher tension, and tugs the trailing pole, creating a Marangoni force opposing the driving force moving the bubble. Hence the retardation in the bubble terminal velocity.

We consider both theoretically and experimentally the effect of the transport rates of an added surfactant from (to) the bulk phase to (from) the bubble surface on the steady state drag of a spherical bubble rising in an infinite liquid containing the surfactant. Theoretically we calculate the drag on the bubble by solving the complete flow equations coupled with the equations of surfactant transport. Experimentally we study the effect of

adding a poly-ethoxy surfactant (C_iE_j: $CH_3(CH_2)_{i-1}(-OCH_2CH_2)_j-OH$)), $C_{12}E_6$ or $C_{10}E_8$ on the drag of an air bubble rising in a 70:30 Glycerol-Water mixture.

In the limit of the surfactant transport rates being very low compared to the hydrodynamic rates, we develop an exact theory and conduct systematic experimental studies that lets us implement a new technique to determine the kinetic exchange rate constants of the surfactant at the air-liquid interface. In the limit when the surfactant transport rates are very high compared to the hydrodynamic rates, previous research in our group hinted at the possibility of the surfactant adsorbed on the bubble surface being able to desorb and making the interface stress free again like in a surfactant free system. We verify this idea of remobilizing the surfactant laden bubble surface from our numerical simulations and in the process deduce the criteria for its possibility under realistic conditions. We corroborate these conclusions from bubble rise experiments as before where we see the drag on a bubble of any given size showing a maximum with the addition of surfactant to the bulk phase. For the first time this provides a concrete proof of this phenomenon of remobilization.

Acknowledgements

I wish to express my sincere thanks to Professor Charles Maldarelli, my mentor for his great personality that really made me enjoy the course of my Ph.D. His, together with the equally pleasant nature of Professor Demetrios Papageorgiou, my co-mentor, made my doctoral study, a truly gratifying experience to me. Both have been great advisors, and more importantly great friends.

Thanks are also due to Professor Alex Couzis, for his valuable suggestions and encouragement throughout my graduate school.

Thanks are also to the members of my examination committee for consenting to be on the same and for their valuable suggestions towards my research work.

I would like to acknowledge the invaluable help of Mr. Andrew Eng, and Mr. Zhen Rong Xu, in the course of this work.

I am indebted to all my friends both at City College and at the Shirdi Sai Center, Flushing who really made my stay possible and memorable in the City of New York. Their constant support made this place a home away from home for me. I am also indebted to all other friends of mine who, though not in New York, through their whispers from across the miles always kept me going.

Last but not the least, the members of my family. My sister Gayatri and my brother in law Prasad always kept me smiling with their sweet nature. No words of

gratitude exist to thank the efforts my parents, who bearing all the difficulties all along for my sake, have been a constant source of encouragement to me.

.....To My Parents

and My Teachers

Table of Contents

List of Tables

List of Figures

CHAPTER 1
Introduction

1.1 Background and Scope

Bubble motion in liquids, like other interfacial flows, is greatly influenced by the presence of surface active species in the liquid phase. When a bubble rises in an infinite liquid containing surfactant, the surfactant adsorbs on to the front end of the bubble and is swept by surface convection to the trailing end. As the surface concentration of surfactant at the trailing pole is greater than the concentration at the leading pole, the leading pole is of higher tension, and tugs the trailing pole, creating a Marangoni force opposing the driving force moving the bubble[1]. Hence the retardation in the bubble terminal velocity. This retardation in surface mobility of bubbles/drops due to the presence of surfactants has been widely studied theoretically[2-8], and observed experimentally[9-15] (also see the review by Clift, et al[16]). We review this research in detail in Section 1.3. This reduced interfacial mobility due to the presence of surfactants affects technological processes like inter-phase mass transfer during drop-wise extraction[11,12,17,18], the rate of thinning of the fluid between mutually approaching particles in an emulsion or foam[19,20], and in thermocapillary motion of bubbles and drops in a microgravity environment[21,22]. While the reduction in interfacial mobility benefits processes like the ones involving stabilization of emulsions and foams, it hampers processes involving say interphase mass

transfer. Hence controlling the interfacial mobility plays a key role. While we describe in detail in Section 1.2, the specific technological processes that form motivation for our study we note that understanding how the surfactants affect, and could be used to control, the interfacial mobility is a key issue in utilizing them for different processes. This thesis is an attempt in this direction.

We describe here the physico-chemical mechanism by which the surfactant affects the interfacial mobility when a bubble moves in an infinite liquid containing surface active materials [1,23]. As shown in Figure 1.1, the surfactant is transported from the bulk by convection and diffusion to the sublayer close to the bubble surface. It adsorbs on the moving bubble surface and is convected by the surface flow from the front of the bubble to its trailing end where the increase in surface concentration Γ' causes surfactant to kinetically desorb into the rear sublayer. This desorption locally raises the sublayer concentration C_s, at the back above the bulk value C_o, far from the interface. The difference drives a diffusive flux away from the trailing end. Similarly at the front end, the reduction in surface concentration causes kinetic adsorption from the front sublayer onto the front of the bubble. The front sublayer concentration decreases, creating a diffusive flux from the bulk to the front end. Eventually a steady state develops: The surface concentration at the back end has increased by $\Delta\Gamma'$ above the equilibrium value Γ_e corresponding to C_o (as given by the adsorption isotherm Γ_e (C_o) so that the desorption

rate balances the convection rate. The back sublayer concentration has increased by ΔC above C_o so that the diffusive flux away from the particle surface balances the kinetic desorption. At the front end, the surface concentration has decreased below Γ_e so that kinetic adsorption balances convection, and the sublayer concentration is reduced below C_o sufficiently so that diffusion to the surface balances adsorption. Thus while the average concentration on the surface at steady state scales with $\Gamma_e(C_o)$, the surface concentration is considerably higher at the rear than at the front of the particle, and the interfacial tension (γ) is lower at the back relative to the front. This interfacial tension difference creates a Marangoni stress along the surface opposing the surface flow caused by the driving force causing the motion of the particle (for example, buoyancy or thermocapillary forces). Thus the adsorption of surfactant onto the particle interface acts to reduce the surface flow and hinder the interfacial mobility. The less mobile an interface, the more drag is exerted by the continuous phase on the particle as it moves through the medium, and the smaller is the migration velocity for a fixed driving force on the bubble.

While we describe in detail later in Section 1.3 with scaling arguments, we mention here that the time scales over which the surfactants reach the bulk sublayer close to the interface and exchange with the interface, relative to the hydrodynamic time scale, govern the extent of their influence on the mobility of the bubble. Accordingly three

regimes in the bubble motion could be identified. When the surfactant transport by both bulk diffusion and kinetic exchange at the air/liquid interface are far less than the surface convection rates of the surfactant, the surfactant behaves as if it were insoluble; to leading order, surface convection sweeps surfactant from the front to the back end with no surface to bulk exchange while the front end is clean of surfactant. Under these conditions from the balance of the surfactant on the surface of the bubble, we can show that the region in the back end of the bubble where the surfactant accumulates is stagnant while the front end of the bubble which is clean is stress free. This is the *Stagnant Cap Regime,* which as we see later in Section 1.3, is the most common in physical situations especially at low surfactant concentrations. Though it has received wide theoretical attention, no systematic experimental study has been reported with use of surfactants.

When the rates of bulk diffusion and surfactant desorption are of the same order as the interfacial convection, the *Uniformly Retarded Regime* is obtained where the surfactant exchanges between the bulk and the surface. In this case, the surface of the bubble becomes more uniformly retarded rather than completely mobile at the front end and solid-like at the back end.

In the case when the surfactant transport from the bulk by diffusion and the kinetic exchange rate at the interface outweigh its rate of transport on the surface of the bubble by convection the *Remobilization Regime* is obtained. Here the surfactant adsorbed onto the bubble surface could desorb and in the process could make the

interface mobile, reducing the shear stress on the surface developed in the to the previous two cases. Only theoretical work either in the diffusion limited (at low Peclet numbers of order 100) or the kinetically controlled case has been reported without direct concrete experimental evidence of the possibility of this phenomenon. There is only an indirect experimental evidence [24,25] of this possibility in the case of slug flow through capillary tubes, coming from our research group, as we detail in Section 1.3.

Since a surfactant that could remobilize an interface should have faster kinetics and should be present at higher concentrations, it would reach the interface preferentially than any trace amount of surface-active impurity present in the bulk. So the retarding effect of the impurity will not be felt by the interfacial hydrodynamics. Thus utilizing a remobilizing surfactant could provide a handle on the control of interfacial mobility in real systems where trace amount of surface active contaminants are always present.

While the study of the effect of surfactant transport on the mobility of a bubble rising in a liquid is the focus of our research, the scope of our study has the following objectives:

1) To develop an exact theory with full numerical simulations to describe the drag on spherical bubble rising in a surfactant solution, as a function of the surfactant bulk concentration, in the stagnant cap regime. Here we take care of the high Peclet numbers ($\sim 10^6$) characteristic of surfactant transport in liquids (as we describe later in Section 1.3),

and the finite kinetic exchange rates exhibited by surfactants at the air/liquid interface. We describe these details in Chapter 2.

2) To undertake a systematic experimental study on the effect of surfactants on the rise velocities of bubbles in an infinite liquid in the stagnant cap regime. From the study as part of our first objective, we find an interesting dependence of the amount of surfactant adsorbed or the drag experienced by the rising bubble on the surfactant kinetic exchange rates. We compare our experimental results with our numerical results and explore the possibility of determining the kinetic exchange rate constants of the surfactant at the air/liquid interface. Chapter 3 describes this approach.

3) To develop the theoretical framework in the remobilization regime where the complete flow equations coupled with the surfactant transport equations need to be solved together. We describe the extension of our theory to this regime in Chapter 4, where we show the effect of the high Peclet numbers and the finite kinetic exchange rates on the ability to remobilize the surfactant laden bubble surface.

4) To experimentally verify the possibility of being able to remobilize a surfactant laden bubble interface conducting experiments to study the effect of an added surfactant on the drag (or the velocity) of a bubble rising in a liquid due to buoyancy. In investigating the effect of the surfactants on interfacial flows, the study of a spherical bubble rising in an infinite fluid provides an ideal test case. The drag on a spherical bubble is independent of the interfacial tension between the bubble and the continuous

phase. The only effect of surface tension comes in the tangential stress balance in the form of surface tension gradient on the interface. Hence unlike the experiments of Stebe, et al [24,25] for slug flow through capillary tubes (for reasons we describe later in Section 1.4), we can single out the effect of these Marangoni forces. Thus the experiments with rising bubble could provide a concrete direct experimental evidence for the phenomenon of remobilization in contrast to the indirect evidence from the work of Stebe et al[24,25]. Our numerical simulations developed as part of our third objective could describe these experimental results. Chapter 5 describes our approach towards this objective.

1.2 Motivation

Since its really difficult to do away with trace amounts of surface active impurities in any physical system, the retarding effects always manifest in physical processes of technological importance as we mentioned before. In particular the phenomena that provide the motivation for our research are the reduction in thermocapillary migration of bubble/drops in a microgravity environment[26], and the reduction in interphase mass transfer efficiency in drop-wise extraction [11,12,17,18,27] due to the presence of the surface active impurities. In the following paragraphs, we will describe these two processes.

Microgravity processes must rely on mechanisms other than buoyancy to move bubbles or droplets from one region to another in a continuous liquid phase. One

suggested method is thermocapillary migration in which a temperature gradient is applied to the continuous phase. As shown in Figure 1.2a, when a fluid particle contacts this gradient, one pole of the particle becomes warmer than the opposing pole. The interfacial tension between the drop or bubble phase and the continuous phase usually decreases with temperature. Thus the cooler pole is of higher interfacial tension than the warmer pole, and the interface is tugged in the direction of the cooler end. This thermocapillary or thermally induced Marangoni surface stress causes a fluid streaming in the continuous phase from which develops a viscous shear traction and pressure gradient which together propel the particle in the direction of the warmer fluid. (For a general discussion of thermocapillary driven motions of fluid particles and their relevance to microgravity processes, see for example the review article by Subramanian, et al[26]). A significant and as yet unresolved impediment to the use of thermocapillary migration to direct bubble or drop motion is that these migrations can be significantly retarded by the adsorption onto the fluid particle surface of surface active impurities dissolved in the continuous or (if the particle is a liquid) droplet phases [21 22 28,29]. Because of the adsorption of the surfactant onto the fluid/fluid interface, as per the mechanism described before, the surface tension gradient created by the applied temperature gradient is reduced (as shown in Figure 1.2b). In a microgravity environment, processes for making of glass, superconducting materials, and composites (using miscibility gap solidification) rely on thermocapillary phenomena.

The presence of trace amount of surface active impurities may considerably hamper the efficiency of these processes.

The reduced interfacial mobility is known to affect the interphase mass transport processes too. Consider the case of a gas dissolution process, like CO_2 dissolving in water. In particular we consider the simple case of a single bubble of CO_2 rising in water and dissolving simultaneously. If the flow past the bubble were in the creeping flow regime, then since the diffusion coefficients of gases in the liquids are in the order of 10^{-6} cm^2s^{-1}, with the velocities of the order of 10 cm s^{-1} for bubbles of radii 10^{-1}cm, the Peclet numbers will be of the order of 10^6. At these high Peclet numbers, the mass transfer coefficient for the transport of CO_2 for the boundary conditions shown in the Figure 1.3, goes as order of $Pe^{1/2}30$, assuming the bubble surface is stress free.

But in any real system, because of the presence of surface active impurities, the bubble surface would be partially /completely immobilized. These impurities form a stagnant-cap on the surface, giving a no-slip condition on the surface, and reducing the circulation rates inside the bubble. Under these conditions, the mass transfer coefficient for the transport of the solute would be closer to that across a fluid-solid interface, which goes as $Pe^{1/3}$. This is lower than the expected mass transfer coefficient of the order of $Pe^{1/2}$.

The reduction in internal circulation rates because of the presence of surfactants is observed for drops experimentally in the studies of Garner, et al[12] and Elzinga , et al[11]. The decrease in the interphase mass transport rates due to reduced internal circulation rates, has been observed in the experimental studies of Takemura and Yabe[27], where the rising speed and dissolution rates of CO_2 bubbles in contaminated water has been studied. The experimentally calculated Sherwood numbers agree well with the numerically estimated values that took care of the stagnant cap (caused by the contaminants) existing on the bubble surface. Experimental studies of Raymond and Zieminski[14] involving intentional addition of surface active materials (C_5-C_9 alcohols) to the continuous phase (water), show that the mass transport coefficients (for CO_2) decreased with increasing surfactant concentrations. The coefficients plateau off to values that were expected for transport across a fluid/solid interface at the highest concentrations studied. Hence the theoretically predicted efficiency for these kinds of mass transfer processes is never achieved in any real system due to the presence of the surface-active impurities.

Hence we see that if one were to enhance the efficiencies of processes like the above two, controlling the mobility of a surfactant retarded interface becomes an important issue. Previous theoretical[31,32] and experimental [24,25] research in our group has hinted at this mobility control using surfactants which exchange rapidly at the interface when present in high bulk concentrations. We present the theoretical scaling

arguments in Section 1.3 on how the surfactant affects the mobility of a bubble rising in a liquid. While we concentrate on the surfactant induced retardation in Section 1.3.1, in Section 1.3.2 we present the scaling arguments and elucidate the conditions under which, the surfactant retarded interface could be remobilized, and brought back to its original stress free state.

We note that using a remobilizing surfactant would enhance the efficiency of the thermocapillary motion in microgravity when this surfactant at high bulk concentrations and rapid kinetic exchange rates adsorbs at the air/liquid interface preferably than the trace amount of retarding impurity. In the case of inter phase mass transport processes, the solute mass transport rates are increased by having a completely mobile interface at the air/liquid interface through usage of a remobilizing surfactant. But since the remobilizing surfactant would be present at high bulk concentrations in the bulk liquid phase, this would decrease the bulk diffusive transport of the solute. So the balance between these two effects governs the net increase of the solute inter phase mass transfer rate.

1.3 Scaling Arguments

1.3.1 Surfactant Induced Retardation

In this section, the theoretical analysis of how the surfactant affects the mobility of a fluid particle moving in an infinite medium is presented. We first sketch the scaling arguments below along with a discussion of the previous literature, which is reviewed in

the context of the scaling framework. We assume the fluid particle to be a gas bubble, with surfactant present only in the continuous phase. We also consider only concentrations of surfactant below the critical concentration at which micellar aggregates form (CMC) or the surfactant becomes insoluble.

In typical liquid systems (like water) the diffusion coefficient of the surfactants is of the order of $10^{-10}m^2/s$, while bubbles of radii of the order of $5x10^{-4}$ m experience rise velocities of the order of 0.3 m/s, due to buoyancy. This would give a ratio of the order of 10^6 for the relative rates of surfactant transport by convection and diffusion. This ratio becomes the Peclet number Pe defined as Ua/D. At these high Pe, the diffusion process occurs in a very fine boundary layer close to the surface of the bubble, whose thickness δ, scales as $aPe^{-1/2}$ for a fluid/fluid interface[30]. So δ forms the length scale for the diffusive transport of the surfactant in the bulk liquid. Hence the scale for the diffusive flux is $D\Delta C/(aPe^{-1/2})$; where ΔC as introduced above is the characteristic difference between the sublayer and bulk concentration and D is the diffusion coefficient of surfactant.

To scale the kinetic flux, we can use any of the kinetic models (see Borwankar, et al[33] for a review of adsorption models). The simplest form of the Arhenius framework which has been found to model accurately surfactant adsorption at the air/liquid surface (and in particular the polyethylene oxide surfactant used in our experiments) is the Frumkin equation. In this formulation, the activation energy for desorption is independent

of the surface coverage, and the activation energy for desorption is linear in the coverage. The surfactant kinetic exchange flux j takes the following form:

$$j = \frac{d\Gamma'}{dt} = \beta C_s(\Gamma_\infty - \Gamma') - \alpha e^{K\frac{\Gamma'}{\Gamma_\infty}}\Gamma' \qquad [1.1a]$$

where Γ' is the dimensional surface concentration, RT is the thermal energy, Γ_∞ is the maximum packing density, α and β are kinetic coefficients for desorption and adsorption, and C_s as before is the concentration of surfactant adjacent to the interface (i.e. the sublayer concentration). We also use this form since it accurately describes the adsorption kinetics of the surfactant used in our experiments. The dependence of the activation energy for desorption on the surface concentration accounts for interactions among the adsorbed molecules. For K<0, cohesive interactions between the hydrocarbon chains increase the activation energy for desorption and reduce the desorption rate. Negative values of K are restricted to be larger than –4, since phase separation occurs for more negative values of the interaction parameter, When K>0, repulsive interactions between the head groups reduce the activation energy for desorption, and increase the desorption rate. When K=0, we get the Langmuir model, in which case the j takes the following form:

$$j = \beta C_s(\Gamma_\infty - \Gamma') - \alpha\Gamma' \qquad [1.1b]$$

In this chapter, for simplicity we use the Langmuir form in all the scaling arguments for the kinetic flux that follow. The average concentration of surfactant on the surface at

steady state scales with the equilibrium concentration Γ_e. An expression for the equilibrium concentration is obtained by setting j=0 and noting the sublayer concentration is the bulk concentration C_o; thus $\Gamma_e = \Gamma_\infty[k/(1+k)]$ where $k = \beta C_o/\alpha$. The parameter k is therefore the non-dimensional bulk concentration. The maximum value of k varies with the surface activity of the surfactant and the maximum concentration at the CMC or point of insolubility; the typical range for the maximum value of k is from 1 - 10^3, cf. the table in the review article by Chang &Franses [34]. The scale for the convective flux is $\Gamma_e Ua$, where U is the terminal velocity, and a, the particle radius. Thus the ratios of the diffusive and kinetic fluxes to the convective flux is given by:

$$\Lambda_D = \frac{\text{rate of diffusion}}{\text{rate of convection}} \approx \frac{\Delta C}{C_o}\frac{\chi(1+k)}{Pe^{1/2}} \qquad [1.2a]$$

$$\Lambda_K = \frac{\text{rate of kinetic exchange}}{\text{rate of convection}} \approx Bi\left[\frac{\Delta C}{C_o} - (1+k)\frac{\Delta\Gamma'}{\Gamma_e}\right] \qquad [1.3a]$$

where $\chi=\alpha a/(\beta\Gamma_\infty)$, Pe is the Peclet number Pe=Ua/D, the characteristic rate of kinetic exchange has been obtained by linearizing j around the equilibrium surface concentration and the Biot number Bi is the desorption rate coefficient divided by the convective rate ($Bi = \alpha a / U$).

In a Frumkin formulation these ratios become

$$\Lambda_D \approx \frac{\Delta C}{C_o}\frac{\chi(e^{K\frac{\Gamma_e}{\Gamma_\infty}} + k)}{Pe^{1/2}} \qquad [1.2b]$$

$$\Lambda_K \approx Bi\left[e^{K\frac{\Gamma_e}{\Gamma_\infty}}\frac{\Delta C}{C_o}-\left(\left\{K\frac{\Gamma_e}{\Gamma_\infty}+1\right\}e^{K\frac{\Gamma_e}{\Gamma_\infty}}+k\right)\frac{\Delta\Gamma'}{\Gamma_e}\right] \qquad [1.3b]$$

Depending on these ratios of the surfactant transport processes to the hydrodynamics, the following different types of behavior are observed:

* Stagnant cap behavior when either or both of Λ_D and Λ_k $<<1$ [1-3,5-7,10,21,22,35-39],

* Uniformly retarded flow when Λ_D and Λ_k are both of order 1 [1,4,6,8,40-43], and

* Remobilization regime when Λ_D and Λ_k $>>1$ [31,32,42,43].

Stagnant Cap Regime

In the limit in which either Λ_D or Λ_K is small, the surfactant behaves as if it were insoluble; to leading order, surface convection sweeps surfactant from the front to the back end with no surface to bulk exchange. From their definitions, the limit Λ_D $<<1$ will be achieved when $\chi(1+k)/Pe^{1/2}$ $<<1$, and the limit Λ_K $<<1$ is obtained when Bi $<<1$ and Bik$<<1$. With the arguments presented in the beginning of this section, the Peclet number for transport in typical liquid systems are of the order of 10^5-10^6; χ/a is strongly dependent on the surfactant activity but ranges between 10^2-10^5 m^{-1} (see also Chang &Franses [34]). Considering typical fluid particles of radii of 10^{-4}-10^{-3} m, the parameter $\chi/Pe^{1/2}$ is therefore between 10^{-1} (for the largest radii and most strongly active surfactants) and 10^{-5} (for the smaller radii and least active surfactants). Thus at low concentrations,

k<<1, bulk diffusion limitations alone can result in the insoluble limit regime. Kinetic rate constants as we will discuss below are not well established. Values for α are in the range of 10^{-3} -10^{2} sec^{-1} depending on the surfactant; and thus kinetic limitations can also give rise to the insoluble limit as Bi ranges from 10^{-5} - 1. Hence this is the regime which is observed often in most of the physical situations.

When the surface Peclet number (Ua/D_s where D_s is the surface diffusion coefficient and is of the order of the bulk diffusion coefficient), is infinite, surfactant convected to the back end cannot diffuse back to the front. The surfactant forms a stagnant cap at the back end with zero interfacial velocity, while the front end is free of surfactant and therefore stress free. We present a detailed review of the earlier work in this limit in Chapter 2, which takes a closer look at the case of stagnant caps on rising spherical bubbles. We note here that this regime has received wide theoretical attention.

Uniformly Retarded regime

When the rates of bulk diffusion and surfactant desorption are of the same order as the interfacial convection (Λ_k and Λ_D of order one), surfactant exchanges between the bulk and the surface, and the factors affecting the Marangoni force can be identified. The non-dimensional Marangoni force, τ_m is written as,

$$\tau_m = \frac{\text{Interfacial tension gradient}}{\text{Viscous stress}} \approx \frac{1}{\mu U}\left[\frac{\partial \gamma}{\partial \Gamma'}\right]_{\Gamma_e} \Delta\Gamma' \qquad [1.4]$$

From the definitions of Λ_k and Λ_D, we get scales for ΔC and $\Delta\Gamma$ as

$$\frac{\Delta C}{C_o} \approx \frac{Pe^{1/2}}{\chi(1+k)} \qquad [1.5]$$

and

$$\frac{\Delta\Gamma'}{\Gamma'} \approx \frac{1}{Bi(1+k)} + \frac{Pe^{1/2}}{\chi(1+k)^2}. \qquad [1.6]$$

Using the fact that the derivative of the equation of state for Langmuir adsorption is:

$$\left[\frac{\partial\gamma}{\partial\Gamma'}\right]_{\Gamma_e} = -\frac{RT}{1-\frac{\Gamma_e}{\Gamma_\infty}} \qquad [1.7]$$

the retarding Marangoni force can be written as

$$\tau_m \approx Ma\left[\frac{k}{Bi(1+k)} + \frac{kPe^{1/2}}{\chi(1+k)^2}\right]. \qquad [1.8a]$$

At large k, this can be written as $\tau_m \approx Ma\left[\frac{1}{Bi} + \frac{Pe^{1/2}}{k\chi}\right]$. In a Frumkin formulation, at large k, the retarding force takes the form

$$\tau_m \approx Ma\left[\frac{1}{Bie^K} + \frac{Pe^{1/2}}{k\chi}\right] \qquad [1.8b]$$

On a clean interface, $\tau_m = 0$. τ_m being non zero in the presence of the surfactant, causes the retardation to the mobility. The bulk concentration of the surfactant k, and the relative rates of kinetic exchange to surface convection, in the form of Bi, affect this mobility.

Consider the case in which kinetics is fast and bulk diffusion controls the Marangoni gradient ($\frac{\chi(1+k)}{Pe^{1/2}} \approx 1$, $Bi >> \frac{\chi(1+k)}{Pe^{1/2}}$ or $Bi >> 1$). In this regime, the surface and sublayer are in equilibrium as given by the adsorption isotherm ($\frac{\Delta\Gamma'}{\Gamma_e} \approx \frac{\Delta C}{C_o(1+k)}$, and the bulk diffusion gradients allow for the exchange of surfactant between the bulk and the surface. Early studies [1,4,8,40] have examined the case of large Peclet number (since this is the technologically relevant case for buoyancy driven motion in water for particles a millimeter and above in diameter), and used a boundary layer analysis to describe the diffusive flux, while Harper[6] studied for negligible inertia and spherical particles, and Andrews, et al[41] for a deformed particle at order one Reynolds number.

The first studies in the direction of solving the convective diffusion directly have been that of Holbrook & Levan [3] and Levan & Newman[7] for the case of linear adsorption and a spherical particle in the absence of inertial effects. For linear adsorption and infinite kinetic exchange ($Bi >> 1$), the terminal velocity depends on Pe, χ and kMa($\chi = 1/K$ and $kMa = 1/Eo$, respectively, in the notation of Holbrook[3]).This study finds that as Eo decreases the terminal velocity decreases as the surface becomes more retarded. On the basis of the scaling arguments given above for the retarding stress. For fast kinetics ($Bi >> 1$), the non-dimensional Marangoni stress $\tau_m \approx Ma\left[\frac{kPe^{1/2}}{\chi(1+k)^2}\right]$ and at

$k<<1$, τ_m scales with k. This explains Levan's result of the decrease in terminal velocity with increasing k (decreasing Eo) for $k<<1$.

Now consider the case when both the bulk diffusion and kinetics controls the transport($Bi\approx 1$; $\frac{\chi(1+k)}{Pe^{1/2}}\approx 1$). Holbrook [3] has studied this kinetically controlled regime in the absence of fluid inertia and for a spherical fluid particle for low concentration ($k<<1$). This study demonstrates that at fixed Bi as k increases (through the decrease in his Eotovos number ($Eo=1/(kMa)$, the only dimensionless group the concentration appears), the terminal velocity decreases. The scaling framework detailed above demonstrates why this is the case: In the kinetically controlled regime, with Λ_K order one, $\Delta\Gamma' \approx \frac{k\Gamma_\infty}{Bi(1+k)^2}$ and hence the non-dimensional retarding force is $Ma\frac{k}{(1+k)}$. In the linear regime ($k<<1$), the Marangoni retardation increases linearly with k because the adsorption and hence $\Delta\Gamma'$ increase with k, and $\left[\frac{\partial\gamma}{\partial\Gamma'}\right]_{\Gamma_e}$ is of order one for small k.

The early experimental studies of the effect of surfactants on the motion of the bubbles and drops have been those of Savic[35], Garner & Skelland[12], Elzinga & Banchero[11], Griffith[10], and Horton et al[44] who studied drops. They observed the reduction of interfacial mobility and diminishment and shift (to the leading pole) of the circulation vortex in the drop with surfactant present in the system. Systematic and more

quantitative studies of the effect of the bulk concentration of the surfactant on the terminal velocity have been the measurements of Edge & Grant[13] of the velocity of dichloroethane drops in water with sodium lauryl sulfate as the surfactant, and later the measurements of Yamamoto & Ishii[45] of the rise velocities of air bubbles in water again with sodium lauryl sulfate, and of Bel Fdhila & Duineveld[46] of air bubble velocities in water with Triton X-100, Brij 30 and sodium dodecyl sulfate as surfactants. All these studies investigate bubbles or drops of the order of 0.1-1cm. Because of the low viscosity of water, the bubbles or drops are deformed and terminal velocities are of the order of 10 cm s^{-1}. Measurements have been made of the terminal velocity as a function of the increasing bulk concentrations of the surfactant, at concentrations below the point where micellar aggregates form in the bulk. All studies show a decrease in velocity, with the expanded studies of Edge & Grant[13] and Bel Fdhila & Duineveld[46] demonstrating that at high enough concentrations the velocity becomes constant with increasing concentrations. While in the studies done at low bulk surfactant concentrations, the diffusive limitations are not overcome ($\Lambda_D << 1$), the ones at high concentrations[13,46] have kinetic limitations ($\Lambda_k << 1$ or $\Lambda_k \approx 1$). Hence all of them lead to the surfactant induced retarded regime.

1.3.2 Surface Remobilization

Having seen the retarding effect of the surfactant, we now look into the conditions when the surfactant can remobilize the interface. This would mean bringing back the interface back to its original stress state when there was no surfactant.

First consider the case of negligible surface to bulk exchange. If finite values of the surface Peclet number are considered, surfactant convected to the rear can diffuse to the front end of the drop, thereby creating a steady state in which convection balances surface diffusion and surfactant is spread everywhere on the surface with nonzero interfacial velocity. Holbrook[2] (for negligible inertia and a spherical geometry), and Leppinen, et al[47,48] (for order one Reynolds number and fluid particle deformation) have obtained solutions for the drag and interfacial velocity as a function of the surface Peclet number for buoyancy driven motion. Kim & Subramanian[22] have examined the insoluble limit for finite Pe_s for thermocapillary driven motion. All simulations demonstrate that as Pe_s decreases (for the rest of the system parameters fixed), surface diffusion reduces the concentration gradient created by the convection, the interfacial velocity is increased and the drag is reduced. As $Pe_s \rightarrow 0$, the Marangoni force disappears entirely as the surface concentration becomes uniform, and the drag is that of a fluid particle with uniform tension. While decreasing the surface Peclet number allows for a reduction in the Marangoni force, values for the surface Peclet numbers are of the order of 10^5 (for buoyancy driven motion) and of the order of $1\text{-}10^4$(for thermocapillary motion

of bubbles of radii 10^{-3} -10^{-1} cm with corresponding thermocapillary velocities in the range 10^{-3} –10^{-1}cm/sec), and therefore are probably too larger to effectively remobilize the interface.

In the case of Λ_k and Λ_D =O(1), equation [1.8] for the non dimensional Marangoni force shows that, if the surfactant is present such that when

* k>>1 (high bulk concentration)

* kBi>>1 and Bi >>1 (rapid kinetic exchange relative to convection)

  (kBi>>1 and Bie^K>>1 in Frumkin Formulation)

* $\frac{\chi k}{Pe^{1/2}} >> 1$ (rapid diffusive exchange relative to convection)

then the retarding force, τ_m due to the presence of surfactant in the continuous phase goes to zero and the paradigm of remobilization is reached when the surfactant laden interface behaves stress free like a surfactant free interface.

When the kinetic exchange resistance is completely eliminated (Bi—>∞), the non-dimensional Marangoni force, $\tau_m \approx Ma\frac{kPe^{1/2}}{\chi(1+k)^2}$. Thus in the limit of large k, the retardation scales as $Pe^{1/2}/(k\chi)$, and as the concentration increases and exceeds $Pe^{1/2}/\chi$, the retardation should disappear. In the limit of large k, the surface saturates and the concentration difference, which scales as $\Delta C \approx \frac{Pe^{1/2}}{\chi(1+k)}C_o \approx \frac{\Gamma_\infty}{R}\frac{kPe^{1/2}}{(1+k)}$, is constant with

the difference relative to C_o tending to zero. The surface concentration difference described by quasi-equilibrium ($\frac{\Delta\Gamma'}{\Gamma_e} \approx \frac{\Delta C}{C_o(1+k)}$ or $\Delta\Gamma' \approx \frac{k\Gamma_\infty Pe^{1/2}}{\chi(1+k)^3}$) then scales as $1/k^2$ reflecting the fact that the isotherm becomes flat ($\Delta\Gamma'/\Delta C \rightarrow 0$ as $1/k^2$) at high bulk concentration near saturation. Although from the equation of state $\left[\frac{\partial\gamma}{\partial\Gamma'}\right]_{\Gamma_e}$ scales as $1/k$ at saturation, since the concentration difference scales as $1/k^2$ the retarding force decreases as $1/k$ overcoming the fact that the surface becomes more incompressible. Unlike the first case of having $Pe_s \rightarrow 0$ for remobilization, this is more realistic, as the diffusion limitations could be removed by using the surfactant at high bulk concentrations and the kinetic limitations, by choosing a surfactant with rapid kinetic exchange.

The theoretical studies of Wang, et al[31,32] in the regime of diffusion limited surfactant transport and high kinetic rates ($Bi \gg 1$), have shown that with increasing surfactant bulk concentration, the drag coefficient for the bubble initially increases from a stress-free value, reaches a maximum and starts decreasing, eventually reaching the same stress-free value at large k. This behavior is observed for zero and order one Reynolds number. The higher the Pe, the higher the k found to remobilize, in consistent with the arguments presented. All these simulations were done for $Pe < 100$, which is far below the Pe encountered in real systems with surfactants (10^5-10^6). We note that at these lower Peclet numbers studied, the condition for eliminating diffusive limitations to surfactant

transport is $\frac{\chi k}{Pe} >> 1$ rather than $\frac{\chi k}{Pe^{1/2}} >> 1$ valid at high Peclet numbers due to the formation of the concentration boundary layer.

In the studies of Chen & Stebe[42,43] (for buoyancy and thermocapillary motions respectively), for the case of kinetic control at high bulk concentrations, it has been shown that for increasing k at a fixed Bi, the terminal velocity tends to a limiting value (less than the clean interface velocity) as k becomes large (This is in line with the scales presented for the retarding force in equation [1.8a] where τ_m—>1/Bi at large k). This behavior at large k results from the fact that although $\Delta\Gamma'$ decreases as 1/k with increasing k (see the scaling above), the tension gradient $\left[\frac{\partial\gamma}{\partial\Gamma'}\right]_{\Gamma_e}$ increases as 1/k as the surface becomes more incompressible. As Bi increases, this limiting value tends to the clean value, as is clear from the scaling. Thus we can expect from these kinetic studies that, for sufficiently fast kinetics (Bi large enough), the interface will remobilize at large enough bulk concentration.

Eventhough the above studies[42,43 32] theoretically show the possibility of remobilization, the only available experimental evidence is that of Stebe, et al[24]. These authors study a three-phase periodic slug flow in a capillary tube in which a train of alternating air and aqueous segments (containing the surfactant Triton X-100 or Brij 35) ride on an annular wetting film of fluorocarbon oil. The surfactant adsorbs onto the

oil/aqueous interface, where it is convected to the trailing edge of the slug. Slug velocities are of the order of $1 cms^{-1}$ and the viscosity of the oil was $5 gcm^{-1}s^{-1}$. At low concentrations of the surfactant the pressure required to drive the slug train at a constant velocity is found to increase with the bulk concentration. However at high concentrations the pressure relaxes, indicating remobilization. In this case, the slower velocity of the slugs, and the higher viscosity of the oil allow diffusion to outscale convection and remobilize the surface.

An important outcome of this study is the effect of this remobilizing surfactant in the presence of an already existing impurity in the system. Since the remobilizing surfactant should have faster kinetics and should be present at higher concentrations, it would reach the interface preferentially than any trace amount of surface-active impurity present in the bulk. So the retarding effect of the impurity will not be felt by the interfacial hydrodynamics, and the system would behave 'like a pure system fluid mechanically'. These ideas have been verified in the experimental studies of Stebe, et al[25] for the same three-phase periodic slug flow. Here the remobilization of the air/liquid interface is observed with increasing bulk concentration of Triton X-100, even in the presence of a surfactant BSA, which by itself does not remobilize.

In these experiments, the aqueous/oil interface mobility is inversely related to the pressure drop across an aqueous slug moving at a constant velocity in a capillary tube.

This mobility decreases initially with surfactant concentration and increases eventually at higher concentrations of the surfactant. The pressure drop (Δp) across a slug in a capillary tube scales as $\gamma^{1/3}$ (where γ is the interfacial tension). Hence with increasing surfactant concentrations, as γ decreases, one would expect a decrease in Δp. But because of the Marangoni stresses developed, Δp initially increases with increasing surfactant concentrations. As per the arguments presented before for remobilization, at higher surfactant concentrations when the Marangoni stresses become negligible, the Δp again scales as $\gamma^{1/3}$. Such qualitative arguments for these experimental results support the idea of remobilization. But with the addition of surfactant, as the surface tension decreases, the deformability of the slug increases. This would increase the Δp. The pressure drop measured would have a contribution from this along with the Marangoni force. The effect of the Marangoni force term could be singled out only from the complete modeling of the fluid mechanics problem. Such analysis would only verify if the air/liquid interface is indeed remobilized. This problem of three-phase flow in capillary tubes with the surfactant being able to go into both the oil and the aqueous phases is difficult to model. Hence these experiments as such could provide an indirect evidence of the phenomenon of remobilization. As stated before, the problem of a bubble rising in a liquid provides an ideal test case where we can single out the effect of Marangoni forces due to the added surfactant. In this case the drag on the bubble depends only on the Marangoni forces and

not on the interfacial tension between dispersed and the continuous phase. Explicit experimental verification of surface remobilization brought out by surfactants with this ideal test case is the central point of our research.

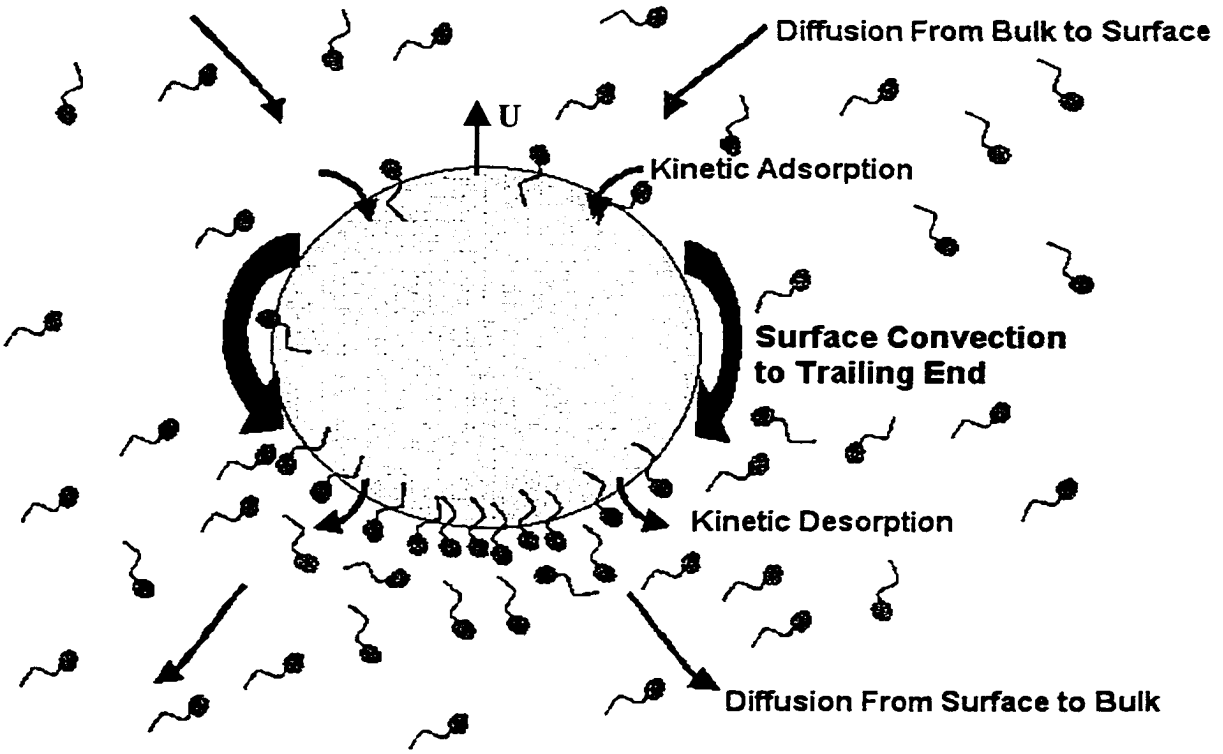

Figure 1.1: Surfactant distribution and transport processes on the surface of a bubble translating upwards.

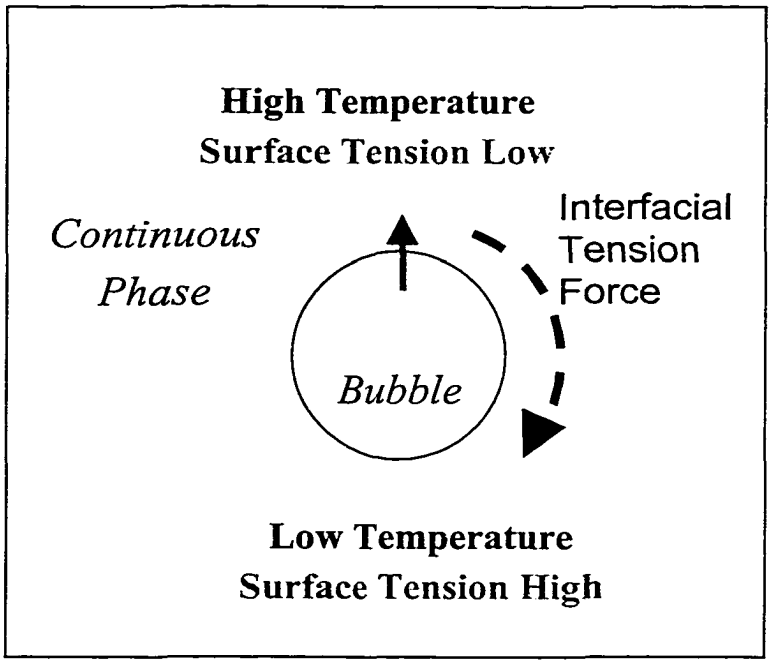

Figure 1.2a: Thermocapillary Motion. With no surface-active materials in the continuous phase, large tension difference between poles creates large thermocapillary velocity.

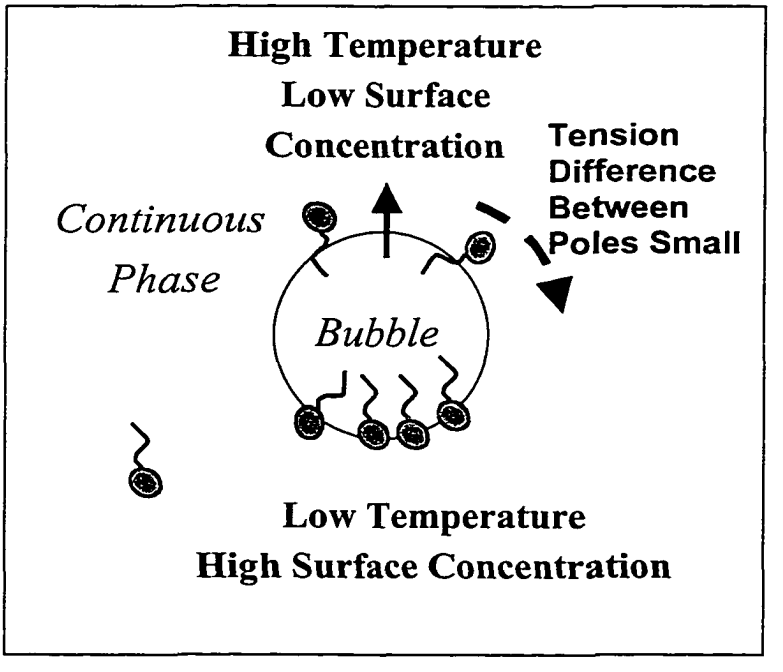

Figure 1.2b: Thermocapillary Motion in the presence of a surfactant impurity in the continuous phase. Surfactant swept to the trailing pole reduces the tension, hence the surface tension gradient created by the applied temperature gradient is reduced. This reduces the thermocapillary velocities.

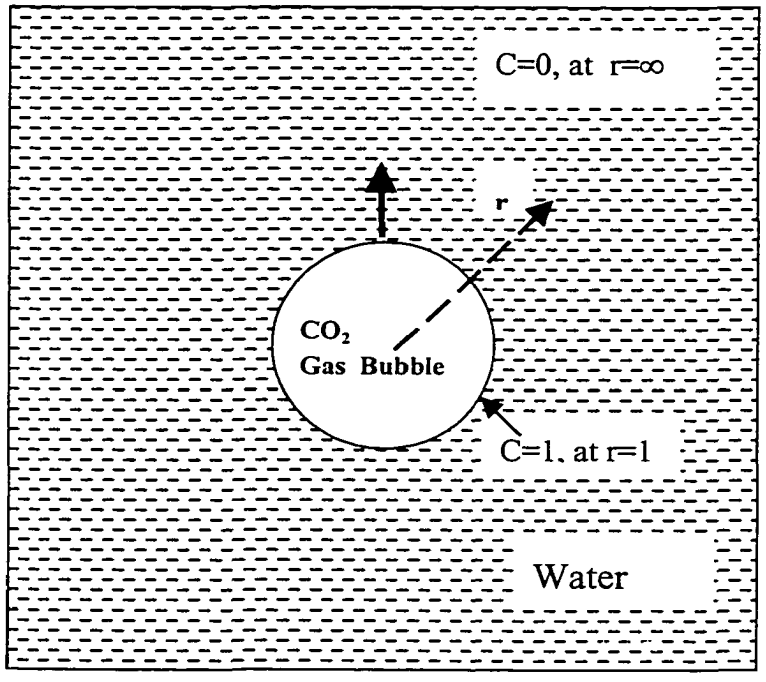

Figure 1.3: Interphase Mass Transfer - CO_2 bubble dissolving in Water.

CHAPTER 2
Theory on the Stagnant Cap Regime in the Motion of a Bubble with an Adsorbed Surfactant Monolayer

2.1 Introduction

As mentioned in Chapter 1, bubble motion in liquids, like other interfacial flows, is greatly influenced by the surfactants present in the bulk phase. When a bubble rises in an infinite liquid containing surfactant, the transport rates of surfactant from (to) the bulk to (from) the bubble surface (both by bulk diffusion and kinetic exchange at the interface) relative to the surface convection, creates a surface concentration gradient of the surfactant on the bubble surface. This creates surface stresses increasing the drag on the rising bubble from that of a stress free clean interface value. Even trace amount of surfactants can immobilize the surface of a rising bubble, and reduce its rise velocity (and hence increase the drag on it) to that of a solid like value.

In this chapter, we study the effect of a trace amount of surfactant present in the continuous phase on the motion of a bubble, in relation to the transport properties of the surfactant. When the surfactant is present in trace amounts, the stagnant cap behavior is observed. Here all the surfactant adsorbed on the bubble collects in the form of a stagnant cap at the rear end, giving a semi-solid like behavior for the bubble. This regime is the focus of our study in this chapter.

From the description in Chapter 1 of the surfactant transport processes occurring on the surface of a bubble moving with velocity U in a static liquid containing the surfactant, we note that the scale for the diffusive flux of the surfactant from the bulk is $D\Delta C/(aPe^{-1/2})$. Here ΔC as introduced above is the characteristic difference between the sublayer and bulk concentration and D is the diffusion coefficient of surfactant. Here Pe is the Peclet number (Ua/D) characterizing the relative rates of bulk convection to bulk diffusion of the surfactant which is typically very high ($\sim 10^6$).

Assuming a Langmuir type kinetics for the surfactant at the air liquid interface, the kinetic exchange rate per unit area of the interface is $\left\{\left(\beta C_o + \alpha\right)\Delta\Gamma' + \beta(\Gamma_\infty - \Gamma_e)\Delta C\right\}$. Here Γ_e is the equilibrium surface concentration at the bulk concentration C_0; Γ_∞ is the maximum packing density; α and β are kinetic coefficients for desorption and adsorption; and $\Delta\Gamma'$ is the difference in the surface concentration from the front and the back end of the bubble. The scale for the convective flux is $\Gamma_e Ua$, where U is the terminal velocity, and a, the particle radius. Thus the ratios of the diffusive and kinetic fluxes to the convective flux is given by:

$$\Lambda_D = \frac{\text{rate of diffusion}}{\text{rate of convection}} \approx \frac{\Delta C}{C_o}\frac{\chi(1+k)}{Pe^{1/2}}$$

$$\Lambda_K = \frac{\text{rate of kinetic exchange}}{\text{rate of convection}} \approx Bi\left[\frac{\Delta C}{C_o} - \left(1+k\right)\frac{\Delta\Gamma'}{\Gamma_e}\right]$$

where $\chi=\alpha a/(\beta\Gamma_\infty)$ is the non dimensional adsorption depth of the surfactant, $k = \beta C_o/\alpha$, is a measure of the bulk concentration. and the Biot number Bi is the desorption rate coefficient divided by the convective rate ($Bi = \alpha a / U$).

The stagnant cap behavior is observed when either or both of Λ_D and Λ_k <<1 [1-3,5-7,10,21,22,35-39].In the limit in which either Λ_D or Λ_K is small, the surfactant behaves as if it were insoluble; to leading order, surface convection sweeps surfactant from the front to the back end with no surface to bulk exchange. From their definitions, the limit Λ_D <<1 will be achieved when $\frac{\chi(1+k)}{Pe^{1/2}} << 1$, and the limit Λ_K<<1 is obtained when $Bi << 1$ and Bik<<1. χ/a is strongly dependent on the surfactant activity but ranges between 10^2-10^5 m^{-1} (see also Chang & Franses[34]). For fluid particles of radii of 10^{-4}-10^{-3} m, with the large Peclet number (of the order of 10^6), the parameter $\chi/Pe^{1/2}$ is therefore between 10^{-1} (for the largest radii and most strongly active surfactants) and 10^{-5} (for the smaller radii and least active surfactants). Thus at low concentrations, k<<1, bulk diffusion limitations alone can result in the insoluble limit regime. Values for α are in the range of 10^{-3} -10^2 sec^{-1} depending on the surfactant; and thus kinetic limitations can also give rise to the insoluble limit as Bi ranges from 10^{-5} - 1. Hence this is the regime which is observed often in most of the physical situations.

When the surface Peclet number (Ua/D_s where D_s is the surface diffusion coefficient and is of the order of the bulk diffusion coefficient) is infinite, surfactant convected to the back end cannot diffuse back to the front, as shown in Figure 2.1. The surfactant forms a stagnant cap at the back end with zero interfacial velocity, while the front end is free of surfactant and therefore stress free. The size of the stagnant cap is characterized by a cap angle ϕ measured from the rear stagnation pole. The particular case of rapid kinetic exchange rates i.e., $Bi \to \infty$, and $\frac{\chi(1+k)}{Pe^{1/2}} << 1$ has been widely studied. For the case in which the inertia of the continuos and fluid particle phases (if the particle is a liquid) are negligible (small Re), the fluid particle is a sphere, and buoyancy drives the motion, Savic[35], Griffith[10], Harper[5] (for small cap angles), Davis & Acrivos[36], Holbrook & Levan[2], Sadhal & Johnson[37] and He, et al[38] solve the creeping flow equations to obtain the drag as a function of the cap angle. The size of the cap as a function of the bulk concentration $\phi(k)$ is obtained by an overall surfactant mass balance which requires that the net flux of surfactant to the surface equal zero at steady state[5,38]. Kim and Subramanian[21] study the analogous problem of stagnant caps formed in thermocapillary driven motion. McLaughlin[49] and Bel Fdhila & Duineveld[46] extend these studies for buoyancy driven bubble flows in water in which the fluid inertia is not negligible, and demonstrated the formation of a wake at the trailing edge due to the

stagnant cap. The experimental measurement of bubble rise velocities in tap water and filtered water by Haberman and Morton[9], shows the case of stagnant cap behavior of the bubbles. The simulations of Mclaughlin[49] support this conclusion. All these studies demonstrate that in the insoluble limit, the cap angle increases rapidly with k and only small concentrations of surfactants ($k<<1$) are necessary to completely immobilize the surface.

The more complete theoretical work taking into account finite rates of both kinetic exchange and diffusive transport of the surfactant has been that of Cuenot, et al [39]. They solve the full convection diffusion equation for the transport of the surfactant with a Langmuir type adsorption isotherm and examines the case of large bulk and surface Peclet numbers ($5x10^4$) at low bulk concentrations ($k=0.112$ and 0.0112) of surfactants with χ equal to 5 or 50, and hence $\frac{\chi(1+k)}{Pe^{1/2}} << 1$. The simulations done for slow kinetic exchange ($Bi<<1$, and $kBi<<1$) illustrate a stagnant cap behavior for bubbles and confirm the formation of wake at order one Reynolds number as noted by Bel Fdhila, et al [46] and McLaughlin[49].

In the present work we would like to study the effect of surfactant transport rates, the diffusion in the bulk and the kinetic exchange at the interface, on the drag of a rising spherical bubble in the stagnant cap regime. In this chapter here we present an exact theory for this problem. In Section 2.2, we first formulate the model problem for the flow

past a spherical bubble rising in a surfactant solution. Next in Section 2.3 we present our approach in solving the governing equations for the hydrodynamics and surfactant transport taking care of the finite rates of transport of the surfactant by diffusion in the bulk and kinetic exchange at the interface. In Section 2.4, we discuss the results of our simulations, studying the effect of various parameters. Finally we present our conclusions in Section 2.5. In Chapter 3, we discuss our experimental study on measuring the drag on a air bubble rising in a liquid (70:30 glycerol-water mixture) containing a poly-ethoxylate surfactant ($C_{12}E_6$). For this model system we discuss how our simulations could describe our experiments.

2.2 Model Formulation

Consider a spherical bubble of radius a, moving steadily and axisymmetrically (in the positive x direction) with velocity U due to buoyancy in a continuous phase containing surfactant. We undertake the analysis in a spherical coordinate system fixed to the bubble with the center of the spherical system co-incident with the bubble center, and the spherical angle θ taken from the negative x direction (Figure 2.2). In this moving reference system, the bubble interface is fixed, and the flow far from the bubble is in the positive x direction. The viscosity, density and surface tension of the continuous phase are denoted by μ, ρ and γ respectively. The continuous phase contains surfactant with a bulk concentration (far from the bubble surface) equal to C_0. The assumption of the

bubble being spherical is reasonable if both the inertial and viscous forces are small compared to surface tension forces (i.e., the Weber Number, $We=\rho U^2 a/\gamma$ and the Capillary number, $Ca=\mu U/\gamma$ are small i.e., say < 0.01).

The flow around the bubble is described by the full incompressible Navier-Stokes equations and the surfactant transport equation. In nondimensional form these equations are:

$$Re(\frac{\partial \mathbf{V}}{\partial t} + \mathbf{V}.\nabla\mathbf{V}) = -\nabla P + \nabla^2\mathbf{V} \qquad [2.1]$$

$$\nabla.\mathbf{V} = 0 \qquad [2.2]$$

$$\frac{\partial C}{\partial t} + \mathbf{V}.\nabla C = \frac{1}{Pe}\nabla^2 C \qquad [2.3]$$

Here: the length scale, the velocity **V**, concentration C, and pressure P are non-dimensionalized with the radius of the bubble a, the free stream velocity U, bulk concentration C_0, and $\mu U/a$ respectively; u and v are the radial and azimuthal components of the velocity **V**; Reynolds number $Re=Ua\rho/\mu$ and Peclet number $Pe=Ua/D$, D being the diffusion coefficient of the surfactant in the liquid. Although we are interested in steady state, we formulate the full unsteadily problem for purposes of the numerical solution (see below).

At the surface of the bubble, the normal (r component) of velocity is equal to zero. The presence of surfactant creates a surface tension gradient and causes a force on

the bubble surface that must be compensated by a viscous tangential stress on the interface. This is expressed as

$$\text{at } r=1,\ \frac{1}{r}\frac{\partial \gamma}{\partial \theta}=\frac{1}{r}\frac{\partial \gamma}{\partial \Gamma'}\frac{\partial \Gamma'}{\partial \theta}=-\frac{\mu U}{a}\tau_{r\theta} \qquad [2.4]$$

where $\tau_{r\theta}$ is the dimensionless shear stress, and γ is the surface tension. To model the surfactant adsorption, Frumkin kinetics will be used since this scheme very satisfactorily describes the adsorption kinetics of the polyethylene oxide surfactant adsorbing at the air/glycerol-water bubble interface in the experiments. The equation of state for this kinetic scheme is given by

$$\gamma=\gamma_c+RT\Gamma_\infty\left[\ln(1-\Gamma)-\frac{K}{2}\Gamma^2\right] \qquad [2.5]$$

from which the boundary condition on the surface of the bubble becomes,

$$\tau_{r\theta}\,|_{r=1}=r\frac{\partial}{\partial r}\left(\frac{v}{r}\right)|_{r=1}=Ma\left[\frac{1}{1-\Gamma}+K\Gamma\right]\frac{\partial \Gamma}{\partial \theta} \qquad [2.6]$$

where Γ is the surface concentration Γ' non-dimensionalized by the maximum packing density of surfactant Γ_∞, $Ma=RT\Gamma_\infty/\mu U$, is the Marangoni number, R is the gas constant, T is the temperature, and K is a (non-dimensional) parameter accounting for a linear variation of the activation energy for desorption on Γ(K=0 gives the Langmuir type kinetics). The Marangoni number is a measure of the forces due to surface tension gradients relative to the viscous forces.

The surfactant distribution on the bubble is computed from the surface mass balance. Surfactant transport into the air space of the bubble is neglected. Under these conditions, the balance equation for the interfacial concentration of a surfactant having a negligible surface diffusivity and with kinetics described by the Frumkin scheme can be written as:

$$\frac{\partial \Gamma}{\partial t} + \nabla_s(\Gamma V_s) = \frac{1}{Pe_s}\nabla_s^2\Gamma + Bi\left[kC|_{r=1}(1-\Gamma) - e^{K\Gamma}\Gamma\right] \qquad [2.7]$$

$$Bi\left[kC|_{r=1}(1-\Gamma) - e^{K\Gamma}\Gamma\right] = \frac{\chi k}{Pe}\frac{\partial C}{\partial r}|_{r=1} \qquad [2.8]$$

Here V_s is the azimuthal component of the velocity $\mathbf{V}$ on the surface of the bubble, $\chi=a\alpha/\beta\Gamma_\infty$, $Pe_S=Ua/D_S$ is the surface Peclet number which is assumed to be the same order as the bulk Peclet number in this work all through, and $k=\beta C_0/\alpha$ is the measure of bulk concentration (α and β are the (Frumkin) desorption and adsorption rate constants respectively, $Bi=\alpha a/U$, the Biot number is the ratio of the rate of kinetic exchange of the surfactant at the gas/liquid interface to the rate at which it is convected from the front end to the rear end due to the bulk flow.

At infinity the boundary conditions for the flow match with free stream values.

$$r=\infty,\ \mathbf{V} = u\mathbf{e}_r + v\mathbf{e}_\theta = \mathbf{e}_x \text{ gives } u = -\cos\theta; \text{ and } v = \sin\theta; \qquad [2.9]$$

For the concentration of the surfactant, since the convection term dominates, the boundary condition at $r=\infty$, is treated in a different way. In the computational domain for our simulations, shown in the Figure 2.2, at the inlet boundary where the flow enters the

computational domain, the concentration takes the free stream value. At the boundary of the outflow region, which is arbitrarily fixed for $\pi/2<\theta<\pi$, the concentration is treated as a parabolic variable in the flow direction. Mathematically this translates to,

At the inlet ($0<\theta<\pi/2$) $C=1,$ [2.10a]

At the outlet ($\pi/2<\theta<\pi$) $$\frac{\partial C}{\partial x}=0$$ [2.10b]

On the symmetry axis, ($\theta=0, \pi$) $$\frac{\partial u}{\partial \theta}=0, \quad v=0, \quad \frac{\partial C}{\partial \theta}=0$$ [2.10c]

The Stagnant Cap Regime

In Frumkin type kinetics, the effective surfactant bulk concentration is $ke^{-K\Gamma}$ while the effective Biot number becomes $Bie^{K\Gamma}$. In the limits $Pe_s >>1$ and either $Bie^{K\Gamma}<<1$ and $Bik<<1$ or $\frac{\chi(e^{K\Gamma}+k)}{Pe^{1/2}}<<1$, which are satisfied at low concentrations of the surfactant, the diffusive transport to the interface and the kinetic exchange at the interface are much slower than the convective transport along the surface. In this case, the in the balance equation [2.7] for Γ, the advective term vanishes when steady state conditions are reached[35]. Then [2.7] reduces to

$$\frac{1}{\sin\theta}\frac{\partial}{\partial\theta}\left(\Gamma V_s \sin\theta\right)=0 \qquad [2.11]$$

Applying the boundary conditions of zero fluxes at the stagnation points then leads to

$$\Gamma U_s = 0 \qquad [2.12]$$

This shows that the interface contains essentially two different regions. Between the front stagnation point and the cap, the interface is free of surfactant. Thus according to the equation [2.4], this part is subjected to stress free boundary condition, i.e.,

$$0 < \theta < \pi - \phi \quad \begin{Bmatrix} v(r=1,\theta) \neq 0 \\ \tau_{r\theta}(r=1,\theta) = 0 \\ \Gamma(\theta) = 0 \end{Bmatrix} \qquad [2.13a]$$

In contrast, in the stagnant cap at the back end of the bubble, as per [2.12] the surface velocity is zero.

$$\pi - \phi < \theta < \pi \quad \begin{Bmatrix} v(r=1,\theta) = 0 \\ \tau_{r\theta}(r=1,\theta) = \tau_s(\theta;\phi) \neq 0 \\ \Gamma(\theta) \neq 0 \end{Bmatrix} \qquad [2.13b]$$

Equations [2.13 a & b] form the boundary conditions on the surface of the bubble for the hydrodynamics in this regime. The drag on a bubble is evaluated as

$$C_D = \int_0^{\pi} \left[\left(-P\cos\theta + \tau_{rr}\cos\theta - \tau_{r\theta}\sin\theta \right) r^2 \right]_{r=1} \sin\theta \, d\theta \qquad [2.14]$$

where $\tau_{rr} = 2\dfrac{\partial u}{\partial r}$ and $\tau_{r\theta} = \left[\dfrac{\partial}{\partial r}\left(\dfrac{v}{r}\right) + \dfrac{1}{r}\dfrac{\partial u}{\partial \theta} \right]$.

Here the drag is non-dimensionalized by the viscous force $2\pi\mu a$. In creeping flow limit, C_D takes a value of 2 for flow past a spherical bubble while a value of 3 for flow past a solid sphere.

2.3 Numerical Solution

The flow past a spherical bubble has been a very well studied problem numerically [27,32,46,50-53] both for small and order one Reynolds numbers. For the solution, one can use either the vorticity-stream function formulation [32,46,50] or the primitive variable approach [27,51]. Peyret & Taylor [54] provide an excellent review of these methods. For numerical integration, the governing equations could be discretized using either of the finite difference, finite element or the finite volume techniques. For the spherical bubble, since the numerical domain is not complex, the simple finite difference technique itself could do a good job. The finite volume based approach is adopted in the present work as the discretization developed by this approach would certainly have the conservative property for the scalar whose equation is being discretized, and hence physically making sense. Patankar [55] provides the details of this kind of formulation. Regarding the type of mesh needed for the numerical method, one can use either the same grid points for all the variables involved, the velocities u, v, pressure P, and the concentration C (non-staggered grid) or a staggered grid for different variables. For a primitive variable formulation, it is more advantageous to use the staggered mesh as we describe later.

The literature for the solution to the incompressible Navier-Stokes equations in primitive variables is extensive. Tannehill, et al [56], Peyret & Taylor [54] provide a good description of the various methods. Broadly they fall in two categories. In the first, called

the coupled approach, the discretized conservation equations are solved, treating all the dependent variables u, v, and P as simultaneous unknowns. In the second approach, called the pressure correction approach, the momentum equations are solved for the velocity components without coupling to the pressure, and hence without using the continuity equation. From the continuity equation a Poisson equation is developed for the pressure, or changes in pressure, that will alter the velocity field in a direction so as to satisfy the continuity equation. In our work we use a version of the second approach, the details of which are described later. In the following lines we highlight the salient features of our numerical algorithm.

2.3.1 Spatial Approximations and Time Advancement

A finite volume method is employed to discretize the unsteady governing equations for the momentum [2.1] and [2.2] and the bulk surfactant transport [2.3]. A staggered mesh as shown in Figure 2.3. is employed. The momentum equations are solved in the primitive variables, i.e., velocity pressure variables. The advective and diffusive terms in both the momentum equations and the surfactant transport equation are discretized using a hybrid scheme[55]. This type of upwinding scheme works well over larger ratios of magnitudes of convective terms relative to diffusive terms in a convective diffusive equation(please refer to Patankar for details). The usage of this scheme

becomes even more important for the surfactant transport equation, where the advection terms far dominate the diffusive terms (Pe~10^6).

The discretization for the momentum equation is described here as an example. The momentum equation when written in the conservative form becomes

$$\frac{\partial \mathbf{V}}{\partial t} + \nabla.(\mathbf{VV} - \frac{1}{\mathrm{Re}}\nabla\mathbf{V}) + \frac{1}{\mathrm{Re}}\nabla P = 0, \qquad [2.15]$$

In solving this equations numerically, the nonlinear term is linearized, and then at any time t the governing equations in the r and θ directions take the form,

$$\frac{\partial u}{\partial t} + \nabla.(\mathbf{V}'u - \frac{1}{\mathrm{Re}}\nabla u) + \frac{1}{\mathrm{Re}}\frac{\partial P}{\partial r} = 0$$
$$\frac{\partial v}{\partial t} + \nabla.(\mathbf{V}'v - \frac{1}{\mathrm{Re}}\nabla v) + \frac{1}{\mathrm{Re}}\frac{1}{r}\frac{\partial P}{\partial \theta} = 0$$

Here $\mathbf{V}' = u'\mathbf{e}_r + v'\mathbf{e}_\theta$ is the velocity field evaluated at the previous time step. Then the governing equations for u, v, and C which are of the form

$$\frac{\partial f}{\partial t} + \nabla.(\mathbf{V}f - b\nabla f) + g(r,\theta) = 0 \qquad [2.16]$$

are first written at the corresponding nodes of the staggered mesh, then integrated as shown below over the corresponding control volumes.

$$\int \{\frac{\partial f}{\partial t} + \nabla.(f\mathbf{V}' - b\nabla f) + g(r,\theta)\}d\vartheta = 0$$

$$\frac{f - f'}{\Delta t}\Delta\vartheta + (fu - b\frac{\partial f}{\partial r})dA_e - (fu - b\frac{\partial f}{\partial r})dA_w + (fv - b\frac{\partial f}{r\partial\theta})dA_n - (fv - b\frac{\partial f}{r\partial\theta})dA_s + g(r,\theta)\Delta\vartheta = 0$$

.....[2.17]

Here dA_i is the area of the face i of the control volume of volume $\Delta\vartheta$. When the above algorithm for discretization is used for the momentum equations on a staggered mesh, the pressure difference between two adjacent grid points would become the natural driving force for the velocity component located between these grid points. Also, the discretized continuity equation would contain the adjacent velocity components, rather than the components at the alternate grid points as in a non-staggered mesh. Consequently, problems associated with a non-staggered mesh: wavy pressure fields being felt as uniform pressure fields, and a wavy velocity field satisfying the continuity equation; could be avoided using even a coarser mesh.

Specifically for the solution of the momentum equations, a projection method [57] is used as described briefly here. Time advancement by Δt from time n to $n+1$ is achieved in two steps.

1) In the first half, the momentum equations are considered without the pressure gradient term.

$$\frac{\mathbf{V}^* - \mathbf{V}^n}{\Delta t / 2} + \nabla.(\mathbf{V}^n\mathbf{V}^* - \frac{1}{\mathrm{Re}}\nabla\mathbf{V}^*) = 0$$

Here $\mathbf{V}^*$ is the intermediate velocity

2) The pressure gradient term is considered only in the second half. The pressure at time $n+1$, P^{n+1} is calculated from the fact that the velocity at time $n+1$, $\mathbf{V}^{n+1}$ is divergence free.

$$\frac{\mathbf{V}^{n+1}-\mathbf{V}^{*}}{\Delta t/2}+\frac{1}{Re}\nabla P^{n+1}=0$$

$$\nabla.\mathbf{V}^{n+1}=0 \Rightarrow \nabla^2 P^{n+1}=\frac{2Re}{\Delta t}\nabla.\mathbf{V}^{*}$$

In this Poisson equation for the pressure at time $n+1$, the right hand side is known. This equation is written in the discretized form by integrating both sides over each of the pressure cells. No special boundary conditions are needed for the pressure at this step because of the employment of the staggered mesh.

The steady state solution is obtained by marching in time asymptotically. For the time advancement of the governing equations, ADI (Alternating Directions Implicit Method) scheme is employed, which is second order accurate in time. The steady state is assumed to be reached once the variation in the variables, like u, v, C, is less than 0.01% in 50 iterations.

In the evaluation of the drag, from equation [2.14], we need to know the pressure at the surface of the bubble. Since in the staggered used, there is no node for pressure on the surface of the bubble, its value on the surface is calculated using a three point polynomial extrapolation. Normal stresses (τ_{rr}) which are only known at pressure nodes are extrapolated on the surface using the same procedure as for pressure. The first

derivatives on the surface of the bubble needed in estimating the net flux of surfactant to the bubble surface (as given by equation [2.20] to be discussed later) in solving the surfactant transport equation, are calculated using three-point formulas, which are second order accurate.

2.3.2 Grid Characteristics

The grid is constructed in the following way. The flow will be confined to an outer boundary r_∞, so that $1<r< r_\infty$. Creating a grid directing on the (r,θ) physical domain would give an expanding grid. We therefore choose to grid based on an x,y coordinate system which transforms the physical domain into a rectangular domain, i.e. $\ln (r/r_\infty)=x$ and $\theta/\pi=y$; the grid is then set-up with even divisions in Δx and Δy. The magnitudes of the dimensionless groups are chosen to correspond with our experiments, so that we may model these experimental results. We will discuss in more detail below the values of the groups; here we note that the Reynolds number, Re is of order one, and the Peclet number, Pe is of order 10^6. For the flow field, since at order one Re there are no boundary layer effects, we found that a denser mesh that already dictated by the coordinate transformation is good enough. To avoid any artificial confinement of the flow by the outer boundary, the outer limit of the grid is fixed at 80 bubble radii. A 50x50 grid in (r,θ) is used for the flow problem in all the simulations we did unless otherwise stated.

However, for the transport of the surfactant from the bulk to the interface, the convective terms are dominant, the Peclet number Pe being of the order of 10^6. For a fluid-fluid interface, at these Peclet numbers, there will be steep gradients in concentrations of the surfactant very near the bubble surface. The thickness of this concentration boundary layer scales as $Pe^{-1/2}30$, and hence a finer mesh is needed near the bubble surface. We put a fine mesh (linear in r), containing ten grid points in a distance of $Pe^{-1/2}$ from the surface of the bubble at r=1, along with an exponential grid described before. For the surfactant bulk concentration, because of this boundary layer, we found that a smaller computational domain good enough. So we chose a computational domain extending to 5 bubble radii for this case. Here we chose a 100x100 exponential grid in (r,θ) coupled with a 10x100 fine grid spread within the boundary layer close to the surface of the bubble. Interpolated velocities at the concentration nodes are used in the solution of the concentration problem. We use a cubic spline interpolation for this purpose. Figure 2.4a shows the exponential grid for the velocity while Figure 2.4b shows the enlarged view of the finer mesh near the surface of the bubble used for the surfactant bulk concentration. We also note that the stagnant cap boundary conditions [2.13] indicates a discontinuity in shear stress at the position where the stagnant region begins $\theta=\pi-\phi$. By using staggered grids and a finite volume method, we avoid this discontinuity by having nodes for Γ on either side of, and equidistant from, the discontinuity. Using an

equation of state for the surfactant, we can integrate the shear stress to get the surface concentration as given by equation [2.18] later.

2.3.3 Algorithm for the Numerical Solution

Here we describe the algorithm followed to obtain the drag exerted on a rising bubble, as a function of the surfactant bulk concentration, at very low surfactant concentrations under the stagnant cap regime.

1) For a given value of cap angle of size ϕ, the hydrodynamic flow around a spherical bubble with a solid cap of this size is solved. This is done using: the mixed boundary conditions on the bubble surface of zero stress and zero tangential velocity [2.13 a and b], the zero normal velocity on the bubble surface and the matching to the far field uniform flow [2.9]. These entirely prescribe the flow in terms of the fixed Reynolds number Re. Then the shear stress exerted by the continuous phase on the bubble surface ($\tau_s(\theta;\phi)$) and the total drag on the bubble is numerically calculated.

2) Once the shear stress distribution on the solid part of the cap is computed, the surface concentration in the cap $\Gamma(\theta;\phi)$ can be obtained from the tangential stress balance

$$\int_{\pi-\phi}^{\theta} \tau_s(\theta;\phi)d\theta = Ma\int_0^{\Gamma}\left[\frac{1}{1-\Gamma}+K\Gamma\right]d\Gamma \qquad [2.18]$$

3) From the surfactant surface concentration distribution on the cap region, the surfactant distribution in the continuous phase corresponding to this surface distribution

can be calculated. This needs a value of the surfactant bulk concentration k. To start with a value of k is guessed. When the kinetic exchange is infinitely fast (Bi→∞) the sublayer and surface are in equilibrium, and the dimensionless sublayer concentration can be calculated directly from the surface distribution.

$$C|_{r=1} = \frac{1}{k}\left[\frac{\Gamma(\theta;\phi)e^{K\Gamma(\theta;\phi)}}{1-\Gamma(\theta;\phi)}\right] \qquad \pi-\phi<\theta<\pi$$
$$C|_{r=1} = 0 \qquad\qquad 0<\theta<\pi-\phi \qquad [2.19]$$

4) Once the sublayer concentration is known, the distribution of surfactant in the continuous phase can be obtained by solving the convective-diffusion equation with the velocity given by the hydrodynamic solution for the cap angle ϕ. The net flux to the bubble surface (given by the Nusselt number Nu defined as

$$Nu = \int_0^{\pi} \frac{\partial C}{\partial r}|_{r=1} \sin\theta d\theta \qquad [2.20]$$

is then computed from the surfactant distribution in the continuous phase.

At steady state, the amount of surfactant adsorbing at the front end of the bubble should be equal to the amount of surfactant desorbing at the back end, and hence making Nu zero. We consider the flux to be zero if the absolute value of Nu be less than 0.1. If the net flux is not equal to zero to this accuracy, the value of k is changed, and steps (3) through (4) are repeated, computing the surfactant distribution in the continuous phase and finally the net flux Nu. Once the net flux is zero to the prescribed accuracy, the cap angle and drag for a particular value of k is known. Steps (1) through (4) are repeated for

different cap angles to get the drag as a function of k in the entire stagnant cap regime ($0^0<\phi<180^0$).

For kinetic-diffusive transport, the balance between the kinetic and diffusive fluxes replaces the quasi-equilibrium equations:

$$\frac{1}{Bi}\frac{\chi}{Pe}\frac{\partial C}{\partial r}\Big|_{r=1} = (C|_{r=1}(1-\Gamma(\theta;\phi)) - \frac{1}{k}\Gamma(\theta;\phi)e^{K\Gamma(\theta;\phi)} \qquad \pi-\phi<\theta<\pi$$

$$\frac{1}{Bi}\frac{\chi}{Pe}\frac{\partial C}{\partial r}\Big|_{r=1} = C|_{r=1} \qquad 0<\theta<\pi-\phi \qquad [2.21]$$

The surfactant distribution in the continuous phase is then solved with the above two conditions, and the net flux to the surface can then be calculated. As in the case of diffusion control, the cap angle is changed until this flux is zero to prescribed accuracy.

2.3.4 Model Validation

As a first test, the drag on a spherical bubble is calculated for different Reynolds numbers in the range of our interest, and compared with those in literature[50,51]. The comparison is shown in Figure 2.5. Using a 50x50 grid, at r_∞= 80, the values of the drag predicted by the present simulation differ from those of the earlier works by within 4%, the maximum error being at order one Reynolds number and decreasing with increasing Reynolds numbers. We could predict the drag on a solid sphere with a no slip boundary condition on the surface to within 0.5% when compared to the previous works [51]. In Table 2.1, we tabulate these comparisons for both the cases of a spherical bubble and a

solid sphere. For the stagnant cap case, we compared the results of the present simulations at zero Reynolds number with the analytical solution of Sadhal & Johnson [37]. With a 50x50 grid, we could get the drag at different stagnant cap angles to 5% accuracy. These results are plotted on a dimensional and dimensionless drag scale (defined as $100[C_D-C_{D(Bubble)}]/[C_{D(Solid)}-C_{D(Bubble)}]$) against the cap angle in Figures 2.6 a and b respectively. Here $C_{D(Solid)}$ and $C_{D(Bubble)}$ are the drags on the solid sphere and a spherical bubble as obtained from our simulations at the same Reynolds number. Also plotted are the results for order one Reynolds number. We note that all the results exhibit very similar features, indicating that the Reynolds number has a secondary effect on the reduced drag coefficient. Most of the drag on the bubble changes when the stagnant cap angle changes from around 50^0 to 110^0. From Figure 2.6b, we note that with increasing Reynolds number, the drag increases more steeply with cap angle near the equator of the bubble, as also observed by others[27,51].

Solving the problem of the transport of a passive scalar in creeping flow past a bubble with stress free interface, when the bubble acts as a sink checks the code for the surfactant bulk transport equation. The Nusselt number defined by [2.20] gives the net scalar flux to the bubble surface. We found good agreement for the Nusselt number, between our solution of the surfactant bulk transport problem with a given creeping flow and the asymptotic results of Acrivos and Goddard[30] for the range of Peclet numbers of

our interest (of orders 10^3-10^6) as shown in Figure 2.7. We note that for this problem, at zero and low Peclet numbers we used a numerical domain extending up to 80 bubble radii. But at higher Peclet numbers (>10^3) a domain extending up to 5 bubble radii is found to be good enough all using a 110x100 grid (a 100x100 exponential grid coupled with a 10x100 linear grid spread within the fine boundary layer close to the surface of the bubble).

For the simulations of the combined problem of hydrodynamics and surfactant transport, Table 2.2 shows the values we chose for the various dimensionless groups. These are dictated by our experiments. Here Bi_{min} is the Biot number calculated from the lower bound on the adsorption/desorption rate constants of the surfactant used in our studies from the pendant bubble apparatus as we describe in Chapter 3.

Using the algorithm described in Section 2.3.3, we tried to predict the bulk concentration $k= k_c$ of the surfactant needed to give a stagnant cap that completely covers the bubble (i.e., the case when $\phi=180^0$), for the case of diffusion limited transport of the surfactant. Using the same 110x100 grid for the surfactant bulk transport, the values of k_c we obtained with different grids are shown in Table 2.3. We note that the accuracy with using the 50x50 grid for the flow problem in a computational domain extending to 80 bubble radii and a 110x100 grid for the surfactant bulk transport problem in a computational domain extending to 5 bubble radii is satisfactory.

2.4 Results

In this section we present the results of our numerical study. First we consider the simple case of when the surfactant follows a Langmuir type kinetics (i.e., when K=0 in equation [2.5]). In Figure 2.8a we plot the surfactant surface concentration profiles on the moving bubble (for the cap angles presented in Figure 2.6), for the case of diffusion limited surfactant transport, while Figure 2.8b shows the corresponding surface velocity profiles. For the parameters used in this simulation $\frac{\chi(1+k)}{Pe^{1/2}}<<1$ and hence we are in the stagnant cap regime. We note that in the stagnant cap boundary conditions [2.13] the discontinuity in shear stress at the stagnant cap position $\theta=\pi-\phi$ is a square root singularity (see for example Harper[5]) i.e., $\tau_{r\theta}\approx 1/[\theta-(\pi-\phi)]^{1/2}$. Hence in the stagnant cap region, from equation [2.18], $\Gamma(\theta)\approx\int\tau_{r\theta}d\theta\approx[\theta-(\pi-\phi)]^{1/2}$ in the limit close to the stagnant cap discontinuity i.e.,$\theta\rightarrow(\pi-\phi)$. Same is true for surface velocity $V_S(\theta)$ in the stress free region, i.e., $V_S(\theta)\approx[\pi-\theta-\phi]^{1/2}$. We verify these arguments from our numerical simulations as shown in Figure 2.9. In Figure 2.9a, we plot the surface concentration Γ and in Figure 2.9b, the surface velocity V_S close to the stagnant cap discontinuity for different cap angles. Within the accuracy of our grid size, from the first five grid points close to the point of discontinuity we find the linear dependence of both $\Gamma(\theta)$, and $V_S(\theta)$ on the square root of the distance from discontinuity.

Consider any particular surfactant bulk concentration, say $k=2.3x10^{-2}$ at Re=0.91. We note from Figure 2.8a, that all the surfactant adsorbed onto the bubble surface is swept to the back end where it accumulates, while the front end of the bubble remains clean. The corresponding curve of the surface velocity profile in Figure 2.8b, shows that while the front end of the bubble is completely mobile with non zero surface velocity, the back end of the bubble with all the surfactant is stagnant. The values of surface concentrations in Figure 2.8a correspond to the solution of equation [2.18] corresponding to the fluid mechanics solution with a given cap size ϕ. In Figure 2.10, we show the profile of the sublayer concentration under these conditions, as given by equation [2.19] which gives us that at the front end of the bubble the sublayer concentration $C_{S(Front)}$ is zero while at the back $C_{S(Back)}$ is in equilibrium with the surface concentration distribution.

As we increase the surfactant bulk concentration, we note that more and more surfactant gets adsorbed onto the bubble surface increasing the size of the stagnant cap at the back end (Figures 2.8 a and b). This could be explained as follows. At any given cap angle ϕ, the flux of the surfactant from the bulk to the front end of the bubble scales as $(C_0-C_{S(Front)})/\delta_{Front}$ while at the back end the flux off the bubble surface into the bulk scales as $(C_{S(Back)}-C_0)/\delta_{Back}$. Here the δ's are the thicknesses of the diffusive boundary layers for surfactant mass transfer at the front and the back end of the bubble. Due to the high Peclet numbers for surfactant bulk transport, at the front end of the bubble which is

completely mobile, δ_{Front} scales as $Pe^{-1/2}$ while at the back end of the bubble with a completely stagnant interface δ_{Back} scales as $Pe^{-1/3}30$. With the increase in bulk concentration k or C_0, while the flux at the front end on to the bubble increases while the flux at the back end off the bubble decreases. Since the increase at the front end is of order $Pe^{1/2}$ compared to a lower order $Pe^{1/3}$ at the back end, there would be a net increase of flux onto the bubble surface which increases the amount of surfactant adsorbed, and hence the size of the stagnant cap.

When the complete bubble is covered by the surfactant, the bubble surface becomes stagnant as if it were a solid sphere. This occurs at a value of k approximately equal to 10^{-1}. This change in mobility on the bubble surface modifies the drag experienced by the bubble as shown in Figures 2.11a for this case of Re=0.91. Here we plot variation of the drag experienced by the rising bubble (in the form of the dimensionless drag as defined before) as a function of the surfactant bulk concentration. In the diffusion limited case, we note that as we add more surfactant in the bulk, as the size of the stagnant cap increases, the drag on the bubble increases from that of a clean interface stress free value to that of a completely stagnant interface solid like value.

Now let us consider the effect of adding a finite kinetic exchange resistance to this process. Figure 2.11a also shows the effect of the added surfactant on the drag of the bubble for the case of finite kinetic exchange rates (Bi= $1.5x10^{-4}$). An interesting result in

the stagnant cap regime evident here is the fact that for the finite kinetic exchange, the drag on the bubble is much smaller than for the diffusion limited case for the same value of k because of less surfactant adsorbed on the bubble. In other words, at any given cap size, the case of finite kinetic exchange rates supports a higher surfactant bulk concentration than a diffusion limited case. This could be explained as follows. Let us consider the diffusion limited case with a given cap size ϕ, say corresponding to $k=2.3x10^{-2}$ in Figure 2.8a as before. With the introduction of finite kinetic resistance in the form of a non-infinite Biot number (Bi) the sublayer concentration profile changes for the same surface concentration distribution as shown in Figure 2.10 in accordance with equation [2.21]. While at the front end $C_{S(Front)}$ increases and becomes non zero in contrast to the diffusion limited case, at the back end, $C_{S(Back)}$ decreases from its earlier value. This reduces the bulk diffusive flux to the bubble surface at the front end of the bubble which scales as $(C-C_{S(Front)})/\delta_{Front}$ which would be of the order of $Pe^{1/2}$ as discussed before. At the same time, the surfactant flux from the back end of the bubble into the bulk is also reduced which is of the order of $Pe^{1/3}$. So essentially the net surfactant flux onto the bubble surface is reduced. To maintain the mass balance of the surfactant at both the front and back end, we need to increase the surfactant flux onto the bubble surface at the front by increasing the bulk concentration C_0. This could also be seen from the following expressions for the surfactant bulk concentrations needed to support a given stagnant cap

size and $\Gamma(\theta)$ distribution, for the cases of diffusion limited and kinetically limited surfactant transport.

For diffusion limited case, $$\frac{\beta C_0}{\alpha} = \frac{1}{\frac{\Phi}{1-\Phi} Pe^{1/6} + 1}\left(\frac{\bar{\Gamma}}{1-\bar{\Gamma}}\right)$$

For kinetically limited case, $$\frac{\beta C_0}{\alpha} = \frac{1}{\frac{\Phi}{1-\Phi} + 1 - \bar{\Gamma}}$$

Here $1-\Phi$ is the fractional area of the stagnant cap, and $\bar{\Gamma}$ is the average surface concentration distribution. Due to the large Peclet numbers in realistic systems, the concentration C_0 needed for the diffusion limited case is smaller than the kinetically limited case. Hence from a diffusion limited case, introduction of the kinetic resistance at a given cap size is balanced by an increased surfactant bulk concentration.

Now let us consider the effect of flow Reynolds number on this phenomenon. In Figure 2.12, we plot the similar graphs for the diffusion limited case for three different Reynolds numbers. We note that as the Reynolds number increases, the curves shift to the right. This could be rationalized as follows. At any given cap angle (roughly around the same value of the drag for the Reynolds numbers studied, see Figure 2.6), the shear stress $\tau_{r\theta}(\theta)$ created by the stagnant cap region increases with the Reynolds number. Hence this increases the surfactant surface concentration $\Gamma(\theta)$ necessary to balance this shear stress (from equation [2.18]). A higher surfactant surface concentration could only be achieved

by a higher surfactant bulk concentration C_0. Hence to achieve the same cap angle, we need higher surfactant bulk concentration C_0 or k. In Figures 2.11(a-c) we see the similar effects of kinetic exchange as discussed before for different Reynolds numbers.

In Figure 2.13, we present the results when the surfactant follows Frumkin type kinetics (K is non zero, here K=5.47). These results show a similar trend. At any given surfactant bulk concentration k, a lower drag is achieved in as compared to the corresponding Langmuir case. This is due to the fact that the effective concentration here is $k/e^{K\Gamma}$ rather than k in the Langmuir case.

Above k_c, the stagnant cap extends over the entire surface of the bubble. There are no sharp gradients in shear stress or surface concentration on the surface of the bubble. Further addition of surfactant would make the surface concentration more and more uniform. The hydrodynamics will not be changed as long as the diffusive transport rates (to/from the bulk) and the kinetic exchange rates (at the interface) of the surfactant don't outweigh the its convection rate on the surface of the bubble. In this regime, to get the drag on the bubble as a function of the surfactant concentration, the complete flow equations [2.1] and [2.2] coupled with the surfactant transport equations both in the bulk [2.3] and on the surface [2.7] need to be solved simultaneously. The coupling occurs through the shear stress balance on the surface as given by equation [2.6]. We will describe this solution in detail in Chapter 4.

In Figure 14, we plot the bulk concentration of the surfactant needed to create a stagnant cap on the bubble that covers the complete bubble (cap angle $\phi=180^0$) as a function of the Marangoni number Ma, for the case of a diffusion limited surfactant transport following Frumkin exchange kinetics. We see that with increasing Marangoni numbers, a completely covered stagnant cap is formed on the bubble at lower surfactant bulk concentrations. Physically, from the definition of the Marangoni number $Ma=RT\Gamma_\infty/\mu U$, smaller size bubbles have high Marangoni numbers. Hence the smaller size bubbles have completely covered stagnant caps, hence behave like solid spheres, at lower bulk concentrations than larger size bubbles. In another words, at a given surfactant bulk concentration, the smaller size bubbles behave more solid like than larger size bubbles. We observe this behavior in our experiments, as we describe in Chapter 3 of our study.

2.5 Conclusions

We study the effect of trace amount of surfactants on the drag of a bubble rising due to buoyancy. In the limit in which the transport rates of the surfactant very small compared to hydrodynamics (i.e., Λ_D and $\Lambda_K<<1$) the surfactant behaves as if it were insoluble; to leading order, surface convection sweeps surfactant from the front to the back end with no surface to bulk exchange. Under these conditions, the stagnant cap model presented here is valid, where the front end of the bubble is considered completely

clean and hence stress free, while the back end of the bubble is considered stagnant like a solid surface. This work deals with the theoretical study on the effect of surfactant transport on the motion of a bubble rising in a liquid under these conditions. We develop an exact theory for this regime for the realistic case of the surfactant transport in the bulk characterized by high Peclet numbers ($\sim 10^6$), and finite kinetic exchange rates of the surfactant at the interface.

Our numerical results show that with the addition of even trace amounts of surfactant the behavior of the bubble changes from that with a completely stress free interface into that with a completely stagnant interface, as seen by the change in the drag on the bubble. Due to the high Peclet numbers this transition occurs in a narrow range of concentrations. We studied the effects of surfactant kinetic rate constants, the flow Reynolds number, and the Frumkin interaction parameter on the adsorption of the surfactant on the moving bubble.

We observe this interesting result that in the stagnant cap regime, at any given surfactant bulk concentration, the rising bubble experiences less drag when the kinetic exchange rates of the surfactant are finite, than in a diffusion limited case. This is because of the fact that less amount of surfactant is adsorbed on the bubble surface due to the increased resistance to transport in the former case. This result hints at the possibility of using experiments involving the measurement of the drag on a bubble rising in a

surfactant solution in the stagnant cap regime to measure the kinetic rate constant of the surfactant. We explore this possibility in Chapter 3 of our study.

Table 2.1: Drag on a spherical bubble and a solid sphere as a function of Reynolds number - Comparison of the results from the present simulations and earlier works.

Re	0	1	10	100
Drag on a Spherical Bubble				
Hadamard-Ribczynnski (1911)[58,59]	2.0			
Ryskin & Leal (1984) [50]		2.330	3.525	5.50
Present Study	1.989	2.198	3.460	5.15
Drag on a Solid Sphere				
Stokes Value	3.0			
Magnaudet, et al (1995)[51]		3.724	6.524	19.125
Present Study	3.116	3.672	6.460	19.292

Table 2.2: Values for the Concentration Independent Dimensionless Groups Used in the Numerical Simulations

Re	Ma	Pe	χ	K	Bi_{min}
0.91	12.6	1.2×10^{6}	0.12	5.47	1.5×10^{-4}

Table 2.3: Effect of Grid Refinement on the Numerical Results

	50x50 grid (r_∞=80)	**50x50 grid (r_∞=40)**	**50x100 grid (r_∞=40)**
Drag on a Bubble	2.17	2.16	2.16
Drag on a Solid	3.70	3.77	3.72
k_c (with a 110x100 grid and r_∞=5 for concentration)	0.27	0.29	0.30

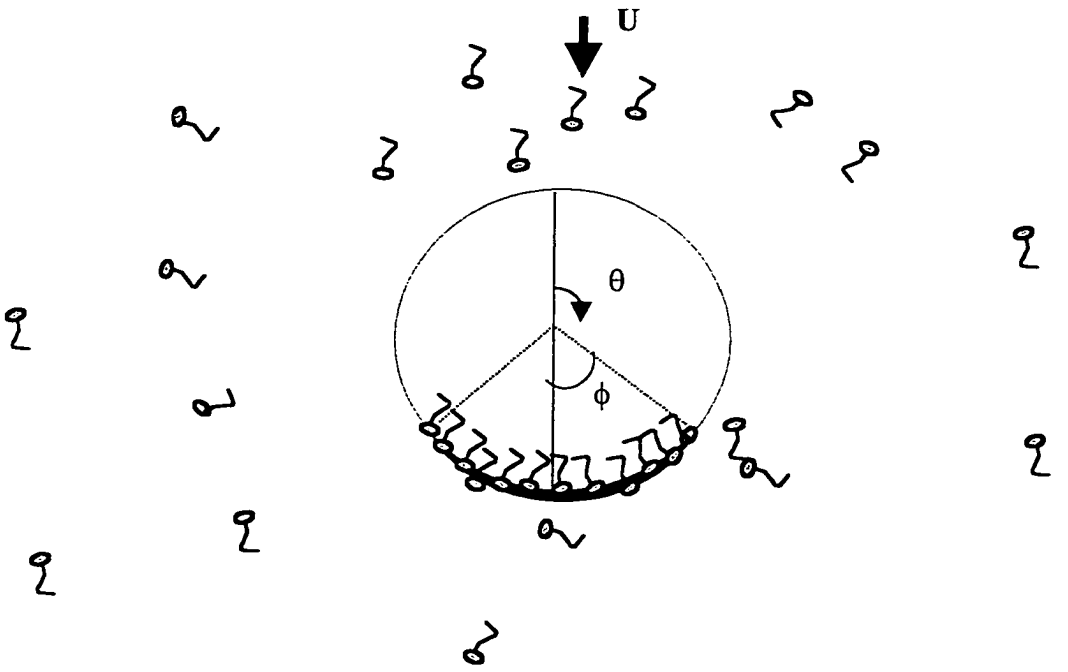

Figure 2.1: Stagnant cap in the flow past a spherical bubble with the surfactant present in the continuos phase.

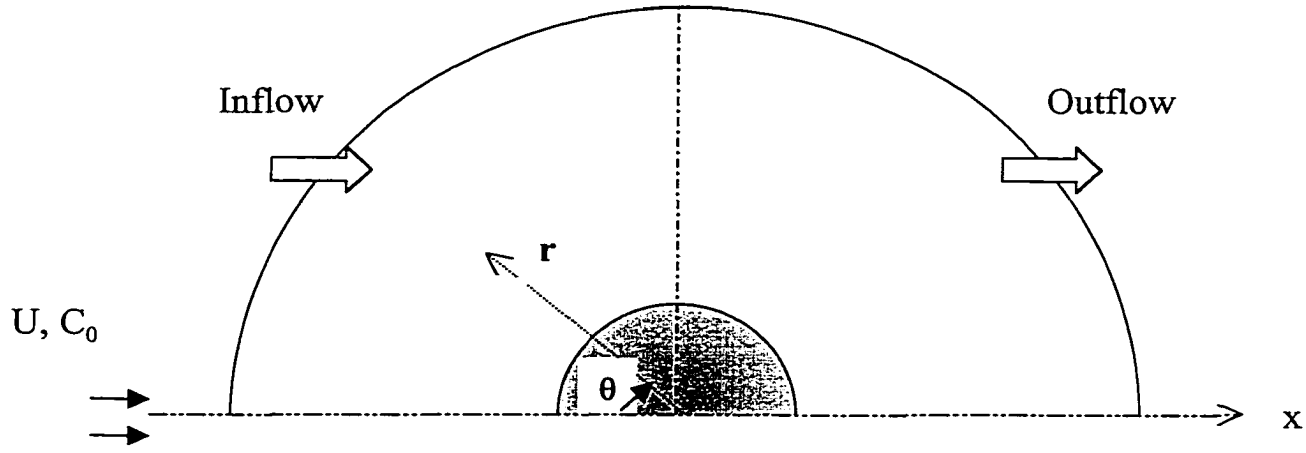

Figure 2.2: Sketch of the problem. The computational domain is restricted from the bubble surface r=1 to infinity r= r_∞. A value of 80 bubble radii is chosen for r_∞. The outer boundary is divided into Inflow and Outflow regions arbitrarily at$\theta=\pi/2$.

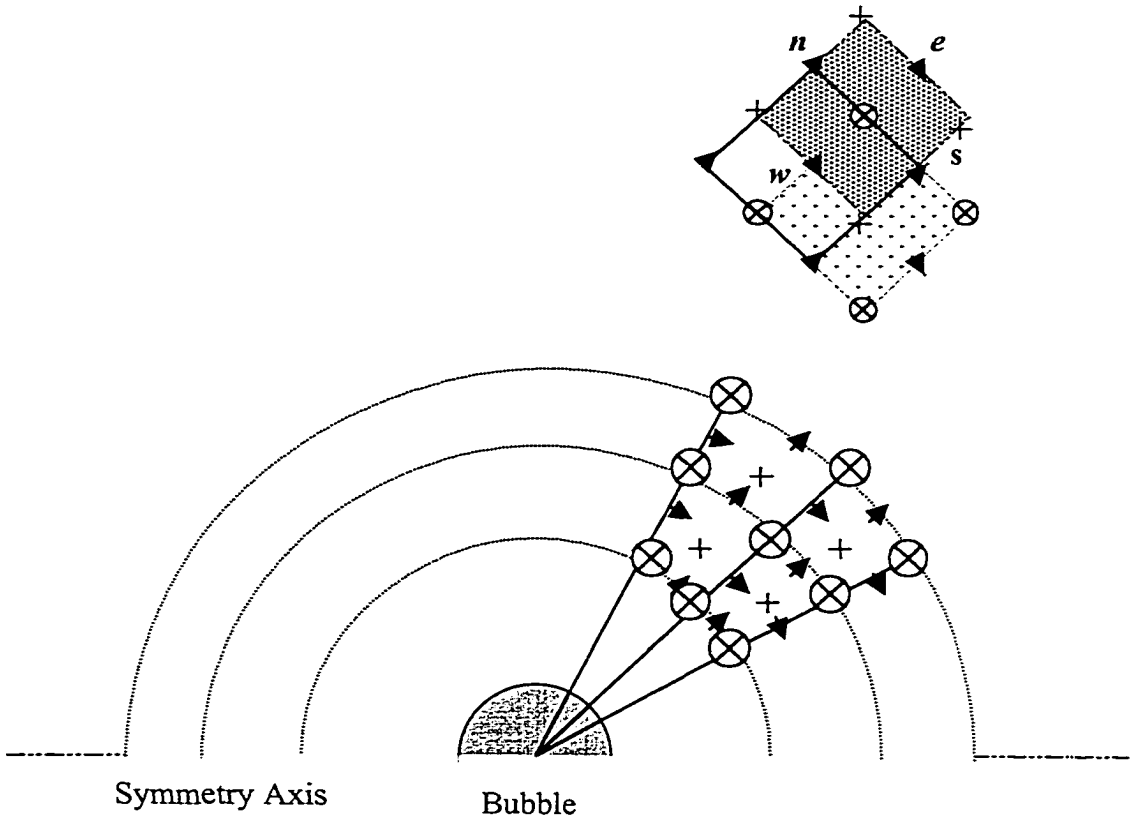

Figure 2.3: Typical staggered mesh for the finite volume method. ⊗ Concentration node; ▼ v node; ◤ u node; + pressure node.

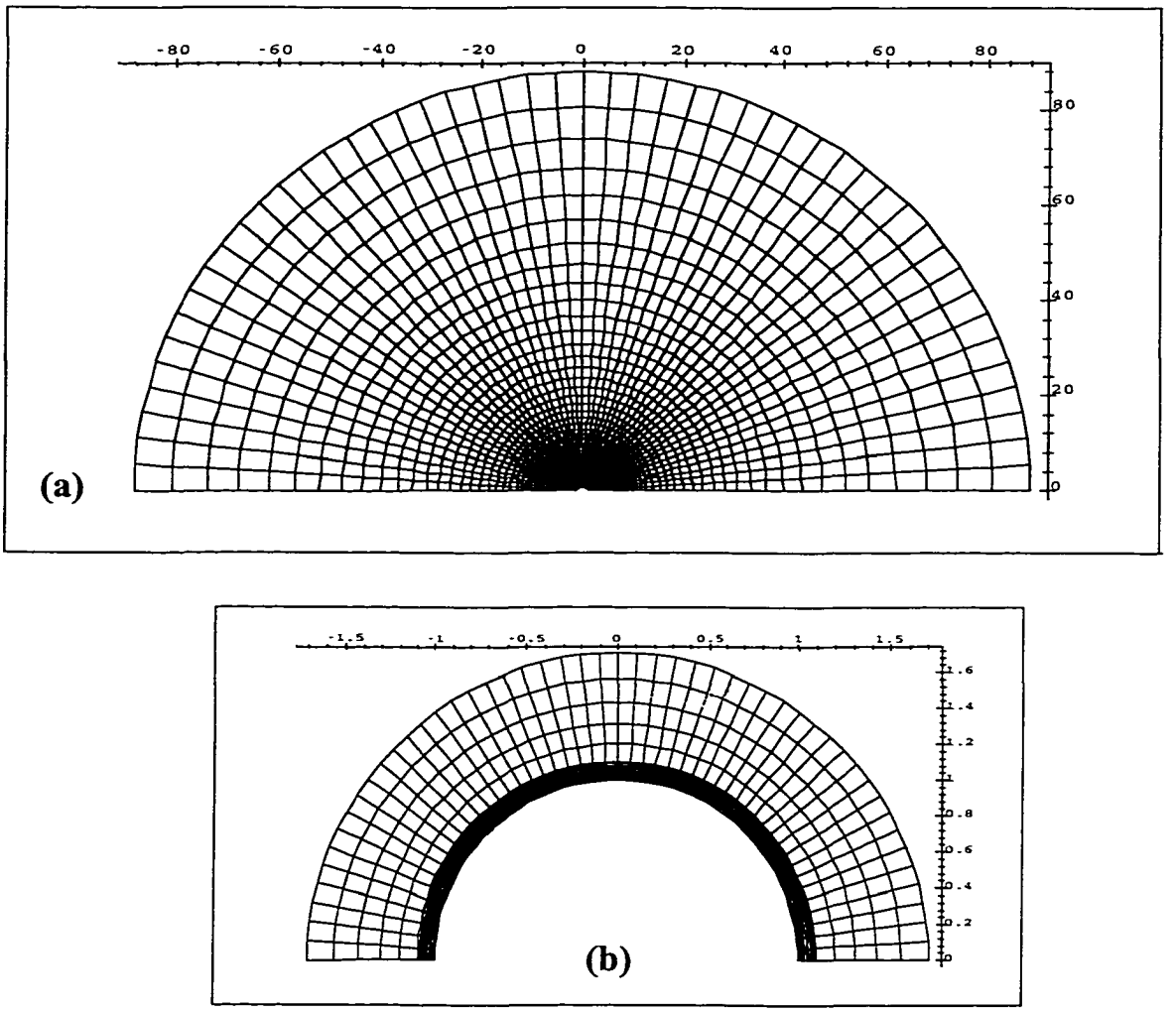

Figure 2.4: Numerical grid. (a) General View, (b) Refinement near the bubble surface needed to capture the happenings in the concentration boundary layer.

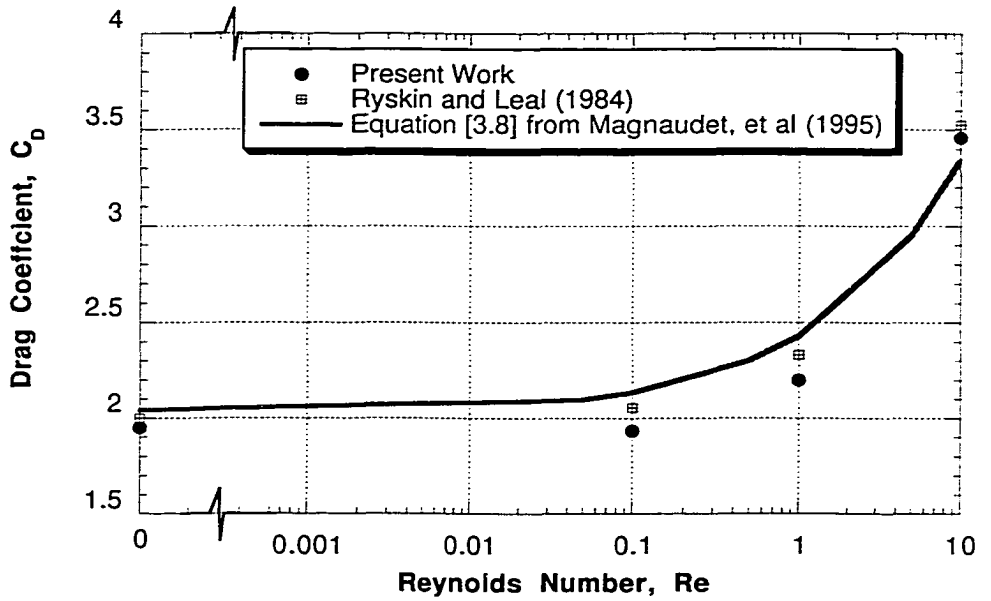

Figure 2.5: Drag on a Spherical Bubble as a function of Reynolds number. Comparison of the results of our simulations with those in previous literature.

(a)

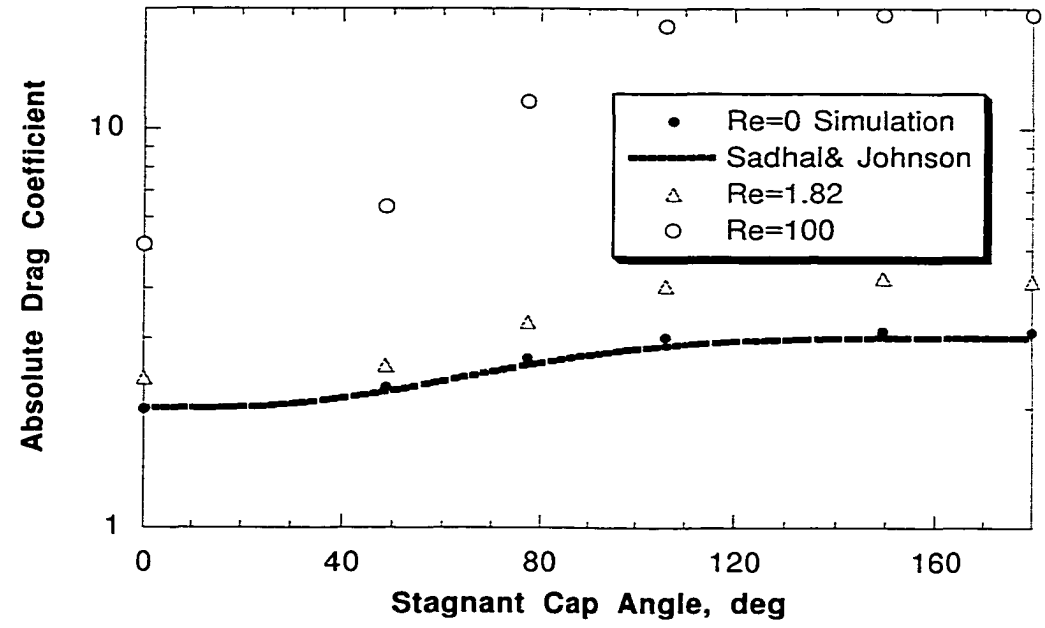

(b)

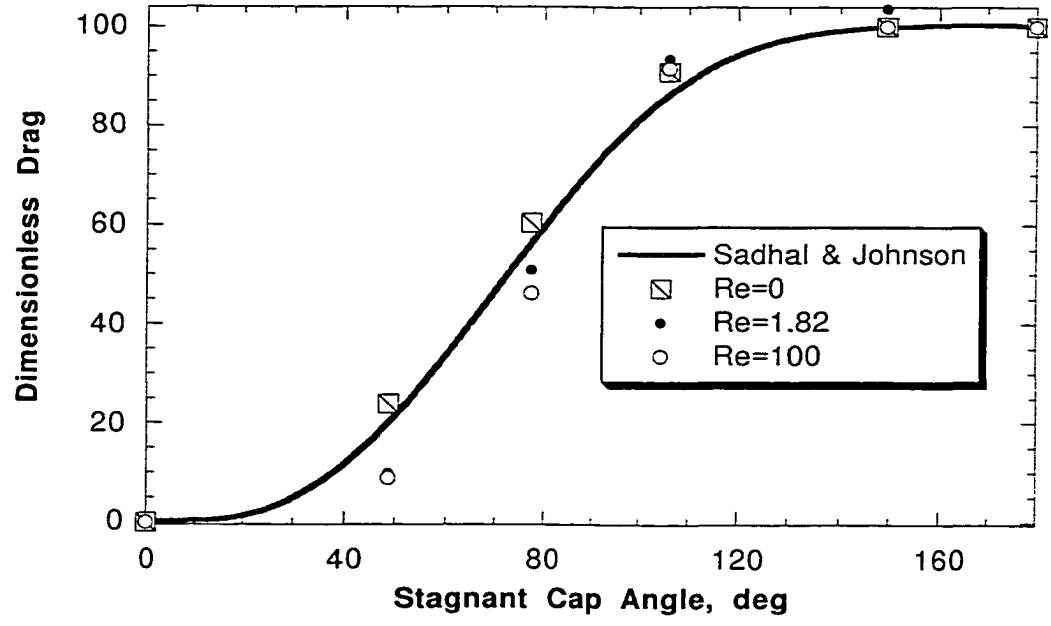

Figure 2.6: Drag on a Spherical Bubble with Stagnant Caps at different Reynolds number- Plotted both in (a) dimensional and (b) non dimensional forms.

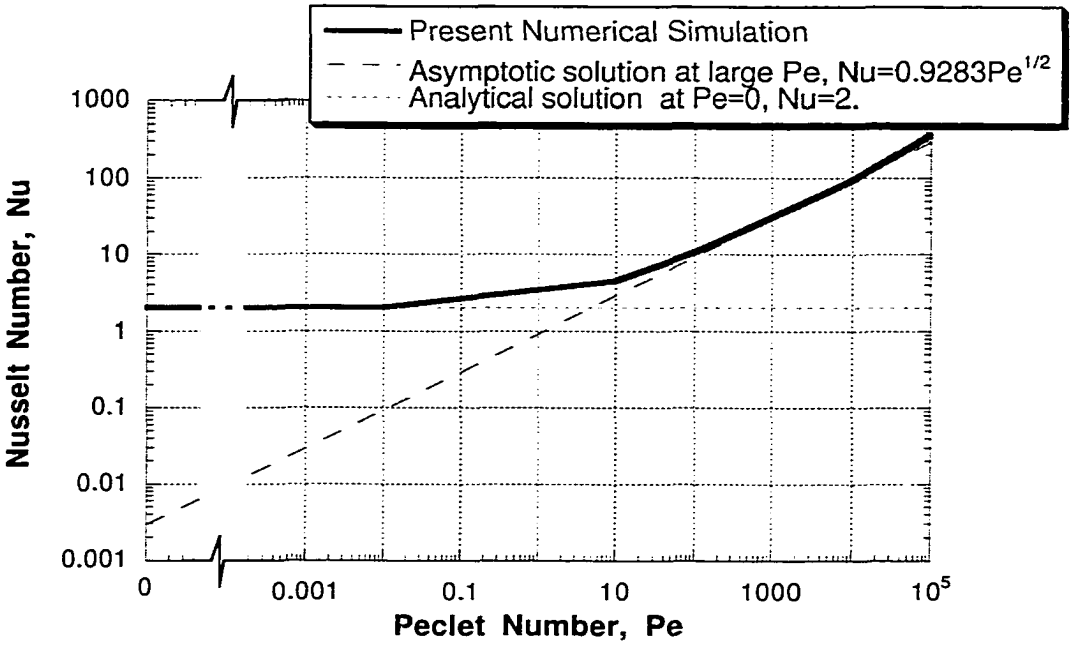

Figure 2.7: Verification of the code for surfactant bulk transport. Comparison of the results from our simulations for the mass transfer rates (Nu) of a passive scalar to the bubble surface for the case of a given creeping flow past the bubble when the bubble surface acts like a sink.

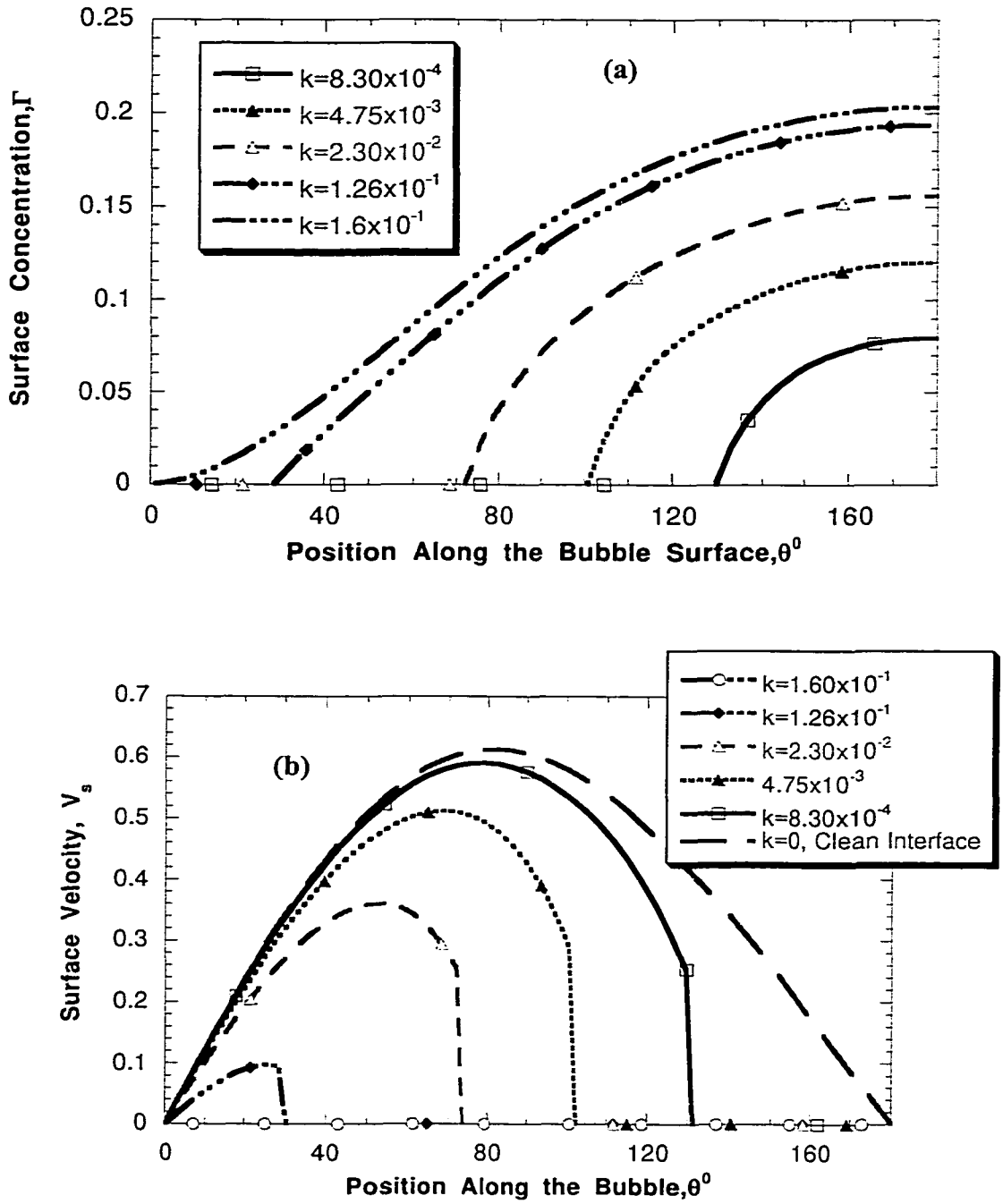

Figure 2.8: (a) Surfactant surface concentrations and (b) Interfacial velocities in the stagnant cap regime for different bulk concentrations of the surfactant (at Re=0.91 for a diffusion limited case)

(a)

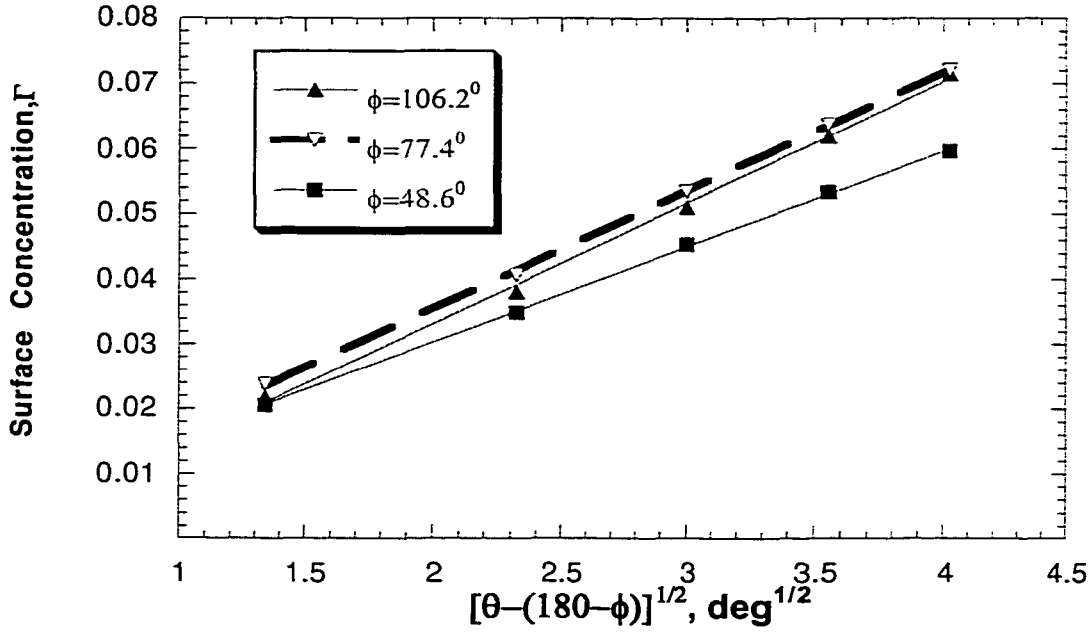

(b)

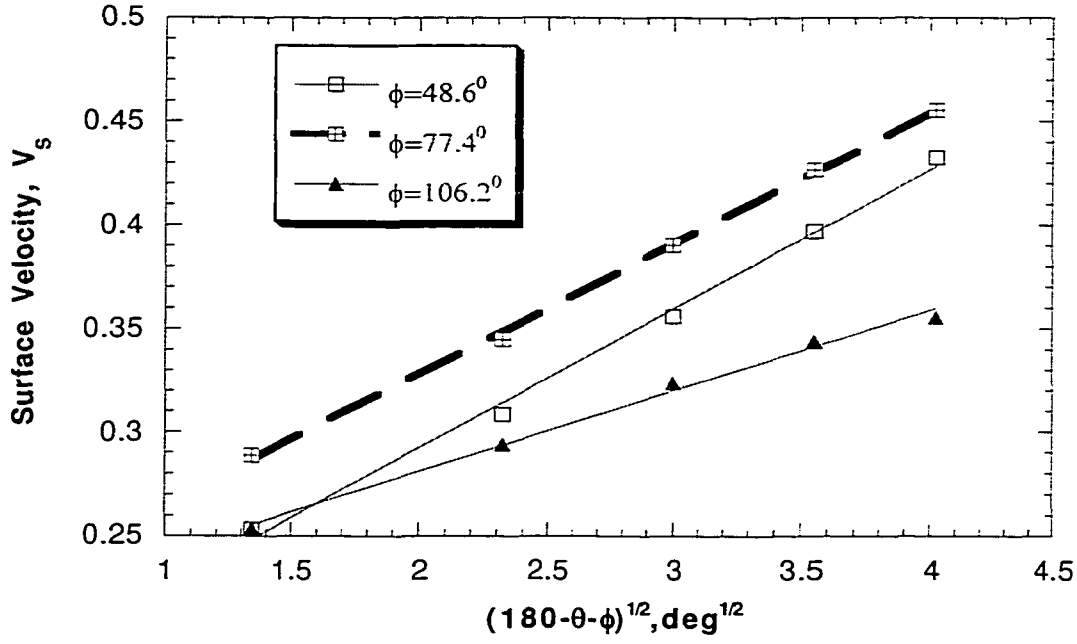

Figure 2.9: (a)Surfactant surface concentrations and (b) Interfacial velocities close to the point of stagnant cap discontinuity(at Re=0.91 for a diffusion limited case). This indicates the square root singularity in shear stress at the position of the stagnant cap.

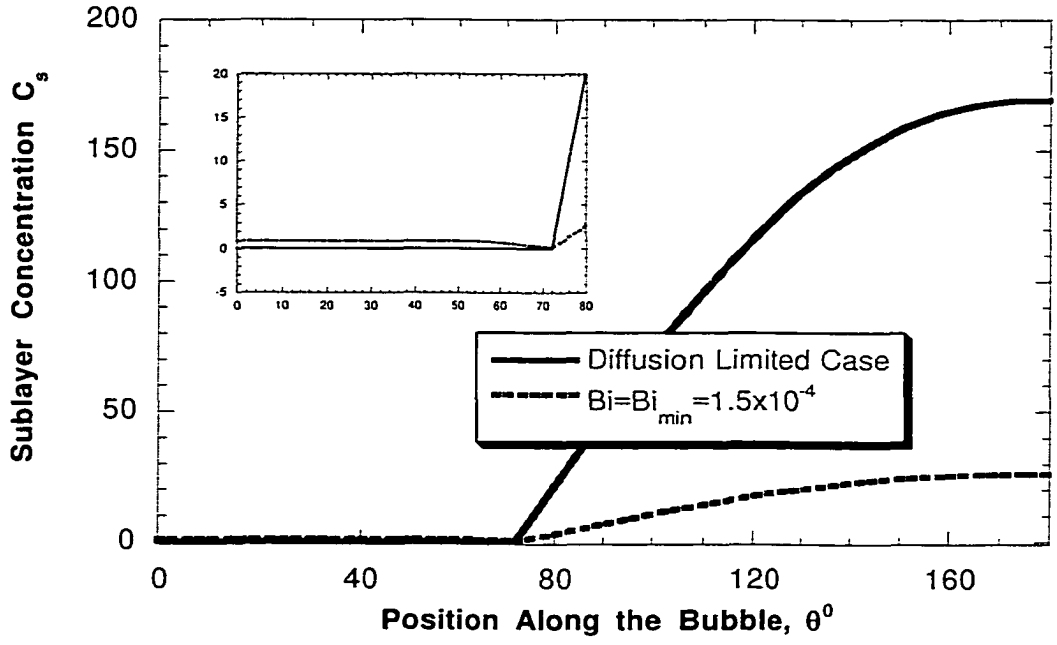

Figure 2.10: Variation of the sublayer concentration profile in the bulk close to the bubble surface for both diffusion limited and finite kinetic exchange case. Shown for a stagnant cap size ϕ= 104.4^0 and Re=0.91.

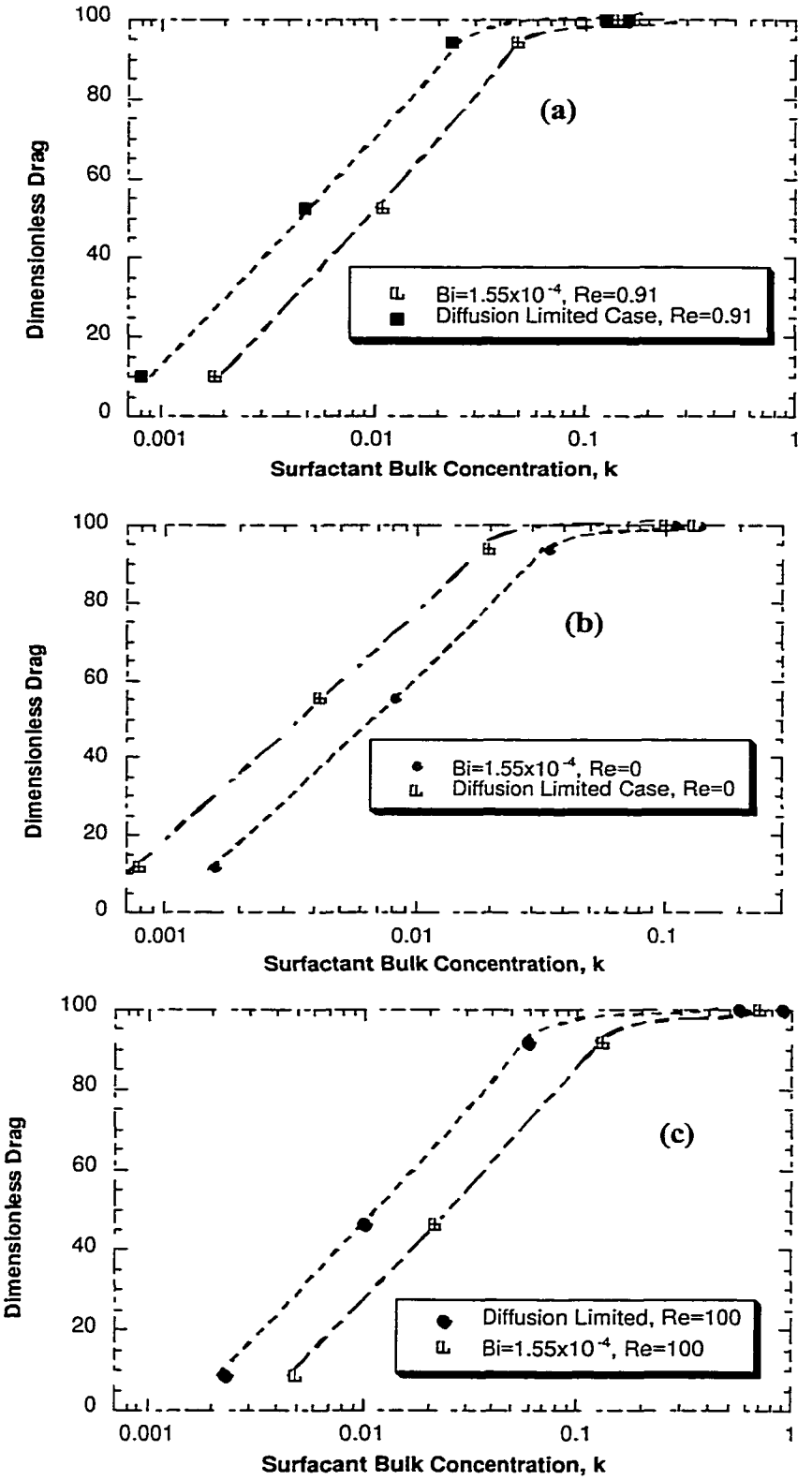

Figure 2.11(a-c): Numerical simulations showing the effect of the surfactant bulk concentration on the drag of a rising bubble, in the stagnant cap regime. Shown for cases when the surfactant follows a Langmuir type kinetics (K=0) at zero and order one Revnolds numbers.

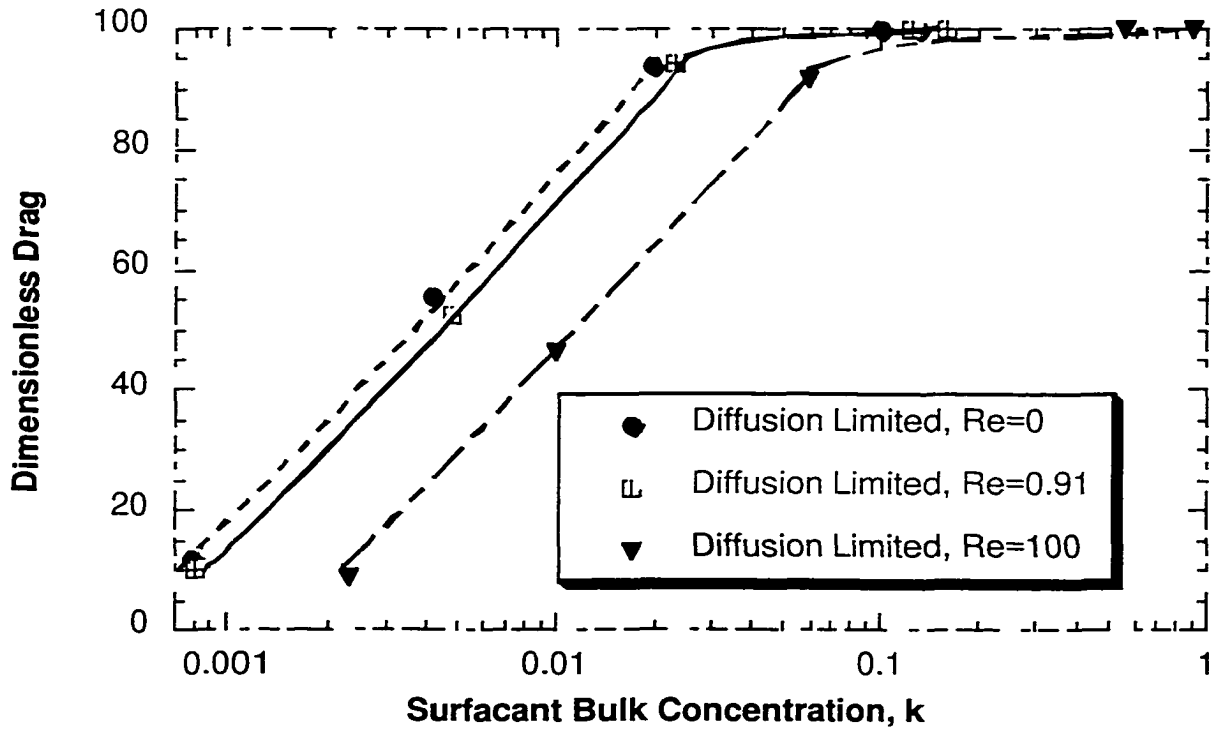

Figure 2.12: The variation of drag on a rising spherical bubble with the surfactant bulk concentration. Effect of flow Reynolds number. Shown for cases when the surfactant follows a Langmuir type kinetics (K=0) and when its transport is diffusion limited.

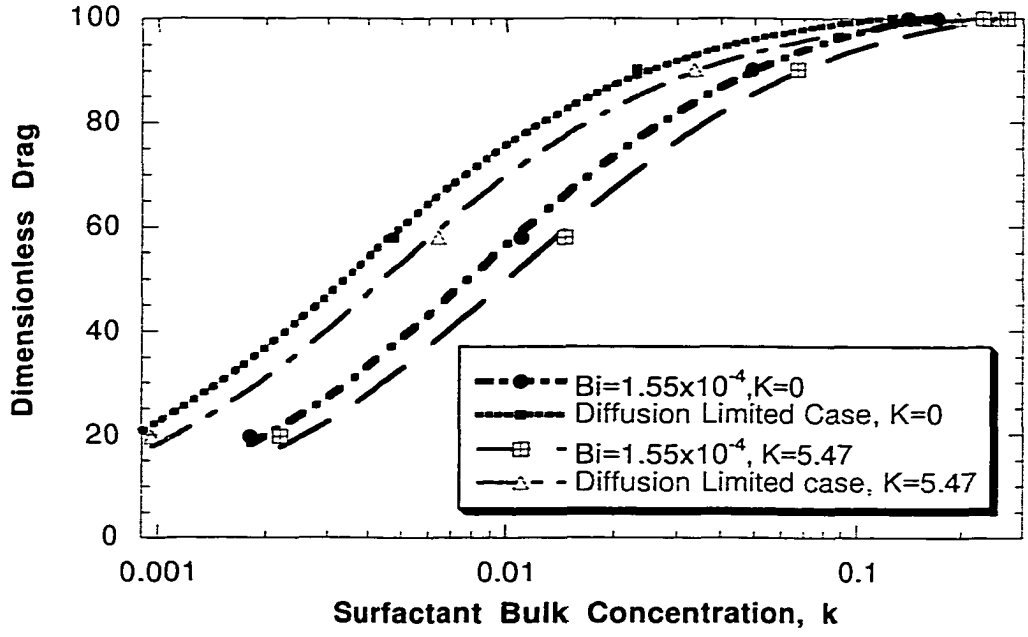

Figure 2.13: Numerical Simulations showing the effect of the Surfactant Bulk concentration on the Drag of a Rising Bubble, in the Stagnant Cap regime. Shown for cases when the surfactant follows a Langmuir type Kinetics (K=0) and when it follows a Frumkin type kinetics (K nonzero, here K=5.47) at Re=0.91

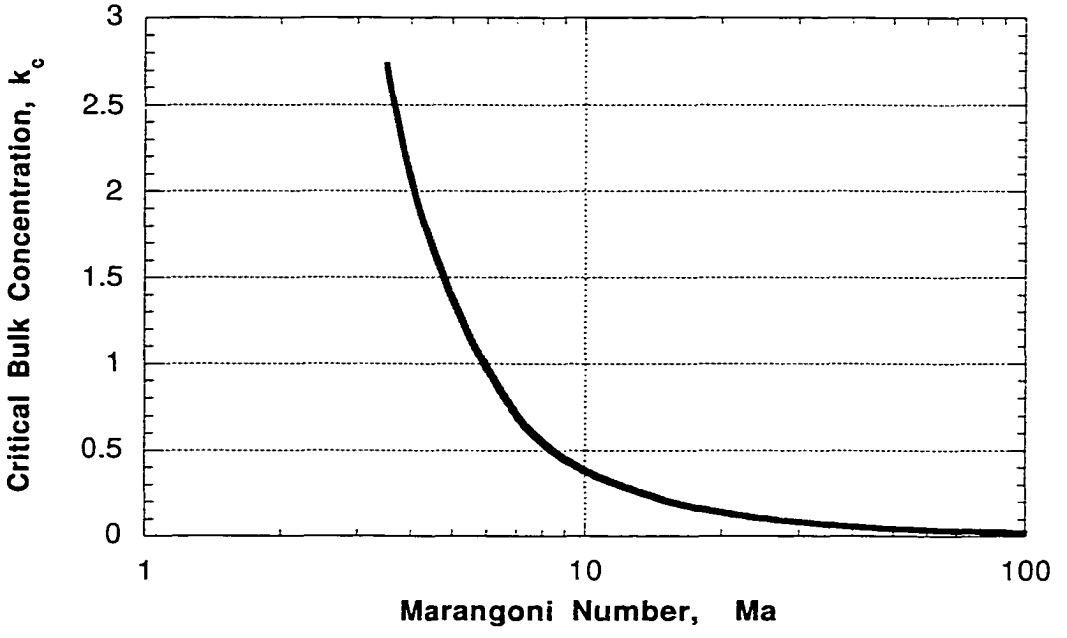

Figure 2.14: Effect of the Marangoni Number on the amount of surfactant (k_c) needed for the stagnant cap to completely cover the bubble surface (diffusion limited case for Re=0.91, K=5.47).

CHAPTER 3

An Experimental Study on the Stagnant Cap Regime in the Motion of a Bubble with an Adsorbed Surfactant Monolayer -Comparison With Theory

3.1 Introduction

Presence of even trace amounts of surface-active species in the continuous phase affects the mobility of bubbles rising in liquids, which affects different technological processes as mentioned in Chapter 1. In an effort to understand this retarding effect of surface active species in relation to their transport properties in the continuous phase, in this chapter we present our experimental work on the effect of trace amount of surfactants on the mobility of bubbles.

The transport of surfactant from (to) the bulk to (from) the bubble surface could be described by diffusion in the bulk and sorption kinetics (adsorption/desorption) at the interface. From the arguments presented in Chapter 1, for a surfactant following Frumkin type kinetics at the air/liquid interface, the rates of these transport processes relative to the convective rates on the bubble surface are given by the following quantities.

$$\Lambda_D = \frac{\text{rate of diffusion}}{\text{rate of convection}} \approx \frac{\Delta C}{C_o} \frac{\chi(e^{K\frac{\Gamma_e}{\Gamma_\infty}} + k)}{Pe^{1/2}}$$

$$\Lambda_K = \frac{\text{rate of kinetic exchange}}{\text{rate of convection}} \approx Bi\left[e^{K\frac{\Gamma_e}{\Gamma_\infty}} \frac{\Delta C}{C_o} - \left(\left\{ K\frac{\Gamma_e}{\Gamma_\infty} + 1 \right\} e^{K\frac{\Gamma_e}{\Gamma_\infty}} + k \right) \frac{\Delta \Gamma'}{\Gamma_e} \right]$$

We noted that in the limit in which either Λ_D or Λ_K is small, the surfactant behaves as if it were insoluble; to leading order, surface convection sweeps surfactant from the front to the back end with no surface to bulk exchange and a stagnant cap behavior is observed. Here all the surfactant adsorbed on the bubble collects in the form of a stagnant cap at the rear end, giving a semi-solid like behavior for the bubble. From their definitions, the limit $\Lambda_D << 1$ will be achieved when $\frac{\chi(e^{K\frac{\Gamma_e}{\Gamma_\infty}} + k)}{Pe^{1/2}} << 1$, and the limit $\Lambda_K << 1$ is obtained when $Bie^{K\frac{\Gamma_e}{\Gamma_\infty}} << 1$ and $Bik << 1$. When the surfactant is present in trace quantities, due to the large Peclet numbers characterizing surfactant transport in liquids, diffusive limitations alone lead to this regime in the bubble motion. Hence this is the regime often observed physically in experiments [9-13,35,44,45,60] and hence received wide theoretical attention[2,5,10,35-39,46,49].

Even though this regime is the most common in the motion of bubbles in liquids containing trace amount of surface active contaminants, there have been very few systematic experimental studies on the effect of surfactant transport on bubble motion. The only study that comes close has been that of Bel Fdhila and Duneveld[46] where the effect of surfactant on the terminal velocity of bubbles in the stagnant cap regime has been compared with a self contained theory (assuming a kinetic exchange limited surfactant transport). But recent studies of Zhang et al[60], showed that for the same

concentrations of the Triton X-100 surfactant used in water, under similar experimental conditions, the rise velocities of bubbles attain the solid like values when allowed to reach steady state, unlike the semi-solid values reported by Bel Fdhila et al. They concluded that in the work of Bel Fdhila et al the bubbles have not reached steady state.

In Chapter 2, we presented our theoretical approach in the stagnant cap regime. There we first formulated the problem of a bubble rise in an infinite liquid containing surfactant. We then solved the governing equations for the hydrodynamics and surfactant transport taking care of the finite rates of transport of the surfactant by diffusion in the bulk and kinetic exchange at the interface. Thus we could describe the effect of the added surfactant on the drag of a rising bubble in the stagnant cap regime. We studied how the surfactant transport properties could alter the drag on the rising bubble. In this chapter, we detail our experiments with a model system. First in Section 3.2, we discuss the measurement of the surfactant properties: the bulk diffusion coefficient and the adsorption/ desorption rate constants, using a pendant bubble apparatus. Then we describe our experiments studying the effect of the surfactant bulk concentration on the velocities of a bubble rising due to buoyancy. In Section 3.3, we discuss the results of our simulations under these experimental conditions, and explore the possibility of using them to determine the kinetic rate constants of the surfactant at the air liquid interface. Finally we present our conclusions in Section 3.4.

3.2 Experimental Section

3.2.1 Materials

We originally intended to measure the velocity of air bubbles in aqueous surfactant solutions, since the adsorption properties of surfactants at the air/water interface have been well studied[61,33] and comparison with the already established theory (which needs the adsorption constants) could be made. However, for air bubbles in the size range we are manufacturing, i.e. 0.3-.7 mm in radius (a), steady rise velocities (U) as experimentally measured by several investigators (see for example the text by Clift, et al[16]), are of the order 150-300 mm/s. At these high velocities, inertial effects are of the order of capillary forces (i.e. the Weber number, $We=\rho U^2 a/\gamma_c$ is between .2 and 1.2, where ρ and γ_c are the density of the continuous phase and clean surface tension, respectively) so the bubbles, as have been observed, are deformed. Our theory is for spherical shapes; since we eventually want to quantitatively compare the theory to these experiments, we decided to increase the continuous phase viscosity (μ) by adding glycerol to water to reduce U. An additional reason for lowering rise velocities is that at the high velocities of bubbles rising in water, although we can measure velocities accurately, the bubble shapes are not distinct and so we can not keep track of the deformation. We chose a glycerol/water ratio of 7:3 by volume, which has a viscosity of 29cP (as measured by a Haake Couette viscometer), and a density of 1.192 g/cm^3 at 25^{0}C. As we will verify, air bubbles with sizes of the order of .3-. 7mm in radius, rise with

velocities of the order of a mm/s keeping the Weber number less than .01, so that the bubbles appear clear and spherical on our video recording. This allows our experiments to be compared to our hydrodynamic simulations, which assume a spherical bubble shape.

In preparing the continuous phase, the water used is purified from tap water using a Millipore Q System (Millipore, MA) with a specific resistance greater than 15M ohm-cm. The glycerol used is obtained from Sigma (ACS Reagent, Cat. No. G-7893) and is used without modification. The surface tension of the aqueous/glycerol mixture against air was equal to 65.6 dyne/cm as measured by a pendant bubble apparatus, and did not vary with time indicating no surfactant impurities. In the range of temperatures studied (22-27°C), the density of the solution did not vary but the viscosity is a strong function of temperature and its effect is accounted for in our study.

For the present study, we chose a member $C_{12}E_6$, of the n-alkyl poly (ethylene glycol) ether surfactant series with the following structure $CH_3(CH_2)_{11}(-OCH_2CH_2)_6$-OH)). This was obtained from Nikkol Surfactants, Japan.

3.2.2 Equilibrium and Sorption Kinetic Properties of the Surfactant

The kinetic rate constants for surfactant exchange at an interface are determined in the following way[34,62,63]. First, experiments are undertaken in which either (i) surfactant diffuses toward and kinetically adsorbs from solution onto a initially clean

interface, and the reduction in surface tension is measured, or (ii) the surface area of an equilibrium monolayer is changed, causing kinetic exchange with the sublayer and subsequently with the bulk, and the re-equilibration in tension is measured. Second, the surfactant mass transfer occurring in each of these dynamic tension experiments is modeled to predict the surface concentration as a function of time ($\Gamma'(t)$). This modeling includes solving the bulk phase diffusion equation (including convection if the dynamic tension experiment involves flow), and the surface conservation equation, which accounts for the kinetic exchange. Third, the equation of state which gives the tension as a function of the surface concentration $\gamma(\Gamma')$ is measured so that the tension relaxation corresponding to the unsteady adsorption can be predicted from the model. Finally, the experimental relaxations are matched to the predictions by adjusting the values of the kinetic constants, and in this way these constants are established.

3.2.2.1 Experimental Apparatus

In our study, we use the pendant bubble technique to measure the reduction in tension as surfactant adsorbs onto an initially clean interface. The technique is based on the analysis of the shape of pendant bubbles formed and tethered to the tip of a needle placed in the surfactant solution [64,65](see Fig. 3.1). A pendant bubble is formed quickly (<1 sec.) by the injection of gas through a needle immersed in the surfactant solution with bulk concentration C_o. Surfactant adsorbs onto the freshly formed interface, reducing the

tension of the bubble surface and elongating the bubble. Digitized video images of the bubble elongation are captured sequentially in time; for each digitized image, the locus of points comprising the bubble interface is constructed, and the surface tension of the bubble interface at that time is computed by matching the bubble profile to theoretical pendant shapes obtained by solving the Young-Laplace equation. Thus from the sequence of images, a surface tension relaxation can be constructed, and the equilibrium tension as a function of the bulk concentration ($\gamma(C_o)$) can be obtained from the long time behavior.

All the experiments are done at 25°C. The surface tension of the glycerol/water mixture against air was equal to 65.6 dyne/cm as measured by the pendant bubble apparatus, and did not vary with time indicating no surfactant impurities. Equilibrium tensions are also obtained for the clean system (and surfactant solutions) by the Wilhelmy plate method in which the force on a (flame blasted) platinum plate immersed in a teflon cell containing the surfactant solution is measured. The surfactant free mixture gave a surface tension of 66.0 dyne/cm by this method. Solutions of the surfactant in the glycerol-water mixture are freshly prepared for each experiment.

3.2.2.2 Equilibrium Surface Tensions and Equation of State

Shown in Figure 3.2 are measurements of the equilibrium tension as a function of C_o as obtained from the longtime behavior of the tension relaxations in the pendant

bubble technique. Separate measurements are also reported of the equilibrium tension using the Wilhelmy plate method. Using the two methods, the equilibrium surface tensions are measured for concentrations in the range from 0.05 to 150 mg/lit (1.11×10^{-6} to 3.33×10^{-4} M). The concentration at which the tension no longer decreases with increasing surfactant concentration is the critical micelle concentration (CMC). At this point and with further increase in C_o, aggregates of surfactant form in the bulk rather than surfactant adsorbing on the interface. The measured value for the CMC (94 mg/l) is approximately twice that of water[61], reflecting the fact that glycerol is less polar then water and hence the glycerol-water mixture is more accommodating of the surfactant chains.

The surfactant equation of state can be obtained from the above γ-lnC_o data because the slope of the data is proportional to the surface concentration as given by the Gibbs equation:

$$d\gamma = -RT\Gamma_e d\ln C_o \qquad [3.1]$$

where Γ_e is the surface concentration in equilibrium with the bulk concentration C_o. The Gibbs equation can be integrated once the adsorption isotherm $\Gamma_e(C_o)$ is specified. The isotherm can be obtained from an Arhenius type kinetic rate formulation for the rate of exchange of surfactant molecules at the interface in which adsorption and desorption rates are proportional to activation energies which can be a function of the surface

concentration. The simplest form of the Arhenius framework, which has been found to model accurately surfactant adsorption at the air/liquid surface (and in particular the polyethylene oxide surfactant used in our experiments) is the Frumkin equation. As described in Chapter 1, in this formulation, the activation energy for desorption is independent of the surface coverage, while the activation energy for desorption is linear in the coverage:

$$\frac{d\Gamma'}{dt} = \beta\Gamma_\infty C_s\left(1-\frac{\Gamma'}{\Gamma_\infty}\right) - \alpha\Gamma e^{K\frac{\Gamma'}{\Gamma_\infty}} \qquad [3.2]$$

where Γ' is the dimensional surface concentration, RT is the thermal energy, Γ_∞ is the maximum packing density, $\Gamma = \Gamma'/\Gamma_\infty$, α and β are kinetic coefficients for desorption and adsorption, and C_s as before is the concentration of surfactant adjacent to the interface (i.e. the sublayer concentration). From [3.2] we obtain the Frumkin adsorption isotherm $\Gamma_e(C_0)$ by setting the kinetic rate equal to zero:

$$\frac{\Gamma_e}{\Gamma_\infty} = \frac{1}{1+(\alpha/\beta C_0)e^{(K\Gamma_e/\Gamma_\infty)}} \qquad [3.3]$$

Finally, from the adsorption isotherm and the Gibbs equation, the equation of state follows:

$$\gamma(\Gamma') = \gamma_c + \quad RT\Gamma_\infty\left[\ln\left(1-\frac{\Gamma'}{\Gamma_\infty}\right) - \frac{K}{2}\left(\frac{\Gamma'}{\Gamma_\infty}\right)^2\right] \qquad [3.4]$$

where γ_e is the tension of the clean surface. In Figure 3.2, a least square fit of the equilibrium surface tension against bulk concentration data using the Frumkin equations is also plotted. The values of the parameters that fit best are Γ_∞= 4.48x10^{-6} mol/m^2, α/β=9x10^{-4} mole/m^3 and K=5.47. The value of Γ_∞ obtained here also agrees with the estimate obtained independently from the slope of the γ vs. ln(C_0) curve. Note also that a positive value of K indicates that repulsive head group interactions dominate in the monolayer.

With the constants K and Γ_∞ determined, we now have obtained an equation of state. We verified this predicted equation of state with the equation of state determined directly from experiment by using the pendant bubble as a Langmuir trough[61]. Here for a given bulk concentration C_0, a pendant bubble is allowed to equilibrate with a surface concentration Γ_e and a surface tension γ_e. The bubble is then rapidly compressed or expanded and the surface tension γ(t) as a function of the surface area of the pendant bubble A(t) is recorded. If the compression or expansion is faster than the kinetic and diffusive exchange, the amount of the surfactant on the interface is conserved and the surface concentration Γ(t) at time t can be written as Γ'(t)A(t)=constant. We choose a reference area A_o during the expansion or compression cycle for which the tension is a particular value. We plot the tension γ(t) as a function of the area A(t) divided by the

reference area to directly map the equation of state. Figure 3.3 shows the results of the measured tension as a function of the surface concentration referenced to the concentration at which the tension is equal to 55.1 dyne/cm. Each set of symbols represents a single expansion or compression cycle, and we note that the cycles are done at different bulk concentrations. The fact that all the data correlates to a single line indicates that exchange with the bulk is negligible, and that the tension is an instantaneous function of the surface concentration.

Also plotted in Figure 3.3 is the prediction of the Frumkin equation of state (Eq. [3.4]) with the constants obtained from fitting the γ-lnC_0 data. The prediction matches the data, and we therefore conclude that [3.4] is an accurate representation of the equation of state. We note that the equation of state obtained from the Langmuir formulation ([3.4] with K=0 and with Γ_∞ obtained by fitting the γ-lnC_0 data) does not agree with the direct measurements.

3.2.2.3 Dynamic Surface Tension and Kinetic Rate Constants

In Figure 3.4, the dynamic surface tension relaxations for adsorption onto the clean air/ glycerol-water interface at five different bulk concentrations (1.1×10^{-5}, 2.2×10^{-5}, 4.4×10^{-5}, 1.1×10^{-4} and 1.9×10^{-4} M) are shown as obtained by the pendant bubble technique. For each concentration, several bubbles were formed and their relaxations were recorded, and these are shown as the different symbols at each concentration. Note

that the rate of relaxation increases with the bulk concentration. This is due to two effects: First, when the clean bubble interface is created, surfactant kinetically adsorbs onto the interface. The larger the bulk concentration, the more rapid is the kinetic adsorption as can be seen from Eq. [3.2]. Second, the kinetic exchange decreases the sublayer concentration C_s below the bulk concentration C_o, creating a diffusive flux to the sublayer. This flux replenishes the sublayer, and thereby increases the kinetic rate. Hence the larger the bulk concentration, the greater is the diffusive flux, the more rapid the adsorption and the faster the reduction in tension.

To model the tension relaxations given in Fig. 3.4, we begin by constructing the following transport model for adsorption to the pendant bubble interface. We assume the bubble to be a sphere with radius b, and we locate a spherical coordinate system with radial coordinate r, and origin at the bubble center. At time t=0 (the moment the bubble stops growing and the adsorption process commences), the surface concentration is assumed to be equal to zero ($\Gamma'(0)=0$), and the bulk concentration is uniform and equal to C_o($C(r,t=0)=C_o$). Transport of surfactant in the bulk is described (in the absence of convection) by the diffusion equation with the transport assumed radial:

$$\frac{\partial C}{\partial t} = D\left(\frac{1}{r^2}\frac{\partial}{\partial r}r^2\frac{\partial C}{\partial r}\right) \qquad [3.5]$$

where D is the diffusion coefficient. The solution of the above equation, subject to the initial conditions, the matching of the diffusive flux to the increase in the surface

concentration $D\frac{\partial C}{\partial r}_{r=b} = \frac{\partial \Gamma'}{\partial t}$, and the requirement that the concentration as $r \rightarrow \infty$ is equal to C_0 can be written as a convolution integral of the (unknown) sublayer concentration $C_s(t)$:

$$\Gamma'(t) = \frac{D}{b}[C_0 t - \int_0^t C_s(\tau)d\tau] + 2(\frac{D}{\pi})^{1/2}[C_0\sqrt{t} - \int_0^{\sqrt{t}} C_s(t-\tau)d\sqrt{\tau}] \qquad [3.6]$$

To obtain the unknown sublayer concentration $C_s(t)$ and the surface concentration $\Gamma'(t)$, [3.6] is solved along with the kinetic equation [3.2] numerically. From the unsteady surface concentration, we calculate the dynamic tension from Eq. [3.4]. In undertaking these simulations, three parameters are unknown, the diffusion coefficient D and the kinetic rate constants α and β. Note, however, that the ratio of the kinetic constants is known, so in principle the simulations require two unknown values. We could run the simulations for chosen values of these parameters, and then adjust the values until the simulations fit the experimental relaxations. However, this two-parameter fitting is not always unique and can be difficult, and so we begin by assuming the process is diffusion controlled. In this approximation, the kinetic exchange is fast enough so that the sublayer and the surface remain in quasi-equilibrium during the adsorption, i.e.,

$$\frac{\Gamma'(t)}{\Gamma_\infty} = \frac{1}{1+(\alpha/\beta C_s(t))e^{(K\Gamma'(t))/\Gamma_\infty)}} \qquad [3.7]$$

We obtain solutions to [3.6] and [3.7] to find $\Gamma'(t)$, and then from [3.4] to obtain the dynamic tension. These simulations can then be fit to the tension data by adjusting only the diffusion coefficient. We find a value for D equal to $1.5 \times 10^{-11} m^2/s$ by fitting all concentrations, and we provide in Fig. 3.4 the simulations in relaxation for this value of D. As the figure shows, the fits are fairly good at all concentrations, and kinetic effects do not appear to play a role in these relaxations. The value of D is an order of magnitude less than that obtained for $C_{12}E_6$ in water in Pan et al (6×10^{-10} m^2/sec). This is expected as the viscosity of the glycerol-water mixture used here is 30 times less than that of water. Measurements of the kinetic rate constants for $C_{12}E_6$ at the air/water surface show that relaxations using the pendant bubble technique at similar concentrations are controlled both by diffusion and kinetics, and a value for the kinetic constants and D are obtained by undertaking a two parameter fit. Here the increased viscosity and reduced diffusion coefficient in the glycerol/water mixture decreases the diffusion rate to the surface relative to the kinetic adsorption rate so that the process becomes diffusion limited.

Although these experiments do not provide values for the kinetic constants, we can obtain lower bounds. We note that as the bulk concentration increases, both the kinetic and diffusion rates increase. However, it is easy to show by scaling arguments[61] that the diffusion rate increases faster: The maximum rate at which bulk diffusion proceeds is obtained when the sublayer concentration is equal to zero; $\Gamma'(t)$ in this case is

given by the first term in the Ward and Tordai expression (neglecting the spherical term), i.e., $\Gamma'(t) = 2C_o\left[\frac{Dt}{\pi}\right]^{1/2}$. Thus the time to achieve an equilibrium monolayer with concentration Γ_e is given for diffusion control by $\tau_d = \pi\Gamma_e^2 / (4DC_o^2)$. The rate at which kinetics alone delivers material to the surface can be obtained by integrating the kinetic equation assuming the sublayer concentration is equal to the bulk value C_o. If we use the Langmuir equation ([3.2], with K=0) which permits analytic integration, we find that the adsorption is given by $\Gamma'(t) = \Gamma_e(1-e^{-(\alpha+\beta C_o)t})$ and the characteristic time to achieve kinetic equilibrium is given by $\tau_{kinetic} = (\alpha + \beta C_o)^{-1}$. As the bulk concentration increases, the ratio of the two time scales becomes of order $\frac{\tau_d}{\tau_{kinetic}} = O(\frac{\beta\Gamma_\infty^2}{DC_o})$, and thus the kinetic time scale increases relative to the diffusion scale. Therefore kinetic effects are most evident at the highest concentrations used. In our experiments this was a concentration of $1.9\text{x}10^{-4}$ M. In Fig. 3.5, we plot alongside the diffusion limited simulation and the relaxation in data, the slower diffusive-kinetic simulation in relaxation for the same value of D but a value for β=1 and 10 m^3/(mole-sec). We note from Figure 3.5, that the kinetic-diffusive curve begins to be distinguished from the diffusion limited curve for β>10 m^3/(mole sec) which leads to a lower bound for α equal to 10^{-2} sec^{-1}.

For the case of a spherical bubble of radius a=0.6 mm rising in this glycerol/water mixture at a speed U= 0.03 m/s would give us a minimum Biot number defined as $Bi=\alpha a/U$, of $Bi_{min}=1.55x10^{-4}$. All the properties of $C_{12}E_6$ are summarized in Table 5.1.

3.2.3 Experiments to Study Bubble Rise Velocities

3.2.3.1 Experimental Apparatus

The experimental apparatus we designed to measure bubble rise velocities is given schematically in Figure 3.6. The apparatus consists of two parts, one, a horizontal capillary tube, in which the bubbles are created, and second, a vertical chamber filled with the continuous liquid phase and connected to the tube, in which the bubbles rise and their velocities and shapes are measured by video recording. A train of gas bubbles is created in a horizontal precision bore quartz capillary tube 0.5mm in bore (Wilmad Glass, NJ) by injecting nitrogen into a flowing stream of the continuous liquid phase. The stream is driven by a syringe pump and enters the capillary tube at the "T" junction. The stream flow is set up first. Teflon tubing from a tank to a stainless steel needle inserted in the capillary tube a centimeter past the "T" junction connects pressurized nitrogen. The outer diameter of the needle (.45 mm) fits loosely into the capillary bore, allowing the continuous liquid phase introduced at the "T" to flow in the annular space between the needle and the inside surface of the capillary tube. The inner diameter of the stainless steel needle is .25mm. Between the tank and the capillary tube is a miniature solenoid

valve (Lee Co., CT). Initially the valve is closed, and then is rapidly opened and then closed by application of an electronic pulse. The nitrogen, which is pushed into the stream, flows the needle; as it emerges from the tip of the needle, it is broken into small segments by the liquid flow. Adjusting the gas and the liquid flow rates can control the sizes of the gas segments formed. We find that with this tube insert, we can form segments with equivalent spherical radii as low as .3-.8 mm. After the segments are created, the flow is stopped and one segment is observed under magnification with a stereo microscope (Nikon, NY). The microscope image is video recorded using a CCD camera (Dage MTI, IN) and digitized (using a VG-5 Scion Frame Grabber on a Macintosh G3 computer) to obtain the volume (using the NIH image analysis program). In the small bore capillary tube, except for the smallest bubbles, the segments are axially elongated, and the measurement of the elongation by video capturing provides a more accurate measure of the volume (since the tube is of precision bore) than can be obtained from the videos of the spherical bubble shape in the vertical measuring chamber. Once formed and measured, the syringe pump is used to push the test segment out of the capillary and into the vertical chamber where it begins to rise. The chamber consists of a vertical quartz tube, 25 mm in diameter (Wilmad Glass, NJ) and 70 cm in length. The upper part, where the bubble motion is recorded, is of square cross section to minimize optical distortion. To minimize surfactant contamination, care is taken in the selection of all the materials for the apparatus so that the experimental fluid comes in contact with

only stainless steel or teflon, or a viton polymer (equilibrated with the liquid being used). Contact with the surrounding air is also minimized, and all glassware is cleaned with Nochromix.

For velocity measurements, the bubble motion is recorded with two CCD cameras (Dage MTI, IN), capable of capturing images at a rate of 30 frames/sec. The cameras are located a known distance apart. The first camera is located at a height of approximately 55cm above the tip of the capillary tube from where the bubble starts to rise. A parallel beam of light from a collimating lens provides the back lighting for each camera. The camera is operated in an auto electronic exposure mode to vary the shutter speed from 1/60 to 1/50,000-sec depending on the light intensity. This helps in decreasing the blur caused by the motion of the bubble. The lens on the camera is a Cosmicar television lens f/1.4 25mm adjusted to a magnification of approximately 20X. Both these cameras are connected to the VG-5 Scion Frame Grabber on the Macintosh G3. Instantaneous bubble velocities can be measured at each of the two locations by capturing successive images while the bubble remains in the field of view of the camera. Times of capture for each image are printed on the video frame by the frame grabber board. From the difference in the times that the bubble passes the two cameras, the average velocity can be obtained and checked with the instantaneous measurements to verify the bubble has achieved its terminal velocity. The digitized images were calibrated by using spheres of known size.

Since the viscosity of the liquid being used is a function of temperature, the temperature is carefully monitored in the course of the experiment by having a probe dipped in the quartz cell.

3.2.3.2 Results

Experiments in the pure liquid without surfactant

Our first step is to use our apparatus to measure bubble rise velocities for the system without surfactant dissolved in the continuous phase, and compare these results with previously established theoretical ones. A successful comparison will indicate that our cleaning procedures are adequate, and all our calibrations are accurate. These results will also function as the baseline for our subsequent experiments in which surfactant is added to the continuous phase.

In Figure 3.7 we show the rise velocities of bubbles plotted as a function of their size. These velocities are the average of the three values: two instantaneous velocities from the two cameras at two different heights and the third from the time of rise of the bubble between the two. Since these measurements differ by within a percent, we assume that these bubbles have reached their steady state. We note that the Weber and Capillary numbers (We and Ca) for these bubbles are of orders 10^{-2}, while the Reynolds number Re is of order 1. So we do not expect to see any inertial or viscous effects deforming the bubbles. This is confirmed by the video images of the rising bubbles, which show spherical shapes.

Also plotted in the same figure are the predicted velocities for these sizes from the numerical work of Magnaudet, et al [51]. The drag coefficient $C_{D(BUB)}$ from their simulations for a spherical bubble is given by (for 0<Re<50, and for Capillary and Weber numbers, Ca and We<<1)

$$C_{D(BUB)} = \frac{8ag}{3U^2} = \frac{8}{Re}(1+0.15[2Re]^{0.5}) \quad [3.8]$$

Here Re is the Reynolds number based on the radius of the bubble. The predicted velocities are obtained by solving for U in this equation. From the same authors also see Clift, et al[16] the drag coefficient for a solid sphere $C_{D(SOL)}$ is given by (valid for 0<Re<150)

$$C_{D(SOL)} = \frac{12}{Re}(1+0.15[2Re]^{0.687}) \quad [3.9]$$

We note that, bubbles of sizes only greater than 0.5 mm rise with velocities agreeing with the predicted values. Smaller size bubbles rise with velocities less than the predicted values. The smaller size bubbles could be feeling the presence of trace amount of impurities present in our system even after our thorough cleaning procedure. Hence we consider only the bubbles of sizes greater than 0.5 mm radius for our analysis of the effect of the added surfactant on the rise velocities.

Experiments With Surfactant

The poly-ethoxy surfactant $C_{12}E_6$ ($CH_3.(CH_2)_{11}(OCH_2CH_2)_6OH$) is used in the 70:30 glycerol water mixture. All these experiments are carried out at temperatures in the

range of 24-27^{0}C, and the data interpreted accounting for the changes in viscosity. The experiments are done from very low concentrations from 10^{-3} mg/lit to around 10^3 mg/lit (10 times the CMC of the surfactant). In Figure 3.8, we plot these results of the dimensionless drag C_D^* on the bubble rising in the surfactant solution as a function of the surfactant bulk concentration. The dimensionless drag is defined as $C_D^* = \frac{C_D - C_{D(BUB)}}{C_{D(SOL)} - C_{D(BUB)}}$ with $C_{D(SOL)}$ and $C_{D(BUB)}$ evaluated from equations [3.8] and [3.9] at the corresponding Reynolds numbers Re. The drag coefficient C_D is calculated from the rise velocity U of the bubble as $C_D = \frac{8ag}{3U^2}$. This way, C_D^* gives a value of 0 if the bubble is behaving with a completely stress free interface, while a value of 100 if it has a completely stagnant interface.

As we notice in Figure 3.8, for a bubble of any given size, as we increase the surfactant bulk concentration, its drag increases monotonically from that of a completely stress free interface in a pure liquid, until it reaches that of a completely stagnant interface. Bubbles of all sizes we studied show similar behavior. From a concentration of 0.9 mg/lit of the surfactant, all the bubbles experience a drag close to that of a solid. At lower concentrations they experience drags between these two extremes. This is when the stagnant cap regime is observed, and when the cap does not cover the bubble completely. We also note that in this regime, at any given surfactant bulk concentration, smaller size bubbles behave more solid like than larger size bubbles. As alluded to in Section 2.3 of

Chapter 2 this is because of the larger Marangoni number for the smaller bubbles, which causes a larger viscous stress as given by equation [2.9], and hence a larger drag. Even though the larger bubbles have a higher Peclet number, which should decrease the stagnant cap size and hence decrease the drag, this decrease is offset by the increase in drag due to the larger Marangoni number. This is verified from the comparison of these experimental results with our simulations in Section 3.3.

We also note that at the lowest two concentrations studied, we could expect a change in the bulk concentration of the surfactant solution due to the adsorption of the surfactant at the air/liquid, liquid/glass interface of our apparatus. We calculated this change in the bulk concentration of the surfactant through simple scaling arguments as follows:

Change in bulk concentration≈(surface concentration)(surface area)/(volume of the cell)

With the surface area/volume of our apparatus of 0.0155 m^{-1}, and a surface concentration scale roughly of the order of Γ_∞=4.48 mol/m^2, the change in the bulk concentration comes to 6.9×10^{-8} mol/m^3 (or 3.13×10^{-5} mg/lit) which is two orders less than the lowest concentration used here. Hence this change is negligible.

3.3 Discussion

From the pendant bubble experiments detailed in Section 3.2.2, we noted that we could describe the surface tension relaxation curves with a diffusion limited model for all

the concentrations we studied below the CMC. Using a mixed kinetic diffusive model for the surfactant transport process in this experiment, we could get the lower bounds on the adsorption and desorption rate constants of the surfactant at the air/glycerol-water mixture interface. At and above this lower bound, the effect of kinetic exchange on the surface tension relaxations becomes indistinguishable from the diffusion limited curve.

Using this diffusion coefficient, in our hydrodynamic model (from Chapter 2), we get the effect of the surfactant on the drag of a bubble rising in a quiescent liquid for a diffusion limited transport case. Using the lower bounds for the adsorption/desorption constants (as a minimum Biot number, Bi_{min}), we can get a similar curve for the case of kinetic finite exchange rates. Plotted in Figure 2.9 are such curves for cases when Bi is 1 and 10 times Bi_{min}. It is interesting to see that even though in the dynamic surface tension relaxations, we could not distinguish the effect of kinetic exchange rates for the case corresponding to Bi_{min}, we could clearly distinguish in the present simulations for the drag on the rising bubble.

This difference in these two problems in distinguishing the effects of kinetic exchange rates from the diffusion limited case could be because of the different length scales for diffusion Γ_∞/C_0 ($=2\times10^{-5}$m, under the experimental conditions) for the adsorption at a clean interface with no flow, while $aPe^{-1/2}$ ($=10^{-6}$ m) for the adsorption of surfactant on a rising bubble (of radius a). The order of magnitude decrease in the

diffusive length scale in the case of a bubble rising in a surfactant solution increases the relative magnitude of diffusive transport rate compared to a given kinetic sorption rate. This suggests that under suitable conditions we could use the bubble rise velocity measurements to determine the kinetic constants of the surfactants at the air/liquid interface. For the case of adsorption of surfactant at a clean interface from an initially uniform bulk concentration C_0, as in the case of experiments with a pendant bubble apparatus, the relative time scales of the diffusive transport and kinetic exchange processes is given by Φ^2 defined as

$$\Phi^2 = \frac{\tau_d}{\tau_{kinetic}} = \frac{\beta\Gamma_\infty\left(\frac{\Gamma_\infty}{C_0}\right)}{D} \text{ for } k=\beta C_0/\alpha >>1 \qquad [3.10]$$

Pan et al[61] showed that in the dynamic surface tension relaxations, the effects of the kinetic exchange rates become distinguishable from the diffusive transport rates of the surfactant in the surface tension relaxations when Φ^2 is smaller than 10. On similar lines, for the case of bubble rising in a surfactant solution, we see that this ratio becomes

$$\lambda^2 = \frac{\tau_d}{\tau_{kinetic}} = \frac{\chi}{Pe^{1/2}Bi} = \frac{\beta\Gamma_\infty\left(aPe^{-1/2}\right)}{D} \text{ for all k} \qquad [3.11]$$

Unlike Φ^2, λ^2 is independent of the surfactant bulk concentration. From our simulations shown in Figure 3.9, under the experimental conditions, we see that all low surfactant bulk concentrations ($k<<1$), the curves corresponding to the cases of Biot numbers of 10^{-3}

and 10^{-2} are close to the predictions of a diffusion limited case, and are essentially indistinguishable from the latter. The values of λ^2 corresponding to these Biot numbers are listed in Table 3.2. We see that the effect of kinetics could be distinguished from a diffusion limited case for λ^2 less than 6.9×10^{-3}. Under these conditions, these kind of studies could be used as a tool for determining the adsorption and desorption rate constants of a surfactant at the air liquid interface.

Table 3.2 shows the experimental data of the drag on bubbles of different radii, rising in surfactant solutions at the lowest two concentrations of the surfactant. At these concentrations the stagnant cap conditions are attained ($\frac{\chi(e^{K\frac{\Gamma_e}{\Gamma_\infty}}+k)}{Pe^{1/2}} << 1$). Hence the steady state experimental dimensionless drag lies between 0 and 100. Also shown are the different dimensionless groups for these cases. Assuming that the effect of Reynolds number is negligible in this range studied, we also present the results of our simulations (for Re=0.91, and χ=0.12) for the diffusion limited, and the finite kinetic exchange case(for $Bi=Bi_{min}$ and $10*Bi_{min}$) at the different experimental Marangoni and Peclet numbers. These values are obtained by running the simulations and obtaining curves like Figure 3.9 for each of the set of non dimensional numbers corresponding to the experimental conditions. Then the drags for the different cases of surfactant transport (finite Bi and diffusion limited case) are read out at each of the two surfactant bulk

concentrations studied. We see that the experiments lie close to the predictions of the simulations with $Bi=Bi_{min}$, at these two different bulk concentrations of the surfactant. Hence the lower bounds on the adsorption/desorption rate constants as predicted from the pendant bubble experiments seem to be close to their exact values.

3.4 Conclusions

As part of our study of the effect of trace amount of surfactants on the drag of a bubble rising due to buoyancy, in this chapter we detail our experimental work. In this work, a poly-ethoxy surfactant $C_{12}E_6$ is used in a 7:3 mixture of glycerol and water. First with a pendant bubble apparatus, from the dynamic surface tension relaxations at a clean interface, the kinetic exchange rate constants at the air/liquid interface, and the bulk diffusion coefficients are determined. We note that while the exact value of the diffusion coefficient could be determined, only a lower bound on the adsorption desorption rate constants could be determined from this technique.

Then experiments to study the effect of the low concentrations of surfactant on the drag coefficient of a bubble rising due to buoyancy are conducted. The hydrodynamic experimental results are compared with the results from our numerical simulations carried out using the kinetic parameters from the dynamic surface tension relaxation experiments. This shows that in the stagnant cap regime, the drag on the rising bubble could be well described by our model with finite kinetic exchange change. Also the lower bounds on the adsorption/desorption rate constants for the surfactant at the air/liquid

interface determined from a pendant bubble apparatus seem to be close to their exact actual values.

For the first time such experiments involving monitoring the drag on a rising bubble in a stagnant cap regime have been used to zero in on the kinetic rate constants of the surfactant at the air-liquid interface. Theoretical analysis shows that these experiments could be used to zero in on the rate constants over a larger range of ratios of kinetic to diffusive rates of surfactant transport, compared to the monitoring of dynamic surface tension relaxations at an initially clean interface.

Table 3.1: Values of λ^2 used in the simulation

Bi	$\lambda^2=\chi/(Pe^{1/2}Bi)$	
$Bi_{min}(1.55x10^{-4})$	0.69	
$10*Bi_{min}$	0.069	Effect of Kinetic Exchange becomes indistinguishable from Diffusive Transport
$100*Bi_{min}$	0.0069	

Table 3.2: Comparison of experiments with simulations in the stagnant cap regime

Bubble Radius (mm)	Re	Ma	Pex10^{-6}	χ	Dimensionless Drag			
					Expt.	Simulation		
						Diffusion Limited	10*Bi_{min}	Bi_{min}
k=0.0024								
0.555	1.23	12.7	1.1	0.127	**35**	38.4	38.4	24
0.611	0.83	10.4	1.34	0.124	**27.8**	33.7	30.6	18.3
0.626	0.88	10.0	1.42	0.127	**28.7**	32.3	29.7	17.3
0.73	1.44	7.14	2.33	0.148	**17.0**	29.3	27.5	16.0
k=0.024								
0.619	0.81	12.2	1.3	0.125	**71.7**	83.2	82.3	68.8
0.605	0.76	12.6	1.24	0.123	**70.0**	84.3	84.3	70.7
0.635	0.83	11.5	1.34	0.129	**70.2**	81.6	79.3	67.9
0.693	1.1	9.58	1.86	0.14	**58.2**	75.8	74.2	62.0

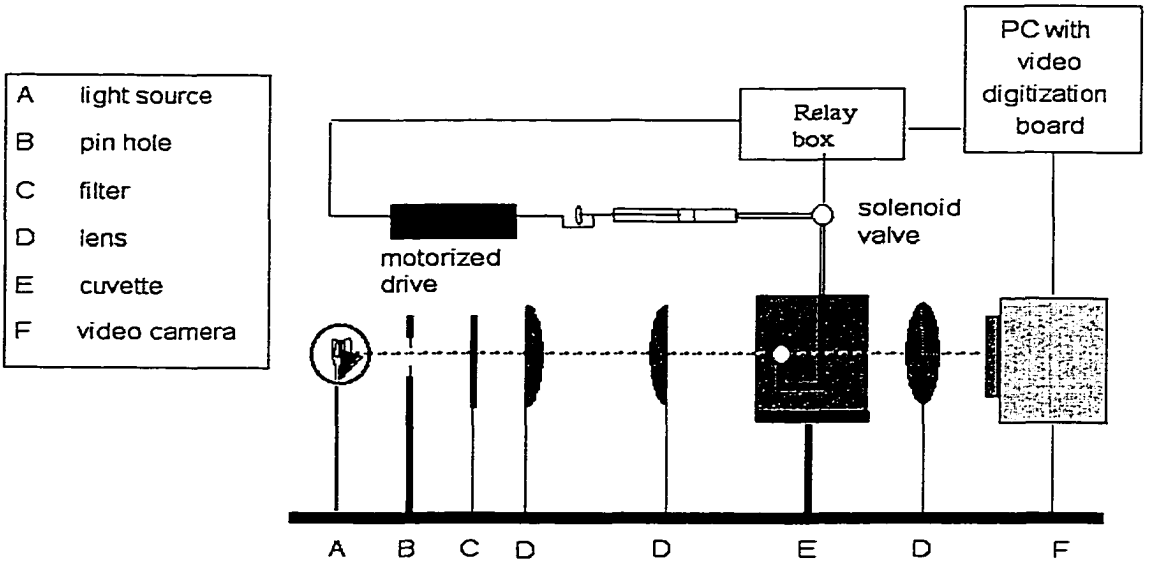

Figure 3.1: Schematic of the pendant bubble technique for the measurement of dynamic surface tension.

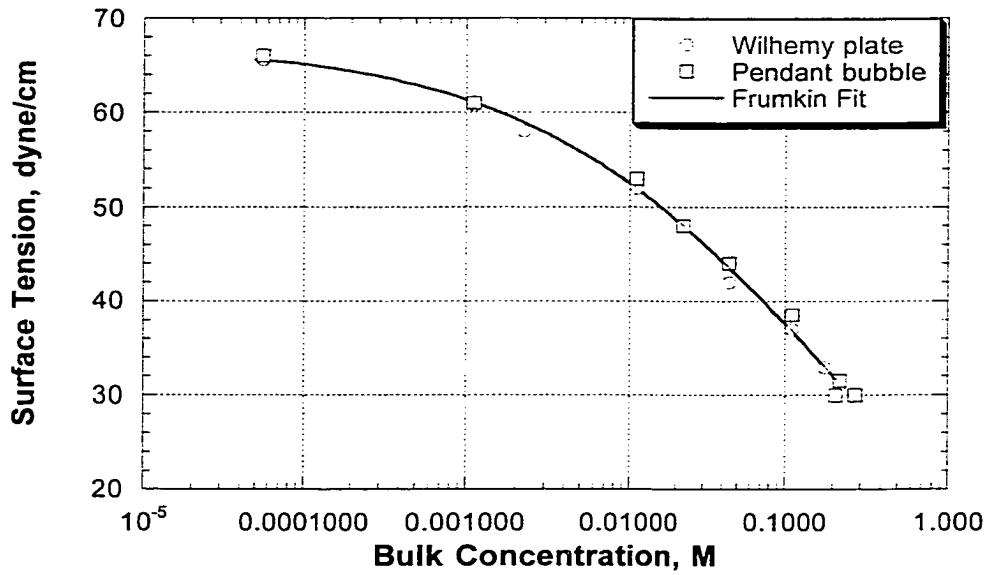

Figure 3.2: Measurements of the equilibrium tension of glycerol/water surfactant solutions of $C_{12}E_6$ at the air/ glycerol-water interface and the Frumkin fit of this data.

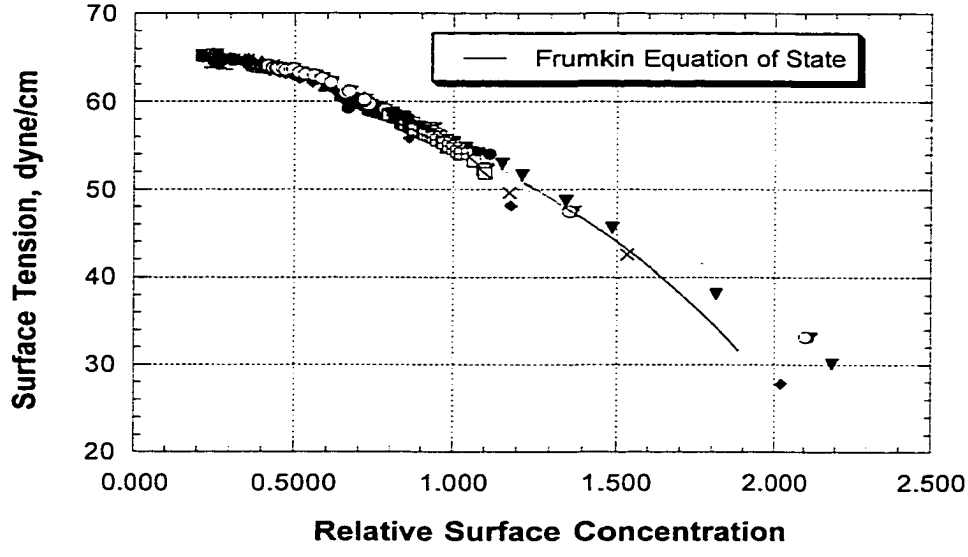

Figure 3.3: Surface Tension as a function of the actual surface concentration divided by the surface concentration at a tension of 55.1 dyne/cm for $C_{12}E_6$ at the air/ glycerol-water mixture interface. Also shown is the prediction of the Frumkin equation of state with parameters obtained from the fitting of the equilibrium tension-bulk concentration measurements of Figure 3.2.

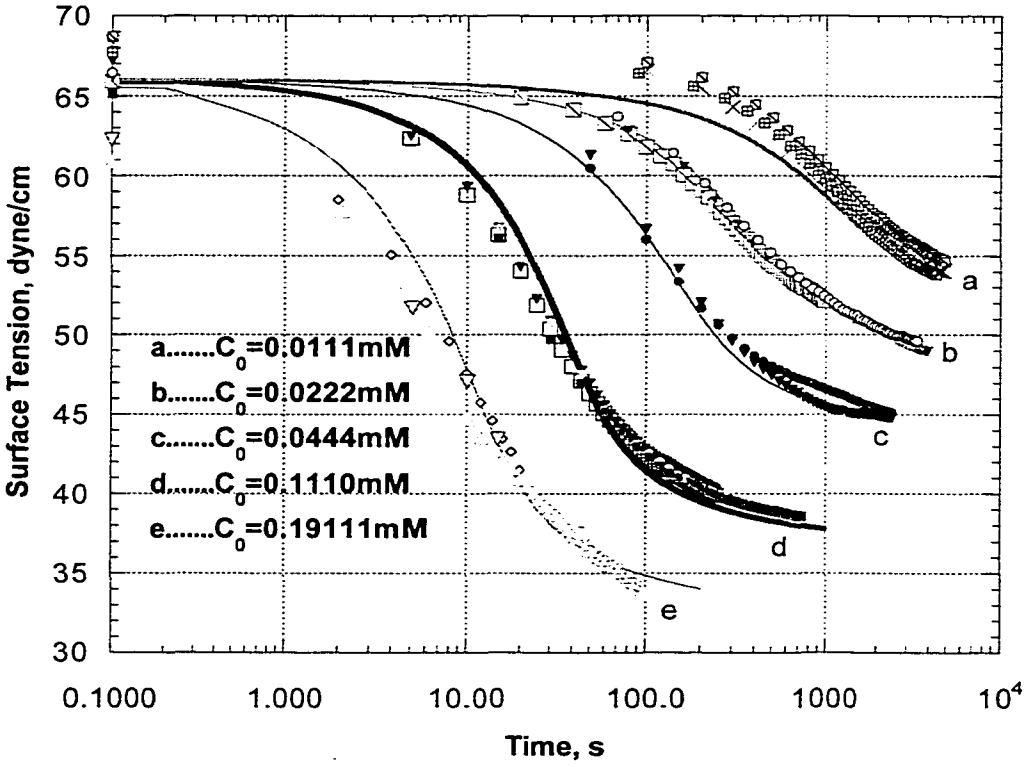

Figure 3.4: Dynamic surface tension relaxations for adsorption of $C_{12}E_6$ at an initially clean air/ glycerol-water mixture interface as measured by the pendant bubble technique. The continuous lines are fitted diffusion-limited simulations of the relaxation for a value of D equal to 1.5×10^{-11} m^2/sec.

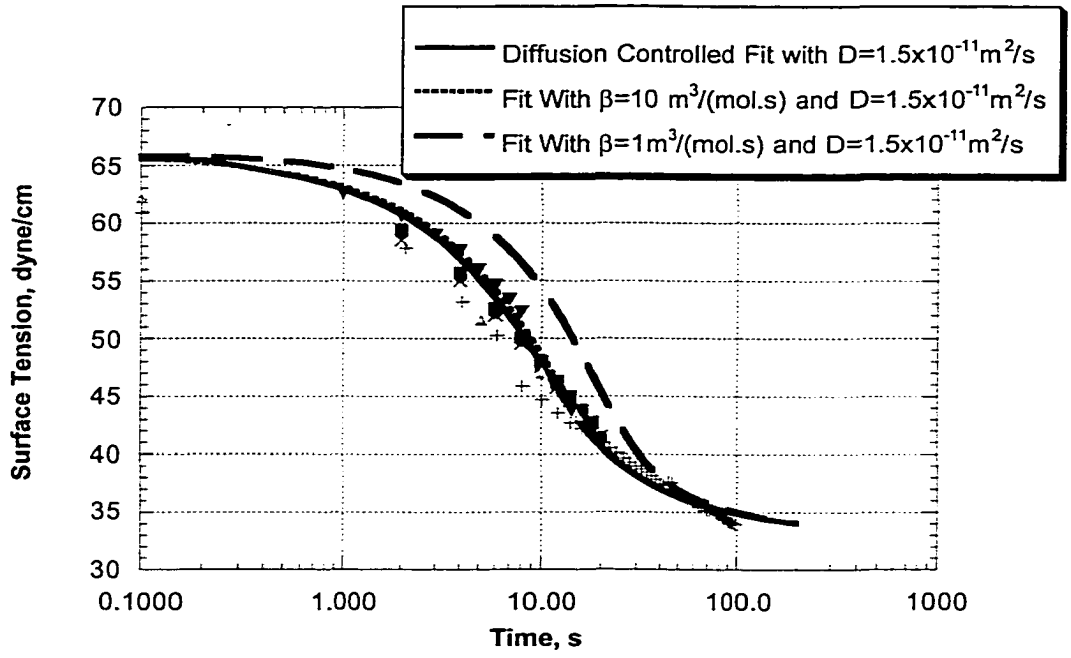

Figure 3.5: Dynamic tension relaxations for $C_{12}E_6$ at the air/ glycerol-water surface, the diffusion limited simulation, and kinetic-diffusive simulations for three values of the kinetic rate constant β.

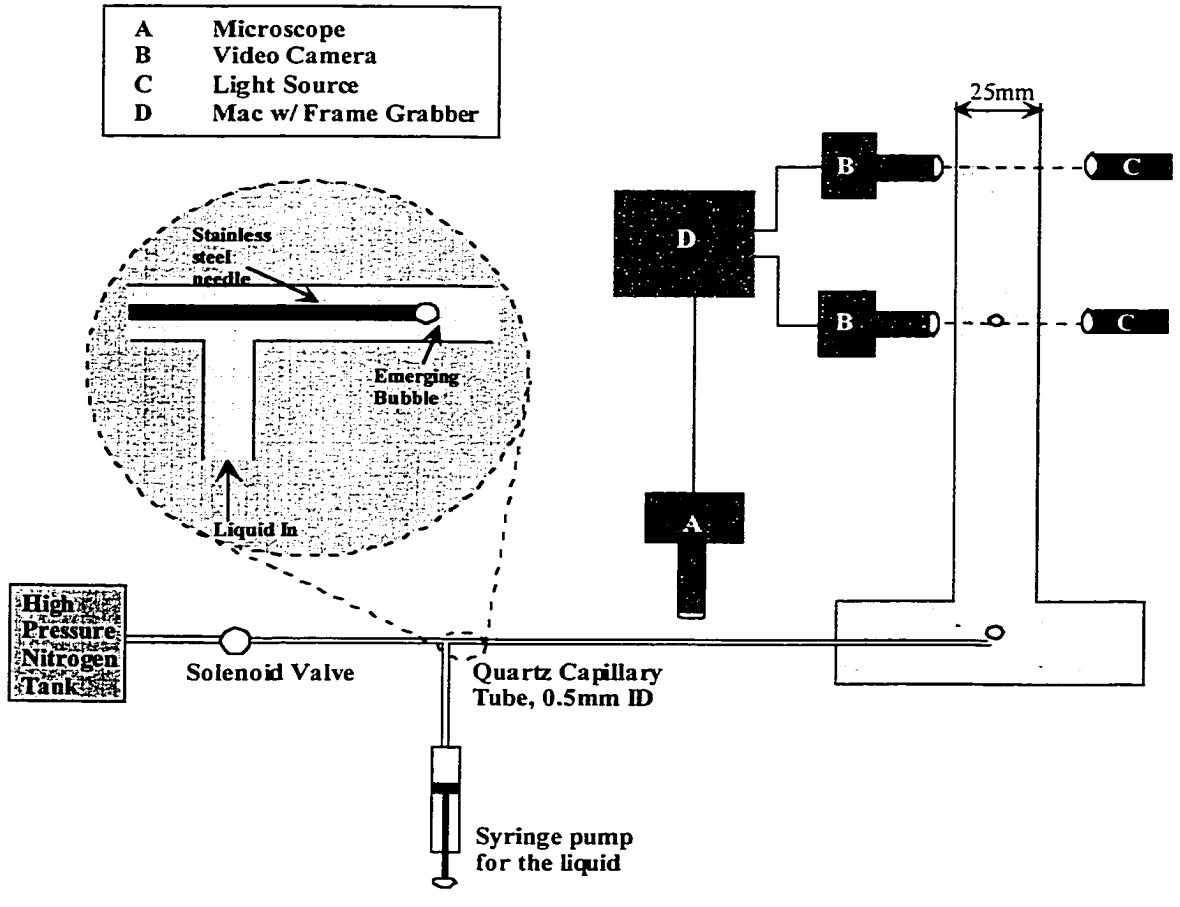

Figure 3.6: Experimental Apparatus for the Measurement of Bubble Rise Velocities.

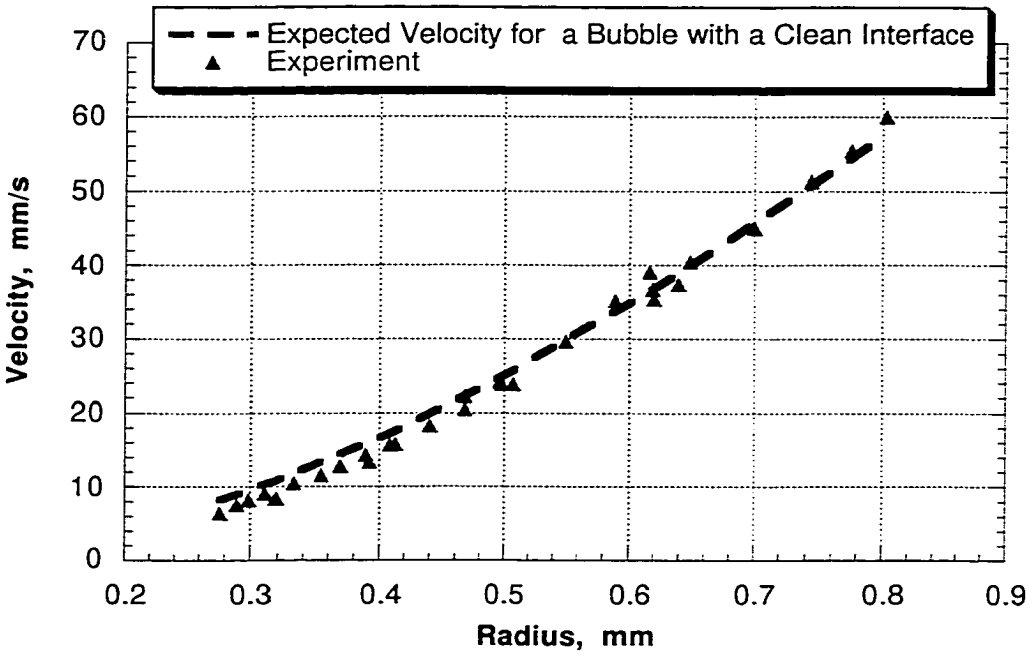

Figure 3.7: Bubble Rise Velocities in a surfactant free 70:30 glycerol/water mixture- Comparison with the theoretical prediction by equation [3.8].

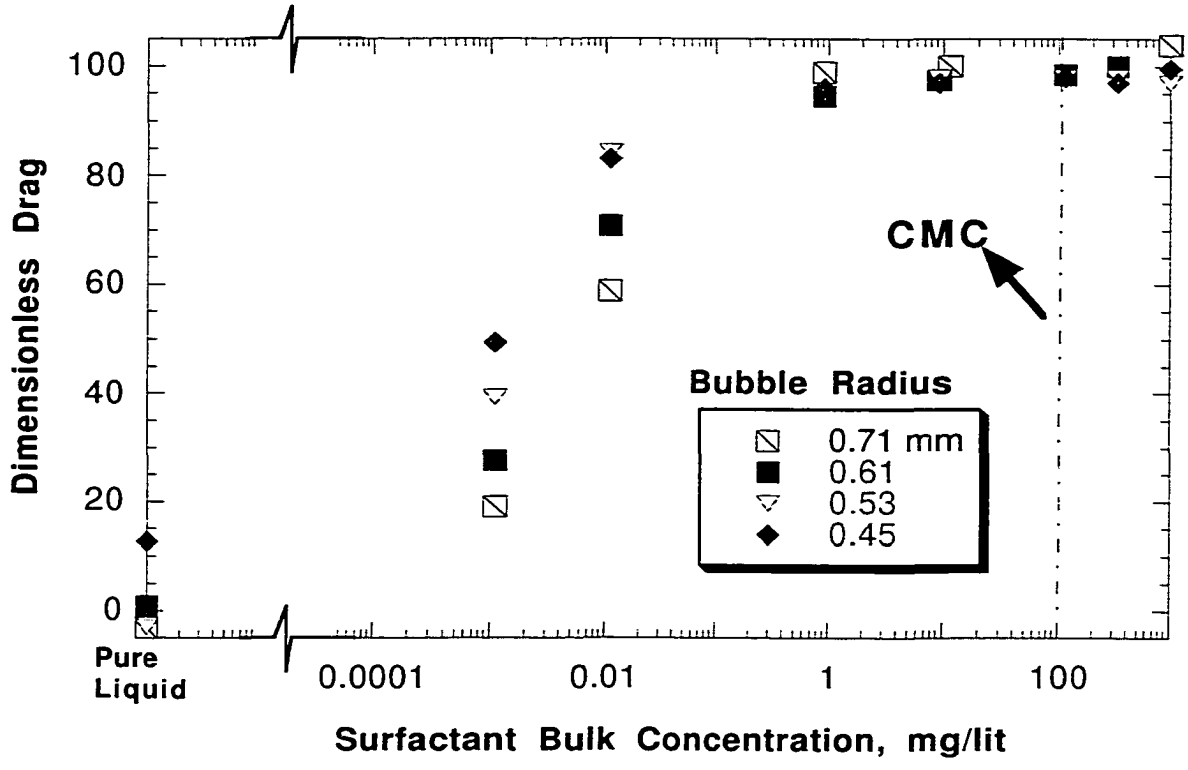

Figure 3.8: Effect of $C_{12}E_6$ Concentration on the Drag of a Rising Bubble.

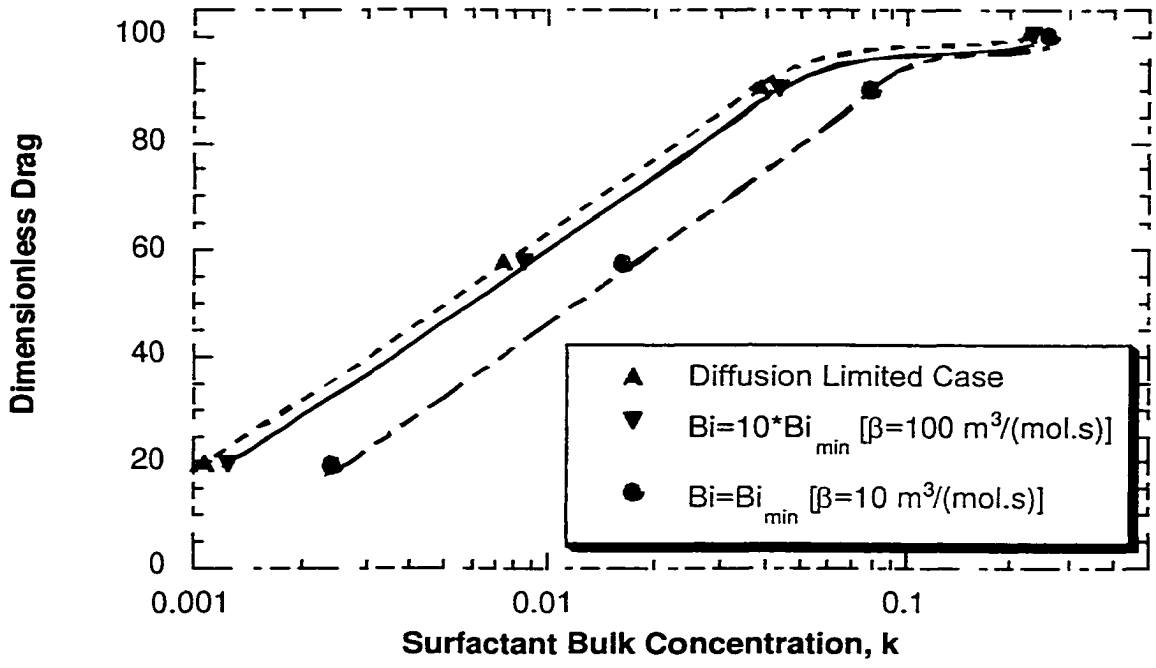

Figure 3.9: Effect of Surfactant Concentration on the Drag of a Rising Bubble-Distinguishing the effect of kinetic exchange rates from the diffusive transport rates of the surfactant.

CHAPTER 4
A Theoretical Study of the Hydrodynamics of Remobilization of a Surfactant Laden Interface at High Peclet Numbers and with Kinetic Barriers

4.1 Introduction

Interfacial flows are greatly influenced by the surfactants present in the surrounding bulk phases. The time scales over which the surfactants reach the bulk sublayer close to the interface and exchange with the interface, relative to the hydrodynamic time scale, govern the extent of this influence. The time scale over which the surfactants reach the bulk sub layer is typically governed either by diffusion (in the case of no flow) or convection (in the case of flow). The time scale over which the surfactant exchanges with the interface from the bulk sublayer depends on the adsorption and desorption rate constants. From the arguments presented in Chapter 1, for a surfactant following Frumkin type kinetics at the air/liquid interface, the rates of these transport processes relative to the convective rates on the bubble surface are given by the following quantities.

$$\Lambda_D = \frac{\text{rate of diffusion}}{\text{rate of convection}} \approx \frac{\Delta C}{C_o}\frac{\chi(e^{K\frac{\Gamma_e}{\Gamma_\infty}}+k)}{Pe^{1/2}}$$

$$\Lambda_K = \frac{\text{rate of kinetic exchange}}{\text{rate of convection}} \approx Bi\left[e^{K\frac{\Gamma_e}{\Gamma_\infty}}\frac{\Delta C}{C_o} - \left(\left\{K\frac{\Gamma_e}{\Gamma_\infty}+1\right\}e^{K\frac{\Gamma_e}{\Gamma_\infty}}+k\right)\frac{\Delta\Gamma'}{\Gamma_e}\right]$$

As mentioned in Section 1.3, when either Λ_D or Λ_K<<1, the surfactant transport limitations (bulk diffusion or surface kinetic exchange) create surface concentration gradients of the surfactant on a moving interface (of a bubble). This creates a surface tension gradient on the interface, which creates a surface stress that retards the interfacial flow. We observed this surfactant induced retardation both theoretically and experimentally in Chapters 2 and 3 respectively, in the case of a spherical bubble rising in a surfactant solution. We also noted in Section1.4 that through scaling arguments that when both Λ_D and Λ_K >>1, i.e., when we could eliminate the diffusional and kinetic exchange barriers for surfactant transport we could in fact remobilize a surfactant laden interface. Λ_D>>1 can be achieved large surfactant bulk concentrations (k>>1) when the surfactant is highly soluble in the bulk phase when $\frac{\chi\,(e^{K\frac{\Gamma_e}{\Gamma_\infty}}+k)}{Pe^{1/2}}$ becomes large, while Λ_K >>1 can be achieved when $Bi(k+e^{K\frac{\Gamma_e}{\Gamma_\infty}})$>>1, when the surfactant adsorbed at the interface rapidly exchanges with the bulk at these high bulk concentrations. Thus the three conditions for remobilization are:

* k>>1 (high bulk concentration)

* kBi>>1 and Bie^K >>1 (rapid kinetic exchange relative to convection)

* $\frac{\chi k}{Pe^{1/2}} >> 1$ (rapid diffusive exchange relative to convection)

At high surfactant bulk concentrations(k>>1), we noted that the retarding force on a bubble rising in a surfactant solution scales as $\tau_m \approx Ma\left[\frac{1}{Bie^K}+\frac{Pe^{1/2}}{k\chi}\right]$ where Ma is the Marangoni number. When complete remobilization of the interface is achieved, this retarding force on the bubble goes to zero. The extent of remobilization achieved when the diffusional barriers are eliminated (when $\frac{\chi k}{Pe^{1/2}} >> 1$ at k>>1) depends on how fast the kinetic exchange rates are as characterized by Bie^K. These observations are supported by the studies of Chen & Stebe[42,43] which deal with the kinetically limited surfactant transport ($Bie^{K\frac{\Gamma_e}{\Gamma_\infty}} \approx 1$, and $\frac{\chi\,(e^{K\frac{\Gamma_e}{\Gamma_\infty}}+k)}{Pe^{1/2}} \to \infty$). Wang, et al[31,32] consider the case of diffusion limited surfactant transport with fast kinetics (i.e., at $Bie^{K\frac{\Gamma_e}{\Gamma_\infty}} \to \infty$, and $\frac{\chi\,(e^{K\frac{\Gamma_e}{\Gamma_\infty}}+k)}{Pe^{1/2}} \approx 1$), and observe that the drag on a spherical bubble initially increases with increasing bulk concentration, and on further increase in bulk concentration, reduces and again reaches the clean interface value. These simulations are done till Peclet numbers of the order of 100. As observed in Chapter 1, in any physical liquid system transport of the surfactant in the bulk is characterized by large Peclet number of the order of 10^6.

Hence we see that there is no work that has been done on the effect of the surfactants on the motion of bubble at high bulk concentrations, in any realistic regime of

interest, i.e., finite Bi, and large Peclet numbers. Cuenot, et al [39] consider the case of finite Bi and large Peclet numbers, but work only in the regime of low bulk concentrations, where remobilization is not possible. In this chapter, we address the theoretical aspects of this particular case of the motion of a spherical bubble in a liquid containing the surfactant at high bulk concentrations, whose bulk transport is characterized by high Peclet numbers (of the order of 10^6) and which has finite kinetic exchange rates at the air/liquid interface ($Bie^{K\frac{\Gamma_e}{\Gamma_\infty}} \approx 1$, and $\frac{\chi\,(e^{K\frac{\Gamma_e}{\Gamma_\infty}}+k)}{Pe^{1/2}} \approx 1$).

In Section 4.2, first we allude to the formulation of the model problem for the flow past a spherical bubble rising in a surfactant solution, described in Section 2.2. Next we present our approach in solving the governing equations for the hydrodynamics and surfactant transport taking care of the finite rates of transport of the surfactant by diffusion in the bulk and kinetic exchange at the interface. In Section 4.3, we discuss the results from our simulations, which verify the above scaling arguments and in particular discuss the effect of high Peclet numbers and the finite kinetic exchange rates on the mobility of a bubble in a surfactant solution. Finally we present our conclusions in Section 4.4.

4.2 Formulation and Numerical Solution

4.2.1 Hydrodynamic Model and Governing Equations

The same model described in Section 2.2 of Chapter 2 is used. The only difference being, we completely solve the flow (Eqs. [2.1] and [2.2])and surfactant transport equations [2.3] and [2.7] with the boundary conditions [2.6],[2.8],[2.9] and [2.10], instead of using the stagnant cap model with boundary conditions[2.13].

4.2.2 Spatial Approximations

The governing equations are discretized in the same way as described in Section (2.3.1) using the finite volume method using a staggered grid. The same spatial approximations as described there in are used.

4.2.3 Grid Characteristics

An exponential grid as described in Section (2.3.2) is constructed for solving the flow equations. The following are the differences followed in this solution compared to the stagnant cap solution. To avoid any artificial confinement of the flow by the outer boundary, the outer limit of the grid is fixed at 80 bubble radii. The same 80 radii outer limit is used for the surfactant bulk concentration also. A 25x25 exponential grid in (r,θ) is used for the flow equations in all the simulations we did unless otherwise stated. For the solution of the surfactant bulk transport equation, we put a fine mesh (linear in r), containing ten grid points in a distance of $Pe^{-1/2}$ from the surface of the bubble at r=1, along with an exponential grid described before. So we have a 35x25 grid for the solution

of the surfactant bulk transport. Also we use interpolated velocities (by linear interpolation) at the nodes of the fine mesh in this boundary layer region.

4.2.4 Algorithm for the Numerical Solution

We use the following algorithm for this problem in contrast to the algorithm presented earlier in Section (2.3.3) for the stagnant cap regime. The steady state solution for the complete set of governing equations with the boundary conditions is obtained by solving them in the unsteady form and advancing in time till steady state is reached. For the time advancement of the governing equations, ADI (Alternating Directions Implicit Method) scheme is employed, which is second order accurate in time. The following algorithm is used for the time advancement.

1) Start with initial values of u, v, C and Γ.

2) Using the momentum equations the velocities u and v are advanced in time Δt. For this step, the fractional step method is used. Time advancement by Δt from time n to $n+1$ is achieved in two steps.

   * In the first half, the momentum equations are considered without the pressure gradient term.

$$\frac{\mathbf{V}^* - \mathbf{V}^n}{\Delta t / 2} + \nabla.(\mathbf{V}^n\mathbf{V}^* - \frac{1}{\mathrm{Re}}\nabla\mathbf{V}^*) = 0$$

   Here $\mathbf{V}^*$ is the intermediate velocity.

* The pressure gradient term is considered only in the second half. The pressure at time $n+1$, P^{n+1} is calculated from the fact that the velocity at time $n+1$, $\mathbf{V}^{n+1}$ is divergence free.

$$\frac{\mathbf{V}^{n+1}-\mathbf{V}^{*}}{\Delta t/2}+\frac{1}{Re}\nabla P^{n+1}=0$$

$$\nabla.\mathbf{V}^{n+1}=0 \Rightarrow \nabla^2 P^{n+1}=\frac{2Re}{\Delta t}\nabla.\mathbf{V}^{*}$$

In this Poisson equation for the pressure at time $n+1$, the right hand side is known. This equation is written in the discretized form by integrating both sides over each of the pressure cells. No special boundary conditions are needed for the pressure at this step because of the employment of the staggered mesh.

Also, in this step, the tangential stress condition [2.6] on the surface of the bubble is based on the values of $\Gamma(\theta)$ at the previous time n, i.e.,

$$\tau^{n+1}{}_{r\theta}\,|_{r=1}=Ma\left[\frac{1}{1-\Gamma^{n}}+K\Gamma^{n}\right]\frac{\partial\Gamma^{n}}{\partial\theta}$$

3) The velocities at the grid points of the fine linear mesh near the surface of the bubble are calculated by linear interpolation.

4) Using the surfactant transport equation, the bulk concentration of the surfactant C is advanced by time Δt. Here also the boundary condition [2.8], is based on the values of $\Gamma(\theta)$ at the previous time n, i.e.

$$\frac{\chi k}{Pe}\frac{\partial C^{n+1}}{\partial r}\Big|_{r=1} = Bi\left[kC^{n+1}\Big|_{r=1}(1-\Gamma^n) - e^{K\Gamma^n}\Gamma^n\right]$$

5) With the conservation equation, for the surfactant on the bubble surface, the values of $\Gamma(\theta)$ are advanced by time Δt.

6) The steps (2), (3), (4) and (5) are repeated till convergence to a steady state is achieved. There are two criteria for convergence. The first criteria is that the relative change over 50 time steps in the values of u, v, and C at each of the node points differ by less than 10^{-2} percent. The second criterion derives from the fact that the net flux of surfactant to the bubble at steady state is equal to zero. This relation follows by integrating the conservation equation [2.7] over the surface of the bubble. Thus:

$$Nu = \int_0^{\pi}\frac{\partial C}{\partial r}\Big|_{r=1}\sin\theta d\theta = 0$$

where Nu defines the overall Nusselt number. We require that the absolute value of Nu be smaller than 0.1; although this may not seem commensurate with the convergence criteria on the node values, because Peclet numbers are large small deviations from the exact solution give large values for the Nusselt number. For example, at the beginning of the simulations, Nu is of order 10^3.

In the limits $Pe_s >> 1$ and either $Bie^{K\Gamma} << 1$ and $Bik << 1$ or $\frac{\chi(e^{K\Gamma}+k)}{Pe^{1/2}} << 1$, which are satisfied at low concentrations of the surfactant, the diffusive transport to the interface

and the kinetic exchange at the interface are much slower than the convective transport along the surface of the bubble. Under these conditions, the stagnant cap regime is attained, when all the surfactant adsorbed on the bubble surface is swept to the back end where it forms a cap region. In this regime, we found that due to the steep gradients in the shear stress and the surfactant surface concentration it's difficult to achieve the steady state solution with the above algorithm. So we used a different procedure as detailed earlier in Section 2.3.3 in Chapter 2 in this regime till the surfactant covers the bubble surface completely.

4.2.5 Model Validation

We described some of the tests done on our code in Section 2.3.4 of Chapter 2. The results presented here for the solution of the full flow equations coupled with the bulk surfactant transport, are solved on a 25x25 node exponential grid for the velocity variables while on this exponential grid couple with a fine grid (as described before) for the surfactant bulk concentration. Solving the same problem on a similar grid but with 40x40 node points on the exponential grid gave results, which are within 3% accurate. We found further grid refinement computationally very expensive, due to the long times taken to achieve steady state. At intermediate surfactant concentrations ($k=10^3$-10^4), the surfactant transport takes long time to reach steady state. For high surfactant concentrations $k=10^5$, though the steady state could be achieved faster in terms of real times, the equation [2.7] becomes very stiff. This could be solved only by taking smaller

type steps $\Delta t(\sim 10^{-6})$, and hence large number of iterations are needed to attain steady state.

4.2.6 Choice of Physical Parameters for the Simulations

The choice of the physical parameters is dictated by our experiments. As we described earlier in Chapter 3 and will again later in Chapter 5, we consider the case of spherical air bubbles of radii around 0.6 mm rising in a 7:3 by volume mixture of glycerol/water. Polyethoxy surfactants $C_{12}E_6$ ($CH_3(CH_2)_{11}(-OCH_2CH_2)_6$-OH)) and $C_{10}E_8$ ($CH_3(CH_2)_9(-OCH_2CH_2)_8$-OH)) dissolved in this liquid has the properties listed in the Table 5.A.1 in Chapter 5. Table 5.1 gives the values of the non dimensional numbers under these conditions for $C_{12}E_6$ and these are the ones considered for the work in this chapter.

4.3 Results and Discussion

In this section we describe the results of our numerical simulation, for the combined problem of bubble hydrodynamics and surfactant transport. First we consider the case of the diffusion limited transport of the surfactant, and when the surfactant follows the simple case of Langmuir type kinetics, i.e., when K=0 in equation [2.5]. In Figure 4.1 we plot the surfactant surface concentration profiles, while in Figure 4.2 the surface velocity profiles on the bubble for various surfactant bulk concentrations. We note that as we add a little amount of surfactant say $k=2.15\times10^{-3}$, the surfactant adsorbed

is swept to the back end of the bubble while the front end remains clean as in Figure 4.1. As shown in Figure 4.2, the front end of the bubble surface remains mobile while the back end remains stagnant. This is in the stagnant cap regime when $\frac{\chi(e^{K\frac{\Gamma_e}{\Gamma_\infty}}+k)}{Pe^{1/2}} << 1$. As we add more and more surfactant (say, till $k=2.6x10^2$) we note that the bubble gets more and more uniformly covered by the surfactant, and the surface of the bubble loses its mobility. The finite surface concentration gradients on the bubble create finite shear stresses close to that of a solid sphere. As we increase the surfactant bulk concentration further, say at $2.6x10^2$, we note that the bubble surface gets even more uniformly populated by the surfactant with the surface concentrations approaching close to their maximum packing values and the surface concentration gradients almost disappear. We also note from Figure 4.2 that the bubble surface starts to regain its lost mobility. This is when the remobilization sets in. Under these conditions, the diffusive transport limitations just start to be over come ($\frac{\chi(e^{K\frac{\Gamma_e}{\Gamma_\infty}}+k)}{Pe^{1/2}}$ becomes large, actually =0.5 at $k=2.6x10^3$). As more and more surfactant is added diffusive limitations are further removed. Hence more and more surface mobility is gained back and the bubble surface becomes more and more stress free. These changes in the mobility on the bubble surface modify the drag experienced by the bubble as shown in Figures 4.3. Here we plot variation of the drag experienced by the rising bubble (in the form of the dimensionless

drag as defined before) as a function of the surfactant bulk concentration. In the diffusion limited case we note that with increasing surfactant bulk concentrations, initially within a narrow range of surfactant concentrations, the drag on the bubble increase from that of a clean interface stress free value to the completely stagnant interface solid like value. In this range of concentrations, the stagnant cap regime is exhibited. Further increase in surfactant concentration above k =0.1 does not change the drag on the bubble from the solid like value over a range of concentrations, till k is order of 10^2. At further higher concentrations when k is order 10^3, the diffusive transport rates of the surfactant overwhelm the surface convection rates as $\frac{\chi(e^{K\frac{\Gamma_e}{\Gamma_\infty}}+k)}{Pe^{1/2}} \approx \frac{\chi k}{Pe^{1/2}}$ becomes large. Then remobilization sets in as noted before with the scaled dimensionless drag on the bubble relaxing and falling below the solid like value. Further increase in surfactant concentration remobilizes the surfactant laden bubble surface further, as shown by the drag falling closer to the stress free value. This verifies theoretically the remobilization arguments, which noted that the dimensionless drag scales as $\tau_m \approx Ma\frac{Pe^{1/2}}{k\chi}$ for the diffusion limited case. We carried out our simulations till k of the order of 10^4. At this value of k, we need time steps as small as 10^{-6} to solve the full systems of governing equations, especially equation [2.7], which becomes very stiff at these high values of k. For the solution of the equations at higher values of k, we would need even smaller of

time steps, which could cause numerical inaccuracies. We emphasize the fact that due to the high Peclet numbers, very low surfactant bulk concentrations are enough to completely cover the bubble surface initially and give a solid like behavior. Also due to the same high Peclet numbers, we need very high surfactant bulk concentrations to remobilize the bubble surface, since we need $\frac{\chi(e^{K\frac{\Gamma_\infty}{\Gamma_\infty}}+k)}{Pe^{1/2}} \approx \frac{\chi k}{Pe^{1/2}}$ to be very large. Hence we see a large range of surfactant bulk concentrations when the drag on the bubble remains close to that of a solid like value.

Consider next the case of finite kinetic exchange rates (when the Biot number is finite). In Figure 4.3 we show the results for this case for two different Biot numbers, $Bi=10^{-3}$ and 1. For any Biot number, at low surfactant bulk concentrations, a stagnant cap behavior is observed as noted before in the diffusion limited case. The drag on the bubble increases with the addition of surfactant. At any given surfactant bulk concentration, less surfactant is adsorbed on the bubble surface than compared to a diffusion limited case, and hence less drag on the bubble. With further increase in concentration, the bubble surface is completely covered by the surfactant giving a stagnant interface like a solid. We have seen that for $k>10^3$ and infinite kinetic exchange, the diffusion limitation relaxes, and the bubble surface once covered completely with a stagnant monolayer is now partially mobile. But for finite values of Bi, the kinetic exchange is reduced relative to surface convection, and adsorbed surfactant at the front end is swept to the back end

increasing the surface concentration gradient, reducing the surface velocity and increasing the drag relative to the diffusion limited case. According to the scaling arguments we presented in Section 1.4, at large surfactant bulk concentrations (k>>1), the dimensionless drag scales as $\tau_m \approx Ma\left[\frac{1}{Bie^K}+\frac{Pe^{1/2}}{k\chi}\right]$, and the interface does not remobilize with increasing k unless Bie^K becomes much larger than one. We see that for $Bi=10^{-3}$, we do not see any remobilization of the interface in the range of k studied (till order of 10^4). Even as the diffusion limitation disappears with increasing k, the kinetic barrier does not allow the interface to remobilize. As Bi increases, the kinetic limitation decreases and greater remobilization is achieved as seen for the case of Bi=1. At higher surfactant bulk concentrations k, when kBi becomes large, the drag on the bubble is less when Bi=1 than when $Bi=10^{-3}$. Larger values of Bi would yield progressively greater remobilization, with the diffusion limited case providing the limit of remobilization achievable at any given bulk concentration k.

As shown in Figure 4.4, similar behavior is observed for the case when the surfactant follows a Frumkin type kinetics (K is non zero=5.47 in this case).

4.4 Conclusions

When a bubble rises in an infinite liquid containing surfactant, the transport rates of surfactant from (to) the bulk to (from) the bubble surface (both by bulk diffusion and kinetic exchange at the interface) relative to the surface convection, creates a surface

concentration gradient of the surfactant on the bubble surface. This creates surface stresses increasing the drag on the rising bubble from that of a stress free clean interface value. This surface concentration gradient of the surfactant can be eliminated when the surfactant transport rates (both by bulk diffusion and kinetic exchange) are faster than the surface convection rates. This could be achieved by using a surfactant in high bulk concentrations if it has rapid kinetic exchange rates at these high bulk concentrations. Under these conditions the drag on the rising bubble could be brought back to that of a clean interface stress free value.

In this chapter, we have reported a full numerical study to verify the above effect of soluble surfactants on the motion of a spherical bubble in an infinite liquid at order one Reynolds number, under realistic conditions of high Peclet numbers and finite surfactant kinetic exchange rates. Computations for the case of diffusion limited surfactant transport show that, due to the high Peclet numbers, even trace amount of surfactant (k~0.1 under the conditions of the present simulations) could transform an initially clean stress free interface to a completely stagnant solid like surface. Also due to the same reason, we need high surfactant bulk concentrations (here k of the order of 10^3) to overcome the diffusive transport limitations (when $\frac{\chi(e^{K\frac{\Gamma_e}{\Gamma_\infty}}+k)}{Pe^{1/2}}$ is made large) to remobilize the surfactant laden bubble surface. Hence we see a wide range of surfactant bulk concentrations when the drag on the bubble remains at the solid like value once the

stagnant cap on the bubble completely covers it. Once the remobilization sets in further increase in surfactant concentrations remobilizes the bubble surface further and further making it more and more stress free.

Similar behavior is observed for the case when the surfactant kinetic exchange rates at the air liquid interface are finite (Bi is order one). At low concentrations of the surfactant, when the stagnant cap regime is observed, less amount of surfactant gets adsorbed onto the bubble surface compared to the diffusion limited case, and hence the bubble experiences less drag than before. At higher surfactant concentrations when the remobilization sets in ($k>10^3$), due to the finite kinetic exchange resistance the bubble surface is always less stress free than in the diffusion limited case. While for the diffusion limited case, by increasing k the bubble surface could be completely remobilized, with the drag reaching the stress free value, in the case of a finite kinetic exchange, the final drag achieved at large k is dependent on the Biot number, Bi. This final drag on the bubble decreases with increasing Biot number.

This verifies the scaling arguments we presented in Section 1.3.2, on remobilization. In the next chapter we present our experimental results, to verify our theoretical work presented here on remobilizing the surfactant laden interface of a moving bubble.

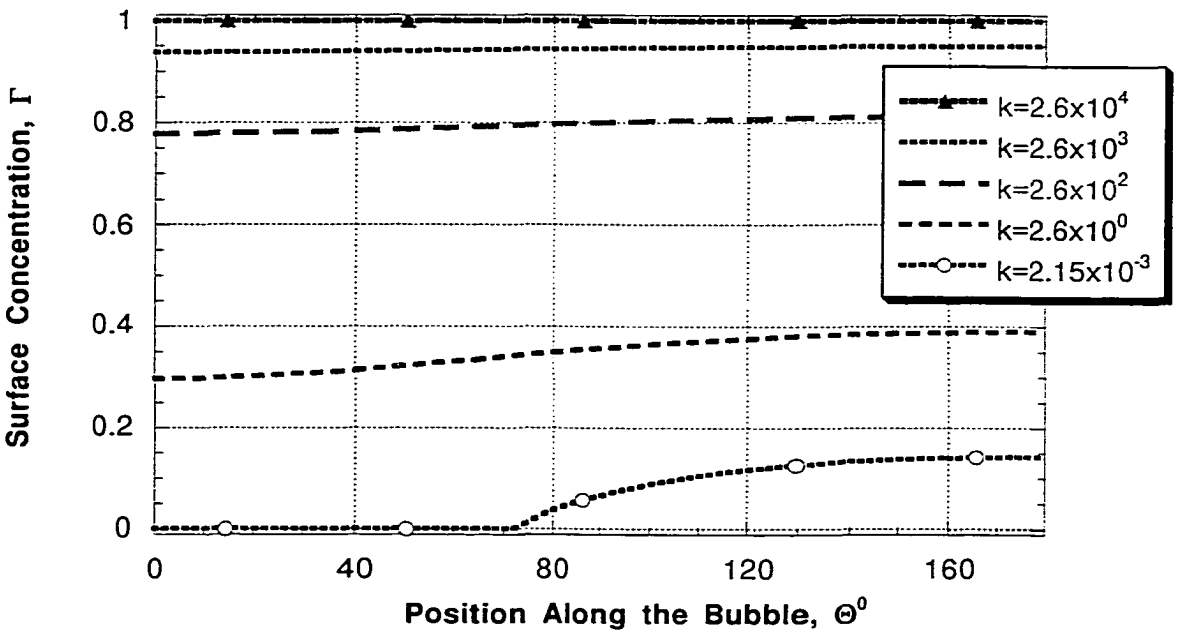

Figure 4.1: Variation of the surfactant surface concentration on the bubble with the addition of surfactant (for a diffusion limited case, when Re=0.91,χ=0.12, Ma=12.6, Pe=1.2x10^6).

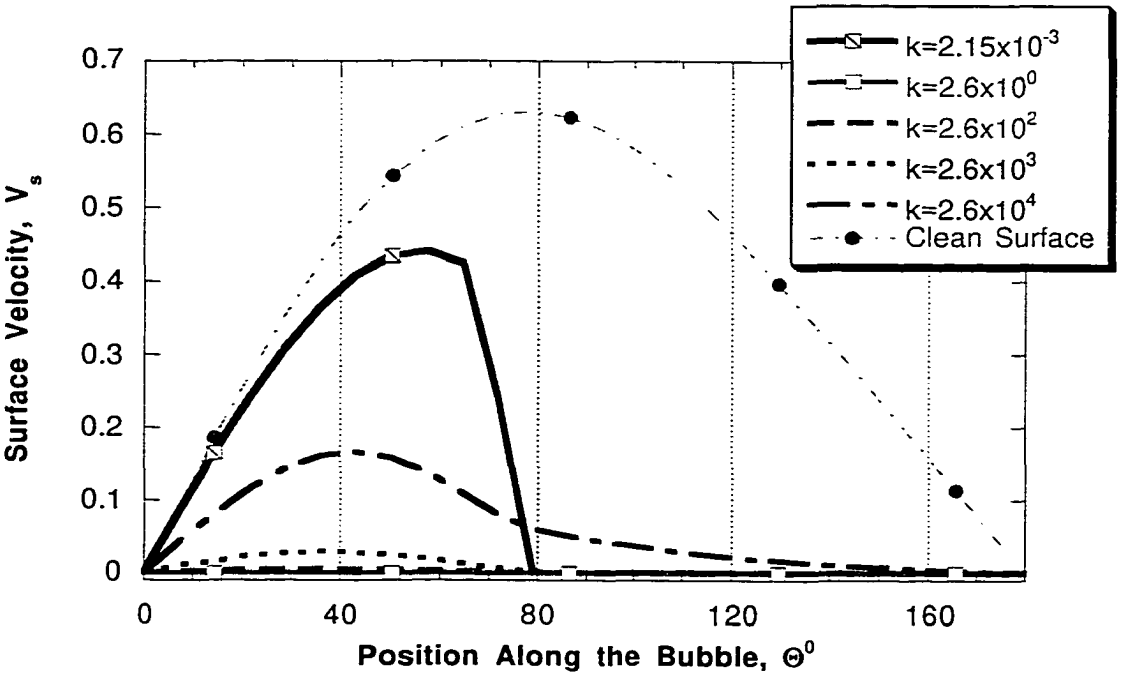

Figure 4.2: Variation of the Surface Velocity on the Bubble with the addition of the surfactant (for the diffusion limited case when Re=0.91, χ=0.12, Ma=12.6, Pe=1.2x10^6).

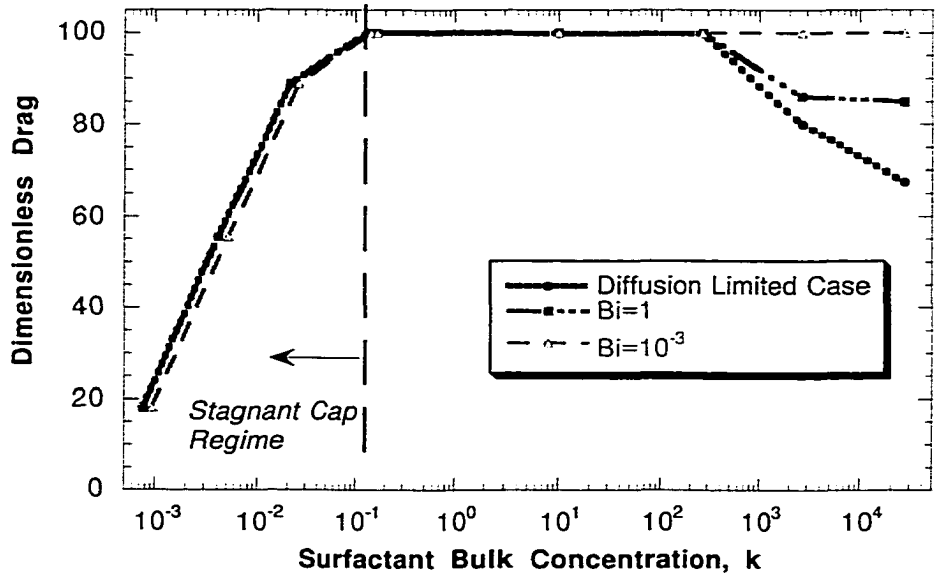

Figure 4.3: Theoretical prediction effect of surfactant bulk concentration on the drag of a rising bubble, for the case when the surfactant follows Langmuir type kinetics (at Re=0.91, χ=0.12, Ma=12.6,Pe=1.2x10^6).

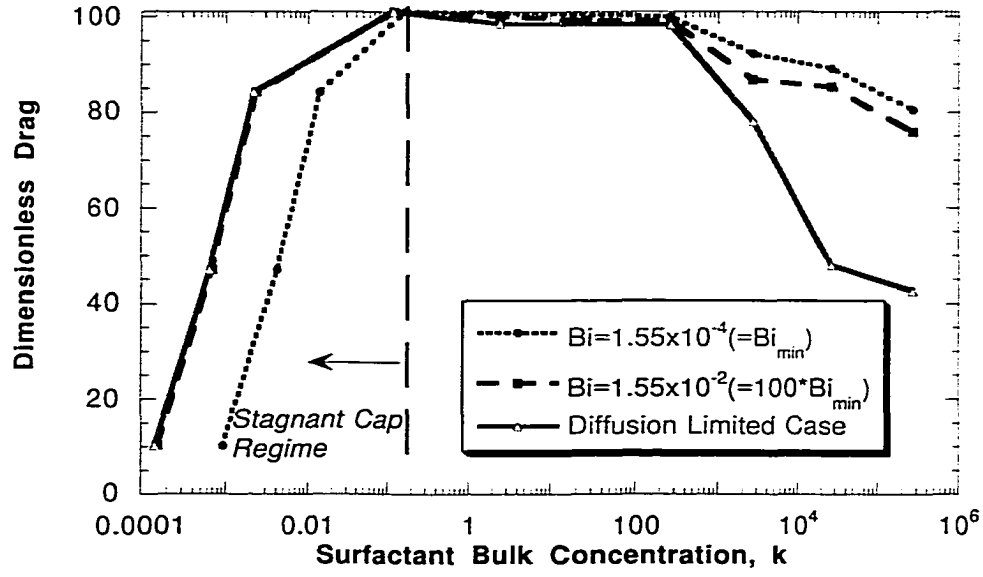

Figure 4.4: Effect of surfactant concentration on the drag of a rising bubble when the surfactant follows Frumkin type kinetics (at K=5.47, Re=0.91,χ=0.12,Ma=12.6, Pe=1.2x10^6).

CHAPTER 5
Experimental Verification of the Increased Mobility of a Bubble Using Surfactants at High Bulk Concentrations

5.1 Introduction

As mentioned in Chapter 1, when a bubble rises in a liquid, presence of even trace amount of surface active species in the liquid phase could create Marangoni forces on the moving bubble surface, retarding its mobility. Then the drag on the bubble would be higher than the stress free clean interface value, and could in fact be equal to that of a solid sphere of the same size, when the bubble interface is completely immobilized. We observed these effects in our numerical studies in Chapters 2 and 4 and in our experimental work in Chapter 3. We presented scaling arguments in Chapter 1, Section 1.3 and later verified with our numerical simulations in Chapter 4 that, if we could eliminate the resistance to surfactant transport due to bulk diffusion and kinetic exchange at the interface, then we could in fact remobilize the surfactant laden bubble surface. Then we could increase the mobility on the bubble surface, and hence make it more stress free, and hence the drag on the bubble would fall back again towards its initially clean interface stress free value. We also noted that by having the surfactant present at high bulk concentrations in the continuous phase, and if it could exchange rapidly at the air/liquid interface at these high bulk concentrations, the resistance to surfactant transport can be eliminated. These could be put quantitatively as the following conditions for remobilization:

* $k \gg 1$ (high bulk concentration)

* $kBi \gg 1$ and $Bie^{K} \gg 1$ (rapid kinetic exchange relative to convection)

* $\frac{\chi k}{Pe^{1/2}} \gg 1$ (rapid diffusive exchange relative to convection)

In this chapter, we present our experimental study to verify the above ideas of the remobilizing a surfactant laden surface of a moving bubble at high surfactant bulk concentrations. We note that the above arguments are valid only when the surfactant exists as a monomer in the bulk phase. Typically, above a critical bulk concentration, called the critical micelle concentration (CMC), real surfactants could form micellar aggregates. Then the surfactant could be present both in the monomeric and micellar form in the bulk phase. Then a different kind of mechanism that takes of micellar transport, break up and formation kinetics could explain the possibility of remobilization.

In Section 5.2, we present the possible mechanism for remobilization when the surfactant bulk concentration is around and above the CMC. In Section 5.3, we present our experimental study and the results on the effect of surfactants on the drag of a rising bubble in different model systems we studied. We discuss our experimental results in Section 5.4 and in Section 5.5 we compare these with the predictions from our simulations. Finally we present our conclusions in Section 5.6.

5.2 Mechanism for Remobilization around and above the CMC of the surfactant

We present here the scaling arguments for the hydrodynamics and surfactant transport processes for the case of a bubble rising in a surfactant solution. We consider the case when the surfactant is present just below and above its CMC. At and above the CMC, the surfactant is present in the bulk fluid in monomeric and micellar forms. The distribution of surfactant in the bulk between the monomer and the different sized micelles is determined by the kinetics of two processes: the exchange of a single monomer with a micelle, and the complete dissociation or break up of a micelle of a critical size to form many free monomers. The size distribution of micelles as a function of bulk concentration is a complex issue and has been the subject of both theoretical and experimental study starting with the models of Annianson, et al[66-68]. The kinetics of a single monomer exchange has been established by several techniques (like pressure jump, and temperature jump[69-72], and ultrasonic adsorption[73]) to be rapid, on the order of microseconds. However, the kinetics of micellar breakup can be slower, can be of the order of milliseconds depending on the surfactant structure and concentration[74-79]. In order for a surfactant to remobilize the interface, and hence be an effective means of controlling the mobility, the kinetics of both of these processes must be faster than the prevailing convective rate of the surfactant on the bubble surface. For this case, rapid micelle-monomer equilibrium maintains the bulk monomer concentration at the CMC.

Also let us also consider that the monomeric form of the surfactant has rapid adsorption/desorption rates at the air liquid interface ($Bie^K >> 1$, and $kBi >> 1$).

Consider first the situation when the bulk concentration is slightly below the CMC. As before the surfactant is present only as monomer in the bulk liquid, and a surfactant concentration boundary layer develops. In this case, however, the accumulation at the trailing end of the bubble increases the local sublayer concentration above the CMC. Therefore in this region, a zone develops in which surfactant is present both in monomeric and micellar form, as shown in Figure 5.1. The presence of micellar zone changes the behavior of the system. Surfactant monomer swept along the interface to the trailing pole, desorbs in to the sublayer. Provided that micelles incorporate monomer rapidly compared to the rate at which it is brought to the rear of the bubble by surface convection, the free monomer concentration in this region is maintained at the CMC. Micelles diffuse toward the outer boundary of this region where they break up to form free monomer.

Because the interface is in local equilibrium with the subsurface monomer concentration, a cap forms on the interface with both uniform surface concentration Γ_{CMC} and uniform surface tension γ_{CMC}. There are no Marangoni stresses exerted in this cap region. Along the remainder of the interface the subsurface concentration is non-uniform, increasing from the leading pole of the bubble to the edge of the cap. A Marangoni stress

results, pulling along the interface from the edge of the cap toward the leading pole. Therefore, in this concentration regime the interface of the bubble can be divided into two regions: a remobilized cap region and the remainder of the interface along which the interfacial mobility is retarded by the Marangoni stress. The size of the remobilized cap increases as the CMC is approached.

Now let us consider the case when the surfactant bulk concentration is above the CMC. Under these conditions, at the leading end of the bubble, monomer is adsorbed and swept to the back end by surface convection. This depletes the leading sublayer of monomer and can lower the local monomer concentration below the CMC, causing a micelle-free zone to form (see Figure 5.2). At the outer edge of the zone, micelles break up, forming monomers, which diffuse toward, and adsorb on to the interface. Surface concentration gradients can develop in this zone, as surface convection sweeps the surfactant out of the region than the monomer can diffuse and replenish it. The surfactant is swept into regions where the sublayer contains micelles, and where rapid equilibration maintains the subsurface monomer concentration, the surface concentration, and the surface tension at their CMC values. In this concentration regime, the interface can be divided into two zones: a retarded cap region extending from the leading pole of the bubble to the edge of the micelle-free zone and a stress-free zone that covers the remainder of the interface.

In the arguments presented in Chapter 1 for the monomeric surfactant transport before, we noted that due to the high Peclet numbers characterizing the monomeric transport, all the changes in the concentration occur in a small region δ_{MON} close to the surface of the bubble, which scales as $aPe^{-1/2}$ for a mobile interface. On similar lines, for micellar transport, all the changes in micellar concentration (from $C_{MIC}=C_{MIC(\infty)}$ to $C_{MIC}=0$, when only monomers exist) are expected to be attained in a small boundary layer δ_{MIC} which would scale as $aPe_{MIC}^{-1/2}$, where Pe_{MIC} is the Peclet number for micelle transport defined as Ua/D_{MIC}, D_{MIC} is the micellar diffusion coefficient. This is shown in Figure 5.2. The micelle-free zone could extend in the bulk from the bubble surface, to a depth δ. The balance of the surfactant transport rates in micellar and monomeric forms gives a scale for this depth, as given below:

$$nD_{MIC}\frac{C_{MIC(\infty)}}{aPe_{MIC}^{-1/2}} \approx D\frac{C_{CMC}}{\delta} \qquad [5.1]$$

Here n is the number of monomers per micelle (assuming micelles with the same aggregation number), $C_{MIC(\infty)}$ is the micellar bulk concentrations. Since the diffusion coefficient of micelles D_{MIC} is less than the diffusion coefficient of the monomer, δ_{MIC} is always less than δ_{MON}.

By increasing the bulk concentration further and further the depth of the micelle-free zone could be decreased until it completely disappears. Thus if micellar breakup is

rapid, the retarded cap can be remobilized (restoring the interface to complete mobility) by increasing the bulk concentration. On the other hand, if the kinetics of micellar breakup is slow compared to the surface convective flux, the retarded cap region at the leading edge of the bubble will persist regardless of how high the bulk concentration.

5.3 Experimental Study

5.3.1 Materials

As mentioned in Section 3.2.1, we choose a mixture of glycerol/water ratio of 7:3 by volume, for the continuous phase in some of our studies. We also conducted some studies using pure glycerol as the continuous phase as we describe later. The density of pure glycerol is 1240 kg/m^3, while that of the 70:30 glycerol-water mixture is 1190 kg/m^3, at 25^{0}C (as measured by a Troemner densiometer). The temperature variation of the viscosity of these two liquids is presented in Figure 5A.1a and 5A.1b. In both these liquids, air bubbles with sizes of the order of .25-. 8mm in radius, rise with velocities of the order of a mm/s keeping the Weber number less than .01, so that the bubbles always spherical, as noted before.

We choose two members $C_{12}E_6$ and $C_{10}E_8$ of the n-alkyl poly (ethylene glycol) ether surfactant series (C_iE_j: $CH_3\,(CH_2)_{i-1}(-OCH_2CH_2)_j$-OH)) in our studies. These are obtained from Nikkol Chemicals Company, Japan. Specifically the case of air bubbles rising in the following three systems are studied.

1) 70:30 glycerol-water mixture containing $C_{12}E_6$

2) 100% glycerol containing $C_{12}E_6$

3) 70:30 glycerol-water mixture containing $C_{10}E_8$

We also note that we do not observe any changes in the viscosity of the continuous phase with the addition of the surfactants in the range of the concentrations that we used in our studies.

5.3.2 Equilibrium and Sorption Kinetic Properties of the Surfactant

On the similar lines as described in Section 3.2.2, the equilibrium and dynamic surface tensions of the air/liquid interface for the above three systems are measured, and the equilibrium and sorption kinetic properties of the surfactants are deduced. While the experimental results for the first system -70:30 glycerol-water mixture containing $C_{12}E_6$ are described in Section 3.2.2, the results for the other systems are described in the Appendix 5A. These properties are all summarized in Table 5A.1.

5.3.3 Experiments to Study Bubble Rise Velocities

The details of the experimental apparatus we designed to measure bubble rise velocities are described in Section 3.2.3. Before the addition of the surfactant, experiments in a surfactant free 70:30 glycerol-water mixture (as shown in Figure 3.7) showed that bubbles of radii less than 0.5 mm rise with velocities less than the expected values, indicating that they feel the presence of trace amount of contaminants present in the system even after our thorough cleaning procedures. Bubbles of sizes 0.5 mm radius and above only behave as if they are in a clean system. The Reynolds numbers of bubbles

of sizes of 0.5 mm radii are of the order of 1. Similar experiments done using pure glycerol showed that bubbles of sizes 0.4mm radius and above rise with their expected velocities (as we show later in Figure 5.4 in terms of their drag coefficients). Here the Reynolds numbers are of the order of 10^{-3}, and hence the flow could essentially be considered creeping flow.

All the experiments with the surfactant are carried out at temperatures in the range of 24-27^{0}C, and the data interpreted accounting for the changes in viscosity. In the first set of experiments, the poly-ethoxy surfactant $C_{12}E_6$ ($CH_3.(CH_2)_{11}(OCH_2CH_2)_6OH$) is used in the 70:30 glycerol water mixture. The experiments are done from very low concentrations from 10^{-3} mg/lit to around 10^3 mg/lit(10 times the CMC of the surfactant). In Figure 3.8 and reproduced in Figure 5.3, we plot these results of the dimensionless drag C_D^* on the bubble rising in the surfactant solution as a function of the surfactant bulk concentration. The dimensionless drag is defined as before as $C_D^* = \left(\frac{C_D - C_{D(BUB)}}{C_{D(SOL)} - C_{D(BUB)}}\right)100$ with $C_{D(SOL)}$ and $C_{D(BUB)}$ evaluated from equations [3.8] and [3.9] at the corresponding Reynolds numbers Re. The drag coefficient C_D is calculated from the rise velocity U of the bubble as $C_D = \frac{8ag}{3U^2}$. This way, C_D^* gives a value of 0 if the bubble is behaving with a completely stress free interface, while a value of 100 if it has a completely stagnant interface.

As we notice in Figure 5.3, for a bubble of any given size, as we increase the surfactant bulk concentration, its drag increases monotonically from that of a completely stress free interface in a pure liquid, until it reaches that of a completely stagnant interface. Bubbles of all sizes we studied show similar behavior. From a concentration of 0.9 mg/lit of the surfactant, all the bubbles experience a drag close to that of a solid. At lower concentrations they experience drags between these two extremes. This is when the stagnant cap regime is observed, and when the cap does not cover the bubble completely. We described these results in Section 3.2.3.2. At higher surfactant concentrations (>=0.9 mg/lit) till the CMC, the bubbles of all sizes experience drags close to that of solid spheres. Further increase in surfactant concentration to 5 and 10 times CMC does not alter the drag on the rising bubbles. Hence we do not see any remobilization of the bubble surface.

In Figure 5.4, we plot the results of similar experiments with $C_{12}E_6$ surfactant in 100% glycerol. We note a similar behavior as before. In the surfactant free liquid, bubbles of sizes 0.4 mm radius and above, rise with velocities equal to the expected stress free values. As we add the surfactant, for a bubble of any given size, we note that the drag on the bubble would increase from that of a clean interface stress free value towards that of a completely stagnant interface solid like value. With further increase in concentrations, to and above the CMC, the drag stays at the solid like value. Hence in the range of concentrations studied till 4 times the CMC, the bubble surface, once

immobilized, remains immobilized. Above this surfactant bulk concentrations, the solution becomes very hazy, indicating the possible solubility limit of the surfactant.

In Figure 5.5, we present the results of similar experiments with $C_{10}E_8$ surfactant in 70:30 glycerol water mixture. As before, at low surfactant concentrations, addition of the surfactant increases the drag on a bubble of a given size, from that of a clean value to that of a solid like value. The drag remains at the solid like value over a range of concentrations. In contrast to the previous results, the experiments at CMC show the drag falling below the solid like value indicating the onset of remobilization. Further increase in surfactant concentration to 5 and 10 times the CMC brings the drag further and further close to the clean interface value. At the highest concentration studied (ten times the CMC), we note that bubbles of all sizes considered, experience drags which are around 55-60% solid like.

5.4 Discussion

As observed in our scaling arguments on the remobilization in Chapter 1, the presence of surfactant concentration gradients on the surface of a rising bubble creates surface stresses that increase the drag on the bubble. These surface concentration gradients of the surfactant could be eliminated if the surfactant transport rates to (and from) the bubble interface into (and from) the bulk both by bulk diffusion and kinetic exchange at the interface, overwhelm the existing surface convection rates. This requires the three conditions listed in Section 5.1 to be satisfied to remobilize the surfactant laden

interface for surfactant concentrations below the CMC. The arguments presented in Section 5.2 apply for concentrations above the CMC.

For the $C_{12}E_6$ surfactant, at CMC, even though the rates of kinetic exchange relative surface convection characterized by Bie^K is large (>0.1), the drag on a rising bubble of any given size, remains at the solid like value at higher and higher surfactant concentrations at and around the CMC. No remobilization is achieved. This could be explained from the fact that at CMC, the relative rates of surfactant transport by bulk diffusion and surface convection, characterized by $\frac{\chi\,(e^{K\frac{\Gamma_e}{\Gamma_\infty}}+k)}{Pe^{1/2}}$, is not large enough (≈0.05). Further addition of surfactant above the CMC does not affect the drag on the bubble. This may hint at the possibility of the micellar breakup or formation rates being not fast enough to balance the existing convection rates of the surfactant on the surface of the bubble.

Similar arguments could explain the behavior of the air bubbles rising in 100% glycerol solutions of $C_{12}E_6$. We note that $\frac{\chi\,(e^{K\frac{\Gamma_e}{\Gamma_\infty}}+k)}{Pe^{1/2}}f$ for this system at CMC is around 0.1.

In contrast, for the $C_{10}E_8$ surfactant, the CMC of the surfactant is an order of magnitude more than $C_{12}E_6$, which gives $\frac{\chi\,(e^{K\frac{\Gamma_e}{\Gamma_\infty}}+k)}{Pe^{1/2}}\approx 0.5$(an order of magnitude more

than before). Even at similar rates of kinetic exchange relative to surface convection as before ($Bie^K > 1$), we note that drag on a bubble of any given size starts falling below the solid like value at surfactant bulk concentrations around the CMC. This indicates the onset of remobilization. Further increase in surfactant concentration above the CMC to 5 to 10 times the CMC reduces the drag even further and further towards the stress free interface value. At these high concentrations above the CMC, the supply of surfactant from the bulk is provided by micellar break up. The fact that in this range of concentrations studied, the drag on the bubble is decreasing with further addition of surfactant shows that the micellar break up kinetics are fast and the retarded cap at the leading edge of the bubble is decreasing with the addition of more and more surfactant. The increased affinity of the surfactant $C_{10}E_8$ for the bulk phase (due to the presence of two more ethoxy groups and two less members in the hydrocarbon chain than $C_{12}E_6$) could explain the increased micellar kinetic rates (on the lines of the observations for octylphenyl polyoxyethylenes in water by Lang et al[75]).

Experiments at further higher concentrations of $C_{10}E_8$, need to be done to see if more remobilization of the surface of the rising bubble could be obtained. Complete remobilization of the bubble surface could be obtained if the micellar breakup/formation rates and their bulk transport rates remain high enough at the higher bulk concentrations of the surfactant.

5.5 Comparison of Experiments with Simulations

In Chapter 4, we have presented a model to describe the effect of the added surfactant on the drag of a rising bubble, when the surfactant exists in the bulk liquid as monomers without forming micellar aggregates. In this section, we compare the predictions of the model with experiments till the surfactant forms micelles (i.e., till the CMC of the surfactant) for each of the cases of $C_{12}E_6$ and $C_{10}E_8$ dissolved in 70:30 glycerol-water mixture. The values of the dimensionless numbers corresponding to the rise of a bubble of radius 0.6 mm in the 70:30 glycerol-water mixture under the experimental conditions are listed in Table 5.1 for the cases of the two different surfactants. In Table 5.2 we present the values of the dimensionless drags predicted by the simulations and observed in the experiments, for different surfactant bulk concentrations described by k. These values of k correspond to concentrations above the limit k_c below which the stagnant cap behavior is observed, which is around 0.29 for $C_{12}E_6$ and 0.28 for $C_{10}E_8$(for the case with minimum Biot number). These values of k_c correspond to the concentration of the surfactant needed to completely cover the bubble surface, to give a completely stagnant solid like surface. The details of evaluating the value of k_c are described in Chapter 2.

From Table 5.2 we note that for $C_{12}E_6$, as we increase the surfactant bulk concentration above k_c, the drag on the bubble as estimated from our simulations for the diffusion limited case, remains at the solid like value till the CMC. At the CMC, the ratio

of the diffusive transport flux of the surfactant relative to its convection rates on the bubble surface characterized by $\frac{\chi(e^{K\frac{\Gamma_e}{\Gamma_\infty}}+k)}{Pe^{1/2}}$ is 0.05. So the diffusion limitations alone create surfactant surface concentration gradients on the bubble surface, creating retarding forces enough to completely immobilize the bubble surface. This prediction from the theory is observed in the experiments.

For $C_{10}E_8$, we also note that as long as $\frac{\chi(e^{K\frac{\Gamma_e}{\Gamma_\infty}}+k)}{Pe^{1/2}}$ is smaller, we get a completely retarded surface on the bubble for the diffusion limited case, with the drag on the bubble closer to the solid like value. In contrast to $C_{12}E_6$, due to the higher value of the CMC now (1.91 mol/m^3, as against 0.209 mol/m^3), at CMC $\frac{\chi(e^{K\frac{\Gamma_e}{\Gamma_\infty}}+k)}{Pe^{1/2}}$ becomes 0.5, an order of magnitude larger than before. Hence the drag on the bubble relaxes and starts to fall below the solid like value. We observe this even for the case with minimum Biot number as determined from our pendant bubble experiments. This onset of remobilization is observed in the experiments also. The remobilization seen at higher surfactant concentrations above the CMC, could only be explained by taking into account, the presence of micelles in the bulk liquid and accounting for their transport and break up/formation rates.

5.6 Conclusions

In this chapter we experimentally verified the scaling arguments presented in Chapter 1 and the numerical solutions presented in Chapter 4 on the concept of remobilizing the surfactant laden bubble interface. We studied the effect of an added poly ethoxylate surfactant on the drag of air bubbles rising in glycerol-water mixture. First we studied the effect of $C_{12}E_6$ concentration in 70:30 glycerol water mixture on the rise velocities of air bubbles in the liquid. We observed that for any given size bubble, as we add more and more surfactant, the drag increased from that of a clean interface stress free value to that of a completely stagnant solid like value at around 0.01 times the CMC. Further increase in surfactant bulk concentrations to and above the CMC (till ten times the CMC) does not show any change in the drag of the bubble from that of a solid like value. Hence no remobilization is observed. Similar results are observed for the case of air bubbles rising in 100% glycerol solutions of $C_{12}E_6$.

In our next set of similar experiments using $C_{10}E_8$ in a 70:30 glycerol water mixture, we notice a similar initial behavior of the drag on a bubble of any given size increasing from the initially clean stress free value to that of a complete surfactant covered solid like value. But further addition of surfactant around the CMC, brings the drag on the bubble below that of a solid like value, indicating the onset of remobilization. At bulk surfactant concentrations above the CMC, we notice that the drag on the bubble decreases further and further away from the solid like value. At the highest concentration

studied (ten times the CMC), we observed a decrease in drag corresponding to around 55% between that of a solid and a completely stress free interface.

Even though similar kinetic exchange rates relative to surface convection rates are observed for both, $C_{12}E_6$ and $C_{10}E_8$ at the air glycerol/water mixture interface ($Bie^K>0.1$ and 1 respectively), the difference in behavior observed for these surfactants could be explained as follows. For $C_{12}E_6$, at CMC the bulk diffusive transport limitations could not be over come as the ratio $\frac{\chi\,(e^{K\frac{\Gamma_s}{\Gamma_\infty}}+k)}{Pe^{1/2}}$ is small (around 0.05). This is not large enough as indicated by our simulations. For $C_{10}E_8$ the CMC being an order of magnitude more than $C_{12}E_6$ makes this ratio around 0.5 which remobilizes the bubble surface, again as confirmed by the results from our simulations. Also for $C_{10}E_8$, above the CMC, faster micellar breakup/formation rates seem to cause the remobilization of the bubble surface, as seen by the drag on the bubble decreasing further and further with increasing surfactant bulk concentration.

Experiments at further higher concentrations of $C_{10}E_8$, need to be done to see if more remobilization of the surface of the rising bubble could be obtained. This, as discussed before, would depend on the structure of the micelles formed at these higher bulk concentrations and their bulk transport and breakup and formation kinetic rates.

APPENDIX
Properties of the Materials Used in our Experiments

As mentioned in Sections 3.2.1, and 5.3.1, for our experimental work on the effect of surfactant concentration on the rise velocities of air bubbles, for the continuous phase we choose either a mixture of glycerol/water ratio of 70:30 by volume, or 100% glycerol. In preparing the 70:30 glycerol-water mixture, the water used is purified from tap water using a Millipore Q System (Millipore, MA) with a specific resistance greater than 15M ohm-cm. The glycerol used is obtained from Sigma (ACS Reagent, Cat. No. G-7893) and is used without modification. The surface tension of the aqueous/glycerol mixture against air was equal to 65.6 dyne/cm as measured by a pendant bubble apparatus, and did not vary with time indicating no surfactant impurities. The surface tension of pure glycerol was 63 dyne/cm.

The density of pure glycerol was 1240 kg/m^3, while that of the 70:30 glycerol-water mixture is 1190 kg/m^3, at 25^{0}C (as measured by a Troemner densiometer). In the range of temperatures studied (22-27°C), the density of the liquid did not vary. The temperature variation of the viscosity of these two liquids is presented in Figure 5A.1a and 5A.1b.

We choose two members $C_{12}E_6$ and $C_{10}E_8$ of the n-alkyl poly (ethylene glycol) ether surfactant series (C_iE_j: $CH_3(CH_2)_{i-1}(-OCH_2CH_2)_j$-OH)) in our studies. These are

obtained from Nikkol Chemicals Company, Japan. Specifically the case of air bubbles rising in the following three systems are studied.

i) 70:30 glycerol-water mixture containing $C_{12}E_6$

ii) 70:30 glycerol-water mixture containing $C_{10}E_8$

iii) 100% glycerol containing $C_{12}E_6$

We also note that we do not observe any changes in the viscosity of the continuous phase with the addition of the surfactants in the range of the concentrations that we used in our studies. We describe in the next section on the measurements of the equilibrium and sorption kinetic properties of the surfactants at the air liquid interface for the different systems.

Equilibrium and sorption kinetic properties of the surfactants

In Section 3.2.2, we described the measurement of these properties for the first system, $C_{12}E_6$ dissolved in 70:30 glycerol water mixture. On similar lines we measured these properties the surfactant bulk diffusion coefficient, and its adsorption desorption rate constants at the air liquid interface for the next two different systems studied. The kinetic rate constants for surfactant exchange at an interface are determined in the following way [34,62,63,80]. First, experiments are undertaken in which the surfactant diffuses toward and kinetically adsorbs from solution onto a initially clean interface, and the reduction in surface tension is measured. Second, the surfactant mass transfer

occurring in each of these dynamic tension experiments is modeled to predict the surface concentration as a function of time ($\Gamma'(t)$). This modeling includes solving the bulk phase diffusion equation (including convection if the dynamic tension experiment involves flow), and the surface conservation equation, which accounts for the kinetic exchange. Third, the equation of state which gives the tension as a function of the surface concentration $\gamma(\Gamma')$ is measured so that the tension relaxation corresponding to the unsteady adsorption can be predicted from the model. Finally, the experimental relaxations are matched to the predictions by adjusting the values of the kinetic constants, and in this way these constants are established. In our study, we use the pendant bubble technique to measure the reduction in tension as surfactant adsorbs onto an initially clean interface. The technique is based on the analysis of the shape of pendant bubbles formed and tethered to the tip of a needle placed in the surfactant solution [64,65] as described in Section 3.2. The results of this experimental work are described in Table 5.A.1.

$C_{10}E_8$ dissolved in 70:30 Glycerol Water Mixture

Figure 5A.2 presents the results of the equilibrium surface tension as a function of bulk surfactant concentration. We see the CMC of the surfactant is 990 mg/lit, an order of magnitude more than that of $C_{12}E_6$ in 70:30 glycerol water mixture. This is due to the fact that $C_{10}E_8$ is more hydrophilic than $C_{12}E_6$, due to the decrease in the hydrophobic hydrocarbon chain, and the increase in the hydrophilic ethoxy groups and hence liking

the bulk phase more. In Figure 5A.2, a least square fit of the equilibrium surface tension against bulk concentration data using the Frumkin equations (equations [3.2] and [3.3]) is also plotted. Using a value of $\Gamma_\infty = 4.5 \times 10^{-6}$ mol/m^2 as determined from the slope of the γ vs. $\ln(C_0)$ curve the values of the parameters that fit best are $\alpha/\beta = 7.037 \times 10^{-3}$ mole/m^3 and K=6.08. Note also that a positive value of K indicates that repulsive head group interactions dominate in the monolayer.

In this case we could not verify the above equation of state parameters by doing an experiment where we compress/expand rapidly an equilibrated pendant bubble, when the amount of surfactant on the bubble surface remains constant under changing area, as in a Langmuir trough (like in Figure 3.3). This is due to the following reason. In our pendant bubble apparatus, for this liquid a maximum areal rate of 30mm^2/s of compression/expansion could be allowed within which bulk hydrodynamic effects do not appear to be important. This is confirmed by compressing/expanding a pendant bubble in a surfactant free glycerol-water mixture. In the absence of hydrodynamic effects, the surface tension as measured from the shape of the compressing/expanding bubble at various times should be the same clean interface value as measured by the static Young-Laplace formulation from the shape of the pendant bubble. We measure at what areal rate of strain the surface tension as measure in this manner goes above the clean interface value, which indicates the onset of bulk hydrodynamics affecting the shape of the bubble.

All the experiments with the surfactant using the pendant bubble as a Langmuir trough, could be carried only below this maximum rate. We found that for this system since the kinetic exchange rates are fast than the maximum possible areal rate of strain, we always see the effect of surfactant kinetic exchange in such experiments. Hence we could not measure the equation of state experimentally this way.

The dynamic surface tension relaxations measured for different concentrations, are shown in Figure 5A.3. On the same lines described in Section 3.2.2.3, we could describe all of them as diffusion limited processes with a diffusion coefficient of $D=1.5\times10^{-11}$ m^2/s, as shown in the same figure. Using a mixed kinetic diffusive model we could determine the lower bounds on the adsorption and desorption rate constants for $C_{10}E_8$ at the air/glycerol-water mixture interface as $\beta=50$ $m^3/(mol.s)$ and $\alpha=0.35$ s^{-1}.

$C_{12}E_6$ dissolved in 100% Glycerol

For this system, in Figure 5A.4 we plot the equilibrium surface tension vs. bulk concentration. The equilibrium surface tensions are measured for concentrations in the range 0.1 to 1000 mg/lit (3×10^{-6} to 2.3×10^{-3} M). The measured value for the CMC (250 mg/lit) is approximately six times that of water[61], and two and half times that of 70:30 glycerol water mixture reflecting the fact that glycerol is less polar then water and hence increasing the glycerol content is more accommodating of the surfactant chains. In Figure 5A.4, a least square fit of the equilibrium surface tension against bulk concentration data

using the Frumkin equations (equations [3.2] and [3.3]) is also plotted. The values of the parameters that fit best are Γ_∞= 4.51x10^{-6} mol/m^2, α/β=3.83x10^{-3} mole/m^3 and K=4.43. The value of Γ_∞ obtained here also agrees with the estimate obtained independently from the slope of the γ vs. ln(C_0) curve.

For this system also we could not do an experiment where we could use the pendant bubble as a Langmuir trough. This is again because of the fact that the bulk hydrodynamic effects become more important even at smaller rates of compressing/expanding the pendant bubble due to the high viscosity of the bulk phase glycerol (1000 times that of water) which leads to high Capillary numbers (Ca=$\mu v/\gamma$).

In Figure 5A.5, we plot the surface tension relaxation at the air/glycerol interface due to the $C_{12}E_6$ interface for two different low concentrations. These could be described by a diffusion limited model with a diffusion coefficient of 3x10^{-13} m^2/s. This is three orders of magnitude lower than the diffusion coefficient of the same surfactant in water [61] in line with the increased viscosity of the bulk phase. This gives lower bounds of 0.1 m^3/((mol.s) and 3.83x10^{-4} s^{-1} on the adsorption(β) and desorption(α) rate constants respectively. Experiments at higher bulk concentrations need to be done to get a better estimate of the lower bounds on these numbers.

Table 5.1: Values of the Dimensionless Parameters in the Simulations corresponding to ~0.6 mm radius bubbles in the experiments for $C_{12}E_6$ and $C_{10}E_8$ in 7:3 Glycerol-Water Mixture.

	Re	**Ma**	**Pe**	**χ**	**K**	**Bi_{min}**
$C_{12}E_6$	0.91	12.6	1.2×10^{6}	0.12	5.47	1.5×10^{-4}
$C_{10}E_8$	0.91	12.6	1.2×10^{6}	0.94	6.08	6×10^{-3}

Table 5.2: Comparison of experiments in 70:30 Glycerol-Water mixture with numerical simulations at higher surfactant bulk concentrations

Surfactant Bulk Concentration, mg/lit	k	Dimensionless Drag		
		Experiment	Simulation	
			Bi_{min}	Diffusion Limited
$C_{12}E_6$				
0.92	2.27	96.8	100	100
9.8	24.17	97.3	100	100
100.1 → **CMC**	**246.67**	**98.3**	**100**	**100**
354.8		100.1		
1003.0		99.7		
$C_{10}E_8$				
24.4	6.70	99.9	100	100
244.0	67.01	98.5	100	100
996.0 → **CMC**	**273.55**	**92.1**	**90.5**	**85.0**
4948.0		67.4		
10324.0		55.4		

Table 5.A.1: Properties of the poly-ethoxy surfactants used in this study in the various systems.

	$C_{12}E_6$ in 70:30 Glycerol Water	**$C_{12}E_6$ in 100% Glycerol**	**$C_{10}E_8$ in 70:30 Glycerol Water**
CMC, mol/m^3	0.209	0.555	1.91
Maximum Packing Concentration(Γ_∞), mol/m^2	$4.48x10^{-6}$	$4.51x10^{-6}$	$4.50x10^{-6}$
Frumkin Interaction Parameter, K	5.47	4.43	6.08
Diffusion Coefficient(D), m^2/s	$1.5x10^{-11}$	$3x10^{-13}$	$1.5x10^{-11}$
Adsorption Rate Constant(β), $m^3/(mol.s)$	>10	>0.1	>50
Desorption Rate Constant (α), s^{-1}	$>9x10^{-3}$	$>3.83x10^{-4}$	$>2.73x10^{-1}$
$\frac{\chi(e^K+k)}{Pe^{1/2}}$ at CMC	0.05	0.11	0.58

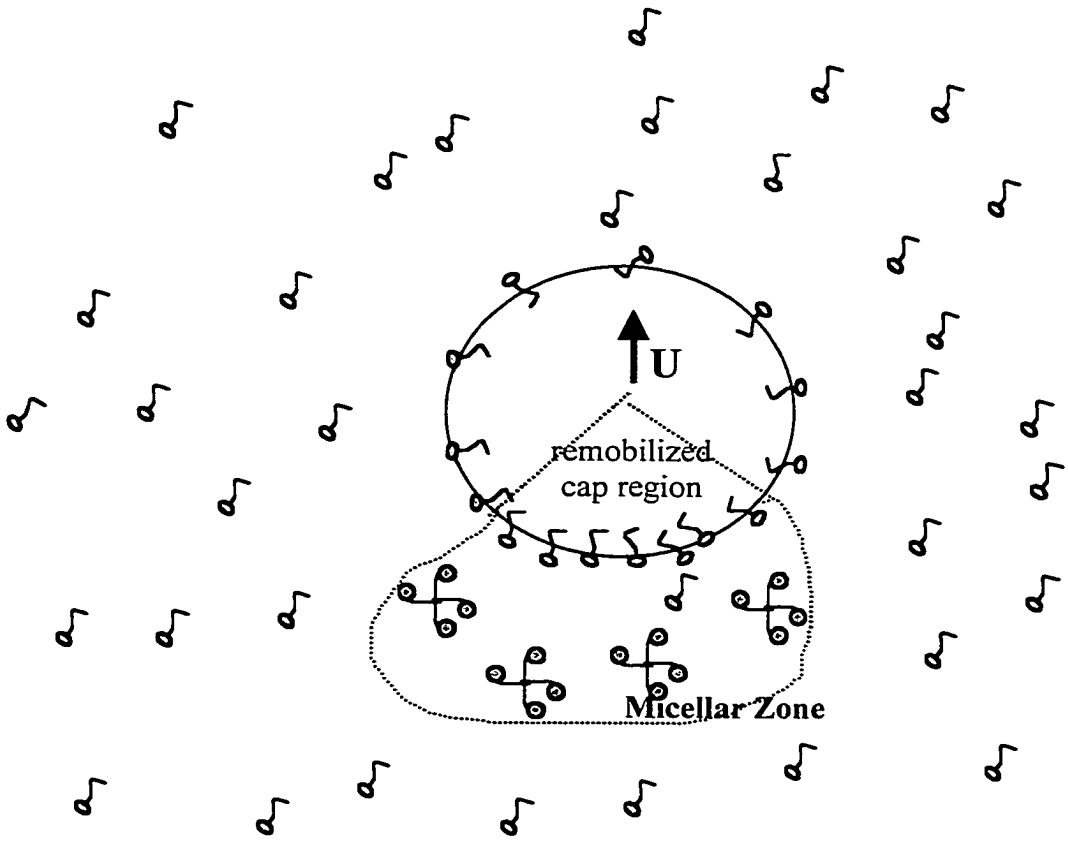

Figure 5.1: The surfactant concentration profile of a diffusion-controlled surfactant just below the CMC. The formation of a micellar zone, along with a remobilized cap region, is shown at the trailing end of the bubble rising in a liquid with terminal velocity U.

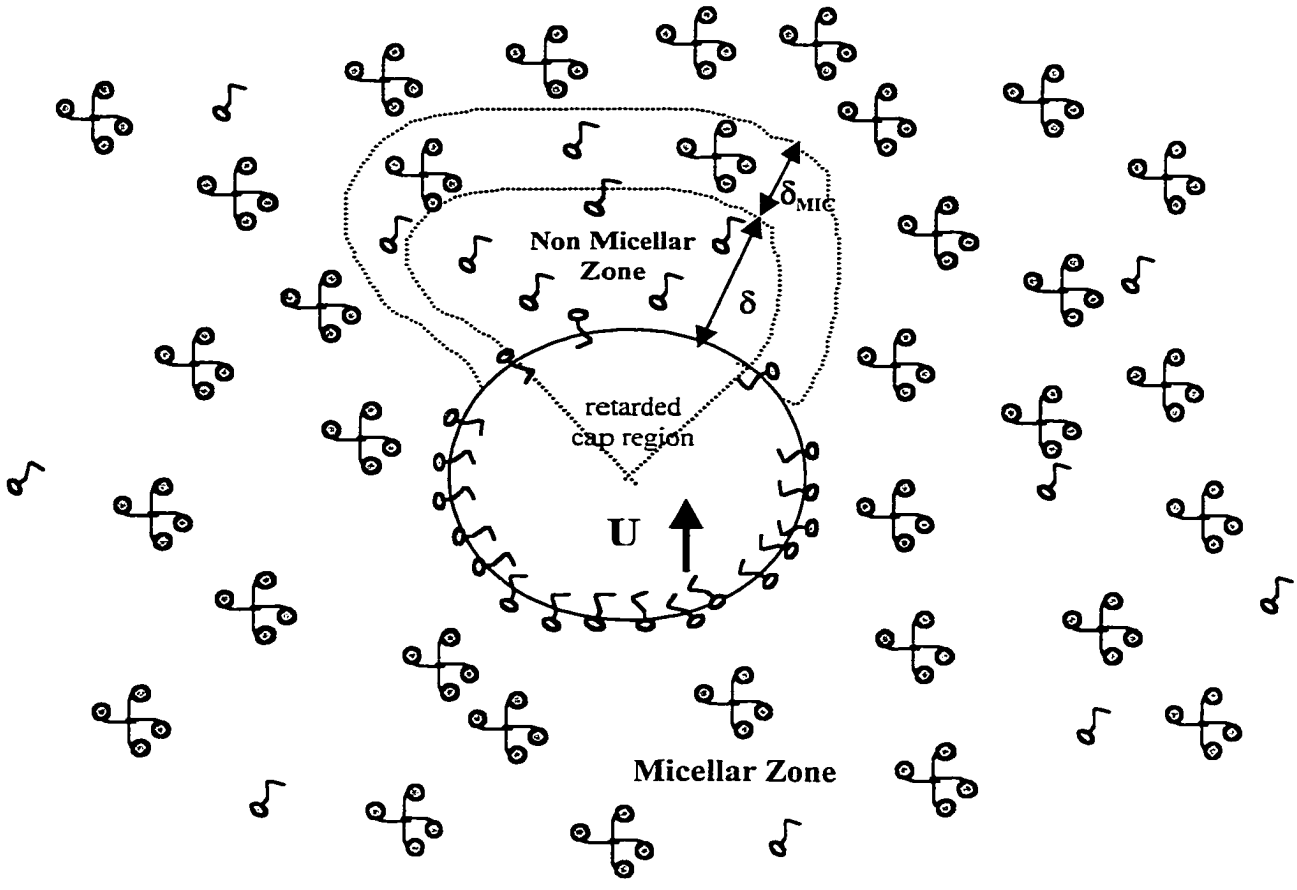

Figure 5.2: The surfactant concentration profile of a diffusion-controlled surfactant above the CMC. The formation of a micelle free zone, along with a retarded cap region, is shown at the leading end of the bubble rising in a liquid with terminal velocity U. δ_{MIC} is the thickness of the boundary layer over which the micellar concentration goes from $C_{MIC}=C_{MIC(\infty)}$ to $C_{MIC}=0$. δ is the thickness of the micelle free zone, where the monomer concentration goes from C=CMC to C=0, near the bubble surface.

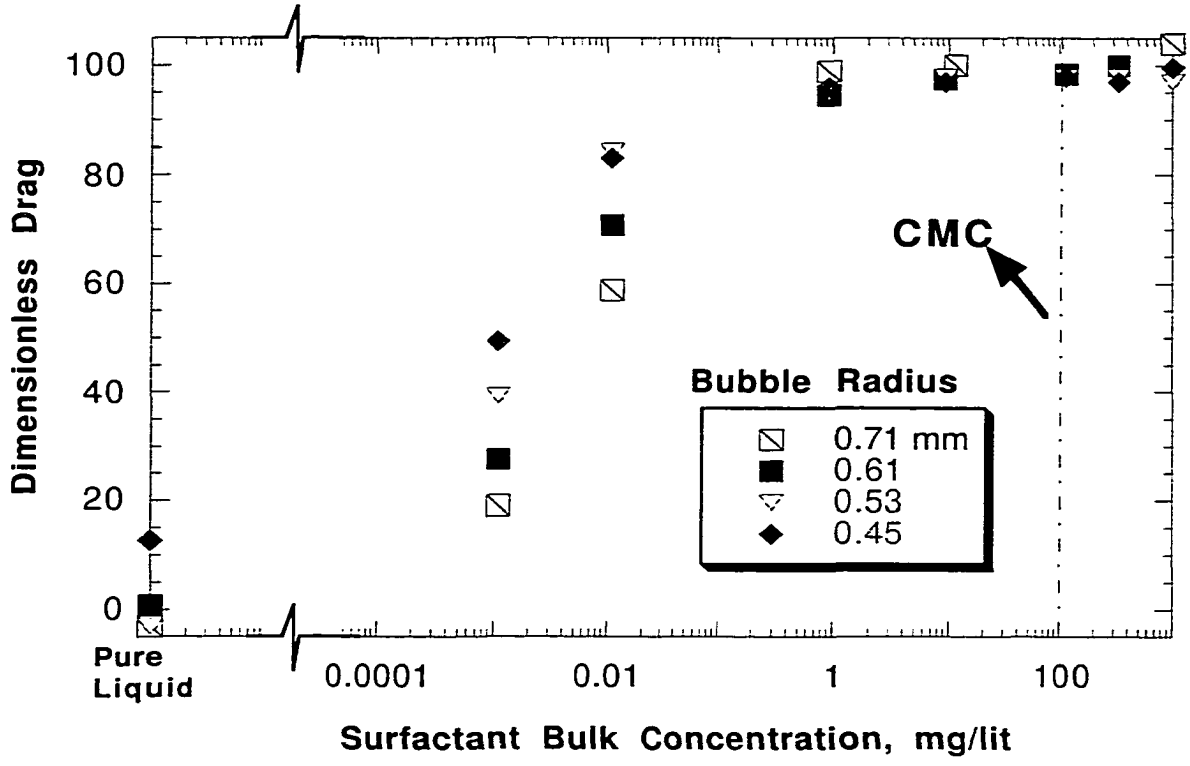

Figure 5.3: Effect of Addition of $C_{12}E_6$ on the Drag of a Bubble Rising in a 7:3 Glycerol/Water Mixture.

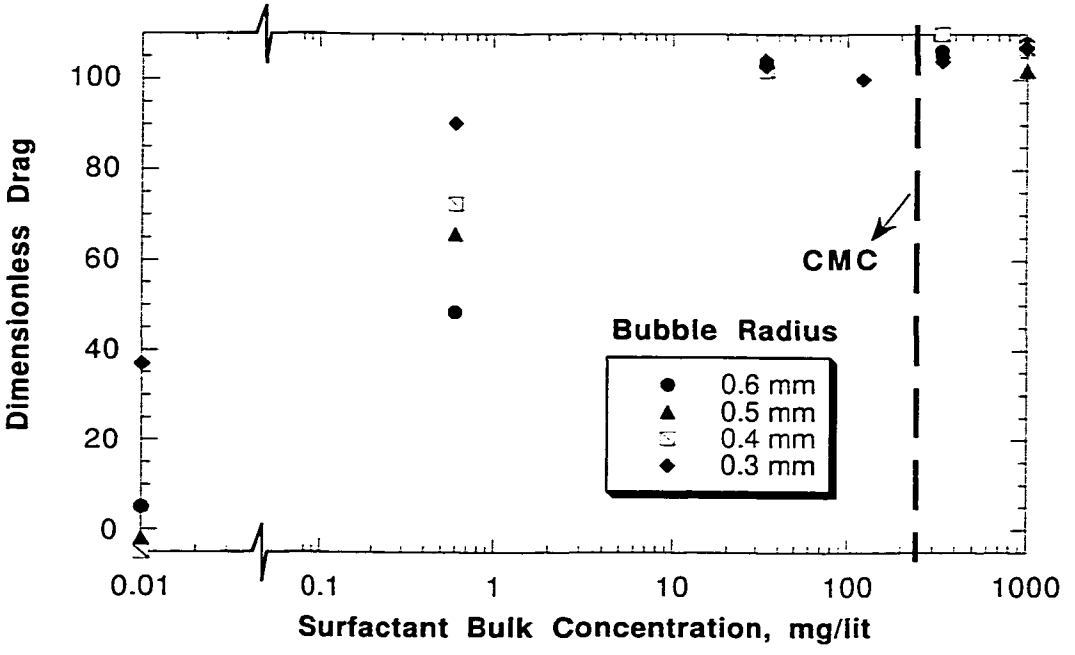

Figure 5.4: Effect of Addition of $C_{12}E_6$ on the Drag of a Bubble Rising in 100% Glycerol.

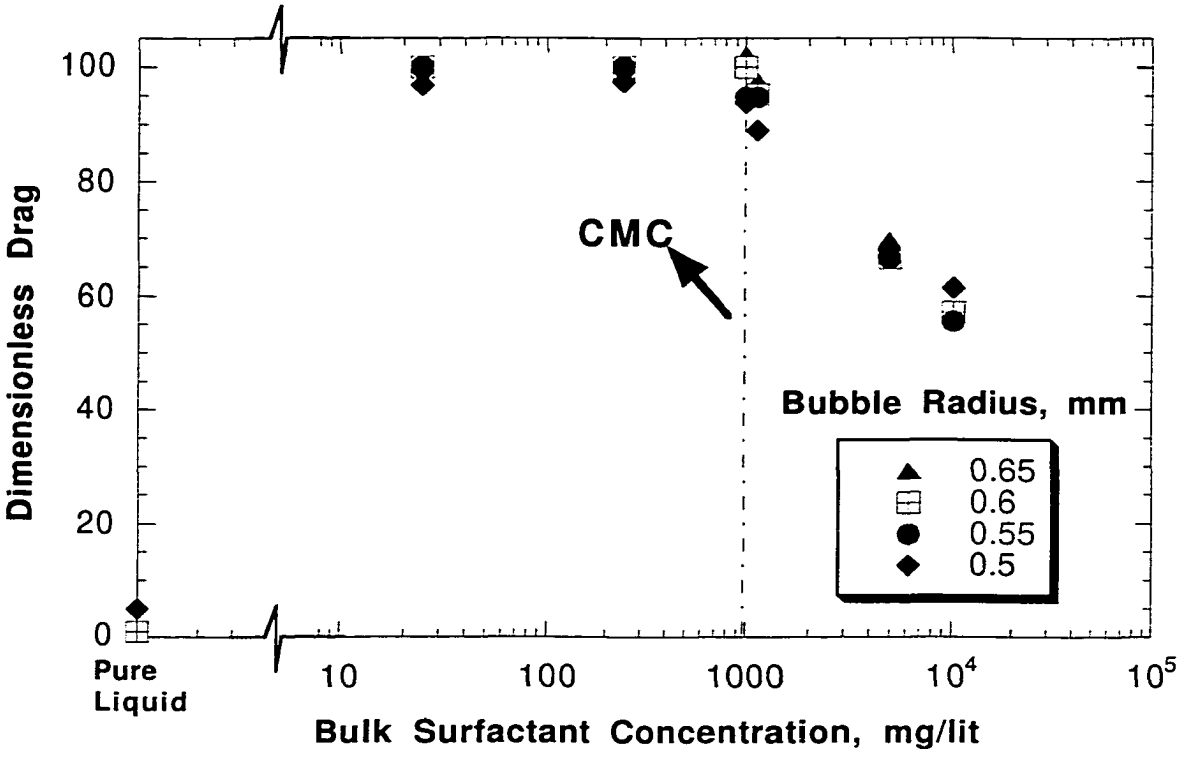

Figure 5.5: Effect of Addition of $C_{10}E_8$ on the Drag of a Bubble Rising in a 7:3 Glycerol/Water Mixture.

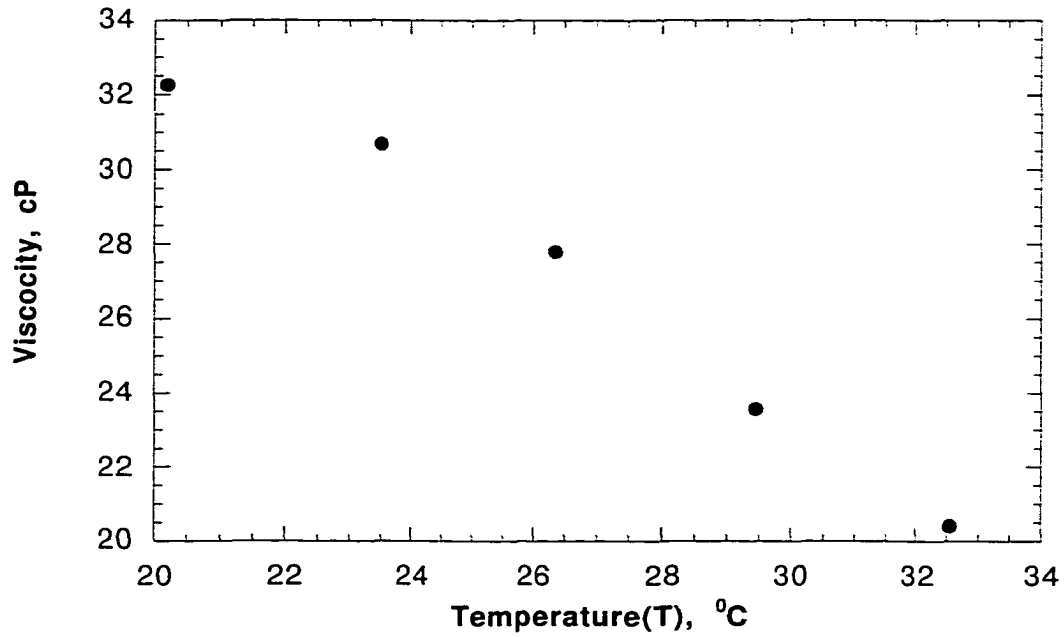

(a)

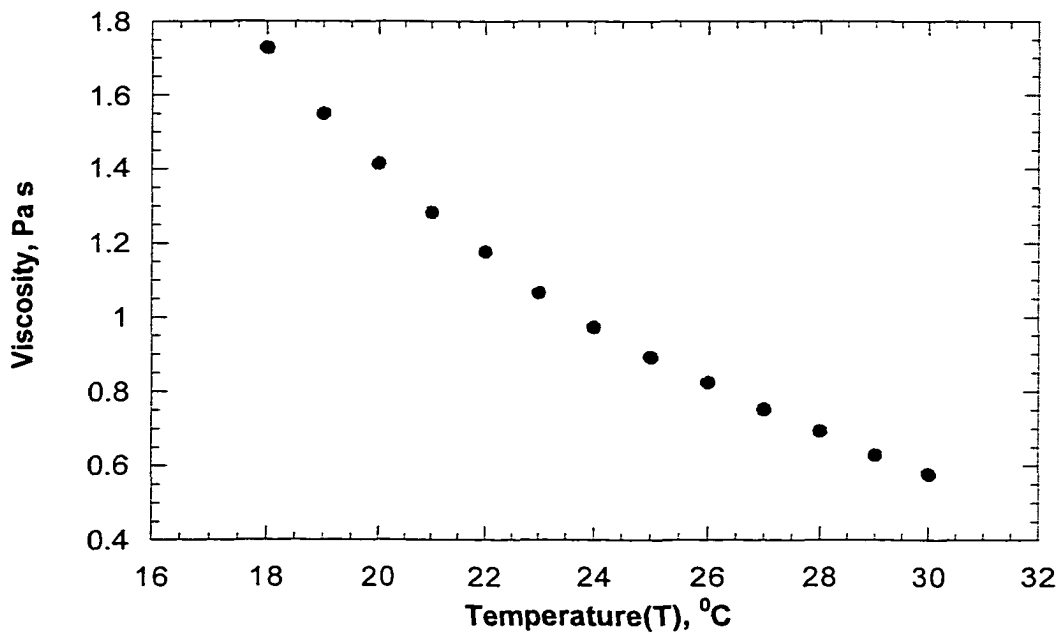

(b)

Figure 5.A.1: Effect of temperature on the viscosity of (a) 70:30 glycerol- water mixture as measured by Haake Viscometer and (b) 100% glycerol as measured by Cambridge Polymer Group, MA

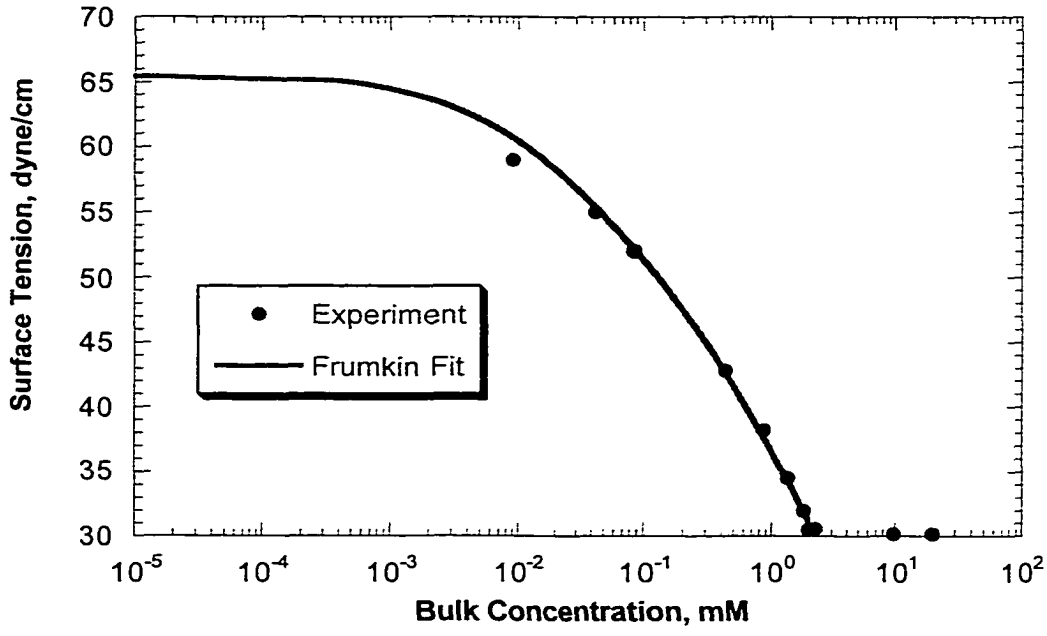

Figure 5.A.2: Measurements of the equilibrium tension of glycerol/water surfactant solutions of $C_{10}E_8$ at the air/ 70:30 glycerol-water interface and the Frumkin fit of this data.

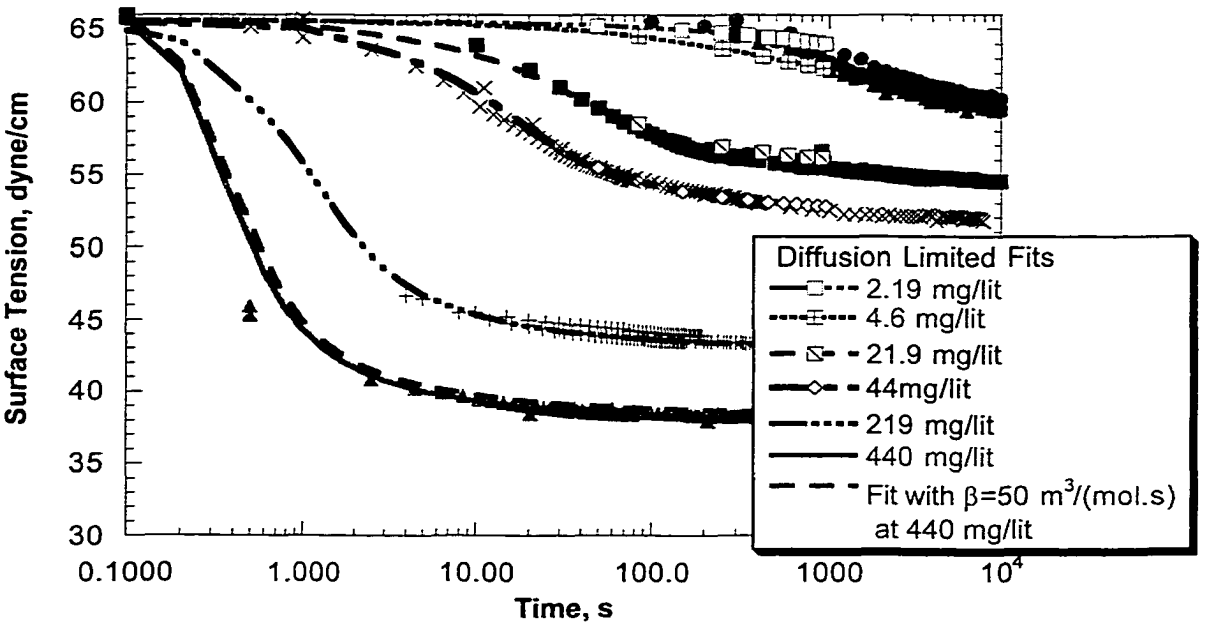

Figure 5.A.3: Dynamic surface tension relaxations for adsorption of $C_{10}E_8$ at an initially clean air/ 70:30 glycerol-water interface as measured by the pendant bubble technique. The continuous lines are fits with diffusion-limited simulations of the relaxation for a value of D equal to 1.5×10^{-11} m^2/sec.

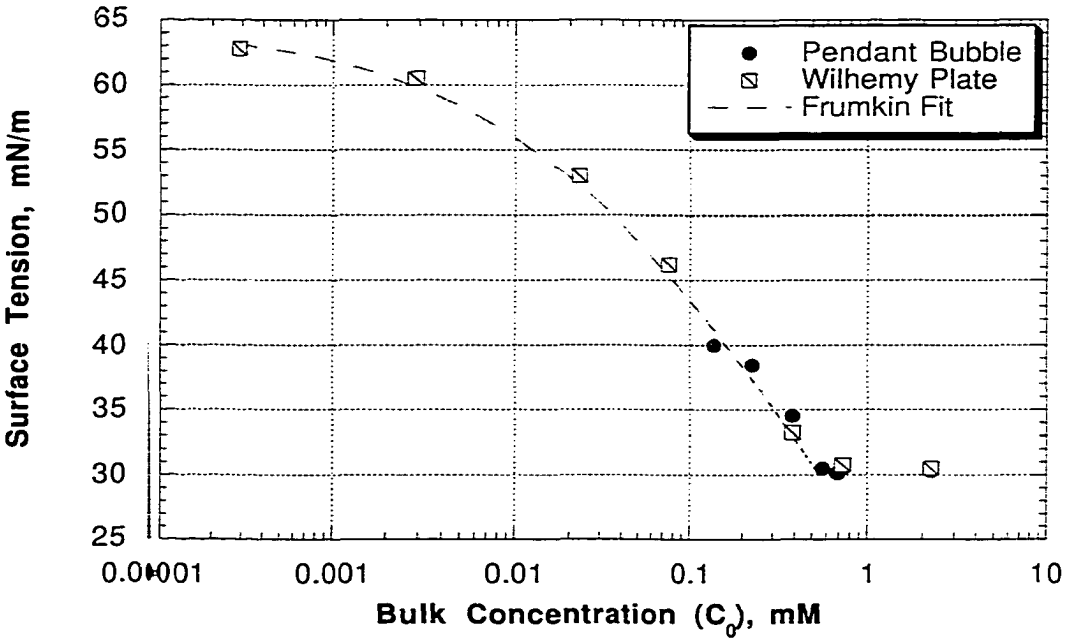

Figure 5.A.4: Measurements of the equilibrium tension of glycerol surfactant solutions of $C_{12}E_6$ at the air/ 100% glycerol interface and the Frumkin fit of this data.

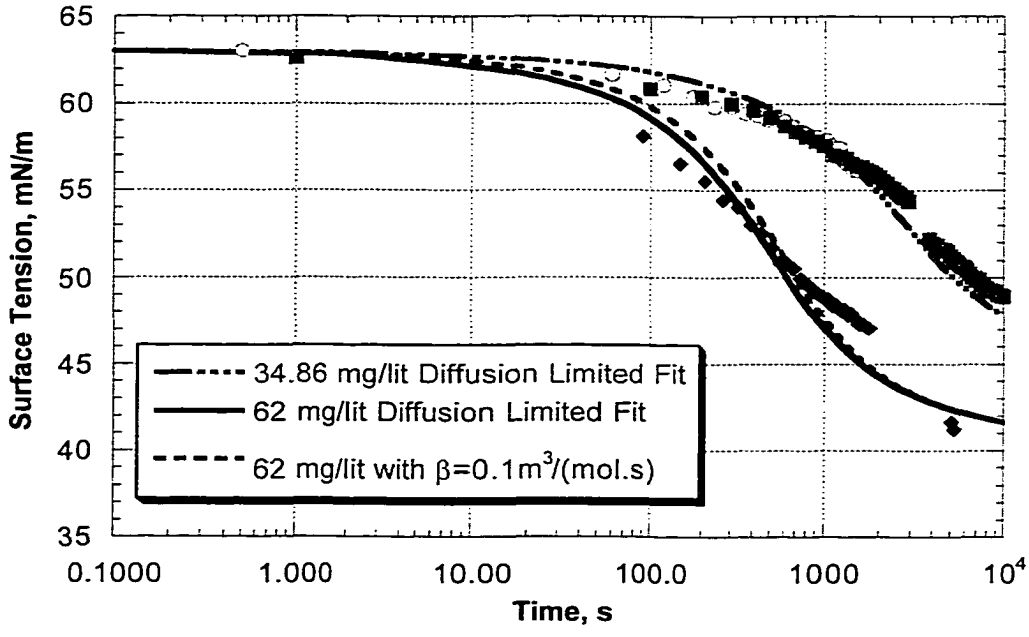

Figure 5.A.5: Dynamic surface tension relaxations for adsorption of $C_{12}E_6$ at an initially clean air/ 100% glycerol interface as measured by the pendant bubble technique. The continuous lines are fits with diffusion-limited simulations of the relaxation for a value of D equal to $3x10^{-13}$ m^2/sec.

CHAPTER 6
Possible Future Work

The results of our computational work in Chapter 2 on the motion of the bubble in the stagnant cap regime, showed the effect of surfactant kinetic exchange rates on the amount of surfactant that could adsorb on the rising bubble and hence the drag on the bubble. We used these results along with results from experiments on the bubble rise velocities, in Chapter 3 to zero in on the adsorption/desorption rate constants of the polyethoxy surfactant $C_{12}E_6$ at the air/glycerol-water mixture liquid interface. We showed how this kind of a technique could be used over a wider range of surfactant transport rates by kinetic exchange relative to bulk diffusion than the standard technique of monitoring the dynamic surface tension relaxations due to surfactant adsorption at an initially clean interface. It would be interesting to use this method in determining the kinetic exchange rate constants of surfactants at a more common air/water interface. The lower viscosity, would give higher rise velocities for air bubbles in water which would decrease the Biot number($Bi=\alpha a/U$). Hence the effect of kinetic exchange could be more distinguishable from the diffusion limited case than what we had seen in the 70:30 glycerol-water mixture case. We note that to be in the stagnant cap regime in water, we need extremely low surfactant bulk concentrations (C_0), lower than the ones we had used

in glycerol-water mixture. This is due to the increased hydrophilic nature of the bulk phase compared to the glycerol-water mixture case, which reduces the ratio α/β.

In Chapter 4, we developed the theory and presented our computational results on remobilizing the surfactant laden bubble surface. All the arguments are valid when the surfactant is present in the bulk in the monomeric form only. As we noted and observed in Chapter 5, to attain remobilization we need high surfactant bulk concentrations. Real surfactant systems form micellar aggregates above a critical bulk concentration called the critical micelle concentration (CMC). Above this, the surfactant exists both in the monomeric and micellar form. Some of our own experiments on remobilization in Chapter 5 have been done above the CMC of the surfactants used. As noted in Chapter 5, under these conditions, we need to take care of both the monomeric and micellar form of surfactant, and the micellar breakup and formation kinetics rates. Developing a theory taking care of these aspects in our computational work could verify the mechanism that we presented in Section 5.2 to explain the experimental results on remobilization of the bubble surface above the CMC. Also in real systems, the surfactants being used being mostly above the CMC, such a theory would form the next step in explaining the effect of surfactant transport in interfacial hydrodynamics in general.

From the discussion in Chapter 1, we see that in general, the accumulation of the surfactants present in the bulk liquid, on the moving interfaces, could result in the

reduction of the interfacial mobility. If there were a mass transport process between the bubble/drop phase and the continuous phase, like a gas dissolution or a drop-wise extraction process, then the mass transfer coefficient would depend on the flow behavior in the vicinity of the interface. Across a solid/ fluid interface, because of the no-slip condition, the mass transfer coefficient would be less than across a fluid/fluid interface with a stress-free boundary and hence higher velocities. As mentioned before, in the limit of high Peclet number (Pe), in creeping flow the mass transfer coefficient would vary as $O(Pe^{1/3})$ at a solid/fluid boundary while there is a $O(Pe^{1/2})$ variation at a fluid/fluid boundary. Since surfactants present in the bulk could alter the behavior of the interface, the efficiency of the interphase mass transfer processes also could be altered. This has been observed in many experimental studies as reviewed in Section 1.2. This alteration in the behavior of the bubbles/drops is caused even in the presence of trace quantities of surface active materials acting as impurities. Since it is difficult to get a pure system to deal with in any physical process, the expected efficiencies for the interphase mass transfer processes are never achieved.

The idea of remobilizing a surfactant retarded interface from the experimental observations of the Stebe, et al[25] and confirmed in this thesis, shows that through the use of remobilizing surfactants at high concentrations, the interface will behave stress free even in the presence of trace amounts of surface retarding impurities in the system. From

the observations made before on interphase mass transfer, one may consider using the remobilizing surfactants to regain the depleted mass transport efficiency in the two phase systems due to the presence of trace amounts of impurities. It would be interesting to see this effect experimentally, by considering the effect of the remoblizing surfactants on a process like say dissolution rates of CO_2 bubbles in water. Here though we expect the mass transfer rates to increase due to the increase in interfacial mobility, presence of surfactants in the bulk phase at high concentrations may change the diffusive transport rates of the solute (CO_2). Selection of the right system where the high concentrations of the surfactant needed for remobilization will not affect the bulk transport rates of the solute, could greatly benefit industrial mass transfer processes.

Bibliography

1)Levich *Physicochemical Hydrodynamics.*; Prentice Hall:, 1962.

2)Holbrook, J. A., Levan, M. D. *Chem. Engr. Commun.* **1983a**, *20*, 191-207.

3)Holbrook, J. A., Levan, M. D. *Chem. Engr. Commun.* **1983b**, *20*, 273-290.

4)Harper, J. F. *Q. J Mech. Appl. Math.* **1974**, *27*, 87-100.

5)Harper, J. F. *J. Fluid Mech.* **1973**, *58*, 539-545.

6)Harper, J. F. *Sci. Res.* **1982**, *38*, 343-351.

7)Levan, M., Newman, J *AIChE J.* **1976**, *22*, 695-701.

8)Saville, D. *Chem. Engr. J.* **1973**, *5*, 251-259.

9)Haberman, W. L., Morton, R.K. *Proc. Am. Soc. Civ. Eng* **1954**, *387*, 227-252.

10)Griffith, R. M. *Chemical Engineering Science* **1962**, *17*, 1057-1070.

11)Elzinga, E. R., Banchero, J. T. *AIChE J.* **1961**, *textbf7*, 394-399

12)Garner, F. M., Skelland, A. H.P. *Chemical Engineering Science* **1955**, *4*, 149.

13)Edge, R. M., Grant, C.D. *Chemical Engineering Science* **1972**, *27*, 1709-1721.

14)Raymond, D. R.; Zieminski, S. A. *AIChEJ* **1971**, *17*, 57-65.

15)Duineveld, P. C. *Bouncing and Coalescence of Two Bubbles in Water*; University of Twente, 1994.

16)Clift, R., Grace, J.R., Weber, M.E. *Bubbles, Drops and Particles*; Academic Press: New York, 1978.

17)Huang, W. S., Kintner, R. C. *AICHE J.* **1969**, *15*, 735-744.

18)Beitel, A., Heideger, W.J. *Chemical Engineering Science* **1971**, *26*, 711-717.

19)Ivanov, I. B., Dimitrov, D.S. ; Marcel Dekker: New York, 1988.

20)Radoev, B. P., Dimitrov, D.S., Ivanov, I.B. *Colloid Polymers* **1974**, *252*, 50.

21)Kim, H., Subramanian, R. *J. Colloid and Int. Sci.* **1989a**, *127*, 417-430.

22)Kim, H., Subramanian, R. *J. Colloid and Int. Sci.* **1989b**, *130*, 112-125.

23)Frumkin, A.; Levich, V. *Zhur. Fiz. Khim.* **1947**, *21*, 1183.

24)Stebe, K. J., Lin, S. Y., Maldarelli, C *Phys. Fluids A.* **1991**, *3*, 3-20.

25)Stebe, K. J., Maldarelli, C. *Journal Of Colloid and Interface Science* **1994**, *163*, 177-189.

26)Subramanian, R. S. ; Chabra, R. P. and DeKee, D., Ed.; Hemisphere Publishing: New York, 1992, pp 1-42.

27)Takemura, F., Yabe, A. *J. Fluid Mech.* **1999**, *378*, 319-334.

28)Nadim, A.; Borhan, A. *PhysicoChemical Hydrodynamics* **1989**, *11*, 753-764.

29)Chen, Y. S., Lu, Y.L., Yang, Y. M., Maa, J. R. *Int. J. Multiphase Flow* **1997**, *23*, 325-335.

30)Acrivos, A., Goddard, J.D. *J. Fluid Mech.* **1965**, *23*, 273-291.

31)Wang, Y., Papageorgiou, D., Maldarelli, C. *J. Fluid Mech.* **2000**.

32)Wang, Y., Papageorgiou, D. T., Maldarelli, C. *J. Fluid Mech.* **1999**, *390*, 251-270.

33)Borwankar, R. P., Wasan, D.T. *Chemical Engineering Science* **1983**, *38*, 1637-1649.

34)Chang, C. H., Franses, E. *Colloids and Surfaces A:Physicochemical and Engineering Aspects* **1995**, *100*, 1-45.

35)Savic, P. *Nat. Res. Counc. Can. Div. Mech. Engng Rep. MT-22* **1953**.

36)Davis, R. E., Acrivos, A. *Chemical Engineering Science* **1966**, *21*, 681-685.

37)Sadhal, S., Johnson, R. *J. Fluid Mech.* **1982**, *126*, 237-250.

38)He, Z., Maldarelli, C., Dagan, Z. *Journal of Colloid and Interfacial Science* **1991a**, *146*, 442-451.

39)Cuenot, B., Magnaudet, J., Spennato, B. *J. Fluid Mech.* **1996**, *339*.

40)Deryagin, B. V., Dukhin, S.S., Lisichenko, V.A. *Russ. J. Phys. Chem* **1959**, *33*, 389-393.

41)Andrews, G. F., Fike, R., Wong, S. *Chemical Engineering Science* **1988**, *43*, 1467-1477.

42)Chen, J., Stebe, K. *J. Colloid Interfacial Sci.* **1996**, *178*, 144-155.

43)Chen, J., Stebe, K. *J. Fluid Mech.* **1997**, *340*, 35-60.

44)Horton, T. J., Fritsch, T. R, Kintner, R. C. *Can. J. Chem. Engr.* **1965**, *43*, 143-146.

45)Yamamoto, T., Ishil, T. *Chemical Engineering Science* **1987**, *42*, 1297-1303.

46)Bel Fdhila, R., Duineveld, P. C. *Phys. Fluids* **1996**, *8*, 310-321.

47)Leppinen, D. M.; Renksizbulut, M.; Haywood, R. J. *Chemical Engineering Science* **1996a**, *51*, 479-489.

48)Leppinen, D. M.; Renksizbulut, M.; Haywood, R. J. *Chemical Engineering Science* **1996b**, *51*, 491-501.

49)McLaughlin, J. B. *J. Colloid Int. Sci.* **1997.**

50)Ryskin, G., Leal, L. G. *J. Fluid Mech.* **1982,** *148*, 1-17.

51)Magnaudet, J., Rivero, M., Fabre, J. *J. Fluid Mech.* **1995**, *284*, 97-135.

52)Oliver, D. L., Chung, I.N. *J. Fluid Mech.* **1987**, *177.*

53)Ryvkind, V. Y., Ryskin, G. *Fluid Dyn.* **1976**, *11.*

54)Peyret, R.; Taylor, T. D. *Computational methods for fluid flow.*, 1983.

55)Patankar, S. V. *Numerical Heat Transfer and Fluid Flow*; Hemisphere Pub;, 1980.

56)Tannehill, C. J., Anderson, D.A., Pletcher, R.H. *Computational Fluid Mechanics and Heat Transfer*; 2 ed.; Taylor & Francis: Washington D.C., 1997.

57)Chorin, A. J. *Math. Comput.,* **1968**, *22*, 745-762.

58)Zhang, Y., McLaughlin,J.B., Finch, J.A. *J. Fluid Mech.* **2000.**

59)Pan, R., Green, J., Maldarelli, C. *Journal of Colloid and Interfacial Science* **1998**, *205*, 213-230.

60)Kretzchmar, G., Miller, R *Advances in Colloid and Interface Science* **1991**, *36*, 65-124.

61)Miller, R., Kretzschmar, G. *Advances In Colloid and Interface Science* **1991**, *37*, 97-121.

62)Rotenberg, Y., Boruvka, L., Newumann, A. W. *Journal of Colloid and Interface Science* **1983**, *93*, 169-183.

63)Cheng, P., Li, D., Boruvka,L., Rotenberg, Y., Neumann, A.W. *Colloids and Surfaces* **1990**, 151-167.

64)Annianson, E. A. G., et al *Journal of Physical Chemistry* **1974**, *78*, 1024.

65)Annianson, E. A. G., et al *Journal of Physical Chemistry* **1976**, *80*, 905.

66)Annianson, E. A. G., et al *Progress in Colloid and Polymer Science* **1985**, *70*, 5.

67)Inoue, T., et al *Journal of Colloid and Interface Science* **1978**, *65*.

68)Inoue, T., et al *Journal of Colloid and Interface Science* **1980**, *73*, 105.

69)Herrmann, C. U., Kahlweit, M. *Journal of Physical Chemistry* **1980**, *84*, 1536.

70)Muller, N. *Journal of Physical Chemistry* **1972**, *76*.

71)Yasunaga, T., et al *Journal of Colloid and Interface Science* **1967**, *23*, 352.

72)Chan, S. K. e. a. *Ber. Bunsenges. Phys. Chem.* **1977**, *81*, 396-402.

73)Lang, J. *Kinetic Studies of the Dissociation of Nonionic Detergent Micelles*; Wyn-Jones, E., Reidel, D., Ed.: Dordrecht, Holland, 1975, pp 195-200.

74)Tondre, C. e. a. *Journal of Colloid Interface Science* **1975**, *52*, 372-379.

75)Oh, S. G., Shah, D.O. *Langmuir* **1991**, *7*, 1316.

76)Oh, S. G., Klein, S.P., Shah, D.O. *AIChE Journal* **1992**, *38*, 149.

77)Patist, A., Oh, S.G., Leung, R., Shah, D.O. *Kinetics of Micellization: Its significance to Technological Processes*: Stockholm, Sweden, 1998.

78)Miller, R., Joos, P., Fainerman, V. *Advances in Colloid and Interface Science* **1994**, *49*, 249-302.